Mass transfer enhanced syngas fermentation using elevated pressure and the spinning disk reactor

Zwaan, Boris B.

Award date:
2023

Eindhoven University of Technology
Research Group of Sustainable Process Engineering

Mass transfer enhanced syngas fermentation using elevated pressure and the spinning disk reactor

Master Thesis

Boris Bert Zwaan

Graduation Committee:

Prof. Dr. J. van der Schaaf
Ir. C.J.W. Hop
Dr. A. Chaudhuri
Prof. Dr. D.Z. Machado de Sousa

Eindhoven, 10 June 2022

Acknowledgement

First of all, I would like to thank my daily supervisor Vince Hop for coaching me during this project. He was always very flexible and wanting to think along to make this project a success. His attitude inspired me keep on working to make this project a success, especially in the first months when 'our' bacteria did not start growing. We've spent a lot of time in the lab together, trying to identify why the reactor set-up was clogged, produced magnetic particles, and so on. Despite all these setbacks, it were the small successes we made that kept us moving forward.

Next, I would like to thank John van der Schaaf for his input during the progress meetings. He gave me many new insights to pursue the project. I found it always very enjoyable that we deliberately had to stop talking about educational matters and switch to discussing this project, as he moreover holds the position of program director. I furthermore would like to thank him, and Vince as well, for giving me the freedom to execute my other activities within TU/e, as it was sometimes difficult to combine these with my graduation project.

Furthermore, I would like to thank all colleagues from SPE and students from the 'Broeikas'. With all the laughter, coffee breaks and activities we did together, you really helped me to enjoy my time in the research group. At last, I would like to thank my roommates from 'Huize Ranonkel', my friends, colleagues at TU/e and my parents for always being available to chat about the project. This made me able to 'zoom-out' and look at the bigger picture of the whole.

Abstract

A pathway that is currently widely researched to transition from the usage of fossil fuels for the production of valuable hydrocarbons is the conversion of bio-based syngas. Many industrial processes that convert syngas operate on metal-based catalysts and are energy-intensive. An alternative method to convert syngas is by means of fermentation using acetogenic bacteria. Currently, bioreactors operating these processes are typically mass transfer limited, requiring high reactor volumes. Consequently, alternative bioreactor configurations are investigated, providing higher productivity and large scale operation. A reactor capable of overcoming mass transfer limitations is the rator stator spinning disk reactor (rs-SDR).

This work investigates mass transfer enhancement of syngas fermentation in a rs-SDR using the acetogenic bacteria *Clostridium autoethanogenum*, producing acetic acid, ethanol and butane-2,3-diol. Focus is placed on fermentation using carbon monoxide (CO) as this gas in particular experiences large gas liquid mass transfer limitations out of the gases present in bio-based syngas. As a starting point, microbes are cultivated in fed-batch glass cultivation bottles. Insights are gained in productivity and selectivity as a function of limitations imposed on the metabolic system. These insights will lead to steering product selectivity towards more valuable end-products.

In addition to the rs-SDR, liquid mass transfer can be enhanced by means of elevating pressure. Continuous fermentation experiments were performed in a stirred vessel at 200 kPa and 500 kPa. Steady state-like behaviour was achieved, resulting in continuous and constant production by *C. autoethanogenum*. A 35% increase in productivity was observed comparing 200 kPa to 500 kPa. CO uptake rate moreover increased, showing successful enhancement of mass transfer during continuous fermentation. Product selectivity seemed to be unaffected however. This study is the first to show continuous syngas fermentation using *C. autoethanogenum* at elevated pressures.

Next, fermentation experiments were performed at various rotational speeds in the rs-SDR. However, no production or bacterial growth was observed, yielding no successful fermentation. Therefore, possible enhancement of mass transfer leading to higher productivity was not quantified. A gradual decline in bacterial concentration was moreover observed after elongated exposure to high shear forces in the rs-SDR. Microscopical analysis of the bacterial cells showed however little to no effect.

Lastly, a literary study on the metabolic system of *C. autoethanogenum* was performed. This system was successfully simplified, reducing the description of the metabolism to a set of 16 reaction equations. An attempt was made to model this set of reactions. However simplified, complexity of the system and lack of kinetic data caused the model to be unable to accurately predict the behaviour of the bacteria.

List of Figures

List of Tables

Nomenclature

Latin

A_{cell}	Superficial cell area	$[m_s^2]$
a_{GL}	Gas liquid mass transfer interfacial area	$[\frac{m_{int}^2}{m_G^3}]$
C	Concentration	$[\frac{mol}{m^3}]$
D	Diffusivity	$[\frac{m^3}{s}]$
D	Dilution rate	$[\frac{1}{day}]$
E_d	Energy dissipation	$[\frac{W}{m_r^3}]$
H	Henry's coefficient	$[\frac{mol}{Pam_L^3}]$
K	Partition coefficient	$[-]$
k_L	Gas liquid mass transfer coefficient	$[\frac{m_L^3}{m_{int}^2 \cdot h}]$
m	Distribution coefficient	$[\frac{m_B^3}{m_L^3}]$
M_w	Molar weight	$[\frac{g}{mol}]$
N	Number of moles	$[mol]$
p	Permeability	$[\frac{m_s}{h}]$
P	Pressure	$[Pa]$
r_d	Rotor Radius	$[m]$
R	Reaction rate	$[\frac{mol}{h}]$
R	Gas constant	$[\frac{J}{K \cdot mol}]$
s	Separation between rotor and stator	$[m]$
t	Time	$[s]$
T	Temperature	$[K]$
V_{cell}	Cell volume	$[m_s^3]$
V_n	Volume of phase n	$[m^3]$
X	Biomass concentration	$[\frac{kg}{m_l^3}]$
X_{death}	Bacterial death rate	$[\frac{kg}{m_L^3}]$
y	Molar gas fraction	$[-]$

Greek

ϵ	Hold-up	$[-]$
ν	Kinematic viscosity	$[\frac{m^2}{s}]$
ρ	Density	$[\frac{kg}{m^3}]$
τ	Torque	$[Nm]$
ϕ	Flow rate	$[\frac{m^3}{s}]$
ω	Rotational speed	$[\frac{1}{s}]$

Subscripts

0	Initial
B	Bacterial
d	Disk
ext	External
G	Gas
in	Inlet
int	Internal
L	Liquid
m	Component m
n	Phase n
out	Outlet
ox	Oxidised
red	Reduced
R	Recycle
s	superficial

Dimensionless number

G	Axial clearance
Re_ω	Bacterial

Abbreviations

ADP	Adonesine diphosphate
ATP	Adonesine triphosphate
ATPase	ATP Synthase
C. autoethanogenum	Clostridium autoethanogenum
C. ljungdahlii	Clostridium ljungdahlii
CoA	Coenzyme A
CODH	Carbon monoxide dehydrogenase
CSTR	Continuously stirred tank reactor
E. coli	Escherichia coli
Fd	Ferredoxin
GC	Gas chromatograph
GCMS	Gas chromatograph mass spectrometry
gDCW	Gram dry cellular weight
HPLC	High pressure liquid chromatography
Hyt	Hydrogenase
NADH	Nicotinamide adenine dinucleotide
NADPH	Nicotinamide adenine dinucleotide phosphate
Nfn	NADH-dependent reduced ferredoxin:$NADP^+$ oxidoreductase
OD	Optical density
Rnf	Rhodobacter nitrogen fixation
rs-SDR	Rotor stator spinning disk reactor
rpm	Rotations per minute
WLP	Wood Ljungdahl Pathway

Table of Contents

1. Introduction

Greenhouse gas emissions need to be reduced to net-zero in 2050 in order to limit global warming to 1.5°C [1]. The chemical industry carries a pivotal responsibility to contribute to this goal, being one of the major emitters [2]. Many of these efforts concern the chemical valorization of the most contributing greenhouse gas to global warming: carbon dioxide (CO_2). Additionally, industry needs to transition from using fossil resources to sustainable carbon resources to provide in the need of valuable hydrocarbons. One technique to achieve this is by producing hydrocarbons from lignocellulosic biomass. This entails the production of syngas, a mixture of CO_2, CO and H_2 from gasification of biomass. Thereafter, the syngas can be chemically converted towards valuable fuels or feedstock for the chemical industry [3].

Currently, metal-based catalytic processes provide an outcome to effectively convert syngas into valuable hydrocarbons. Chemical conversion routes under investigation are the hydrogenation of methanol and catalytic ethanol production, amongst others [4]. Another widely performed and researched process for the hydrogenation of C_1 feedstock (CO_2 and CO) is the Fischer-Tropsch process [5]. However, over the past decades, attention has extended to syngas conversion using bacterial fermentation. Several bacterial species are able to convert this gas mixture into valuable chemicals, with higher selectivities compared to metal-based processes [6]. Another advantage is that fermentation processes usually operate at milder temperature ranges (30-40 °C), making these processes much less energy intensive [7].

This work focuses on the anaerobic bacterial fermentation of biomass-derived syngas by the acetogenic bacteria *Clostridium Autoethanogenum* (*C. autoethanogenum*). This bacteria is able to convert various mixtures of CO, CO_2 and H_2 into acetic acid, ethanol and butane-2,3-diol [8]. These components are both valuable chemical feed-stock as valuable products themselves. Especially butane-2,3-diol is a highly valuable component, which downstream products are estimated to have a global market value of $43 billion in sales [9].

Fermentation processes using bacteria alike *C. autoethanogenum* are commonly performed in stirred tank reactors and bubble columns [10]. However, cell growth and productivity are restricted by the ability of these reactors to transfer sufficient gas into the liquid phase towards the bacteria [11][12]. To obtain reasonable product concentrations and high product volumes, relatively high reactor volumes are required. This makes the economic feasibility of scaling up these processes challenging.

A reactor able to reach high volumetric gas-liquid mass transfer rates is the rotor-stator spinning disc reactor (rs-SDR). This reactor has successfully proven to intensify several mass transfer limited processes. In previous studies, this reactor has shown to reach mass transfer rates higher than bubble columns. Moreover, intensification of gas-liquid mass transfer limited processes of mixtures with higher viscosities, similar in bacterial fermentation processes, has shown benefits using the rs-SDR [13][14][15].

Therefore, this work investigates the promising concept of intensifying bacterial syngas fermentation with *C. autoethanogenum* using a rs-SDR. Off all gasses present in syngas, CO in particular shows to have a low gas liquid mass transfer coefficient [16]. It is therefore important to gain insight in the limitations of this gas. In addition, this substrate usually yields higher and more valuable ethanol production in *C. autoethanogenum* compared to mixtures of CO_2 and H_2 [12]. Consequently, this work focuses on fermentation processes using CO as its sole substrate. Small scale experiments are conducted in a continuously stirred vessel installation to gain insight in the effect of elevated pressures on the fermentation process, in addition to further enhance mass transfer. Furthermore, experiments are conducted in a spinning disc reactor at different rotational speeds. By performing these experiments, insights in limitations are obtained. Additionally, a literary study is performed to understand the metabolic pathway of *C. autoethanogenum* and its uncertainties. Having a clear understanding of the metabolic pathway helps explaining the effect

of process parameters on the final product composition.

Eventually, both insights in mass transfer limitations and the metabolic pathway will lead to steering product selectivity and intensifying continuous fermentation of bio-derived syngas in a rs-SDR.

2. Theoretical background

In this section, all required theory to understand the results presented in chapter 4 are discussed. First, the studied bacterial species is introduced, where-after the literary study on its metabolic pathway is presented. Chemical reactions following from this study are required for understanding the behaviour of the fermentation process of *C. autoethanogenum* in bioreactors. Furthermore, general elaboration on mass transfer in fermentation processes is provided, concluding with a theoretical background of the rs-SDR.

2.1 Clostridium Autoethanogenum

The anaerobic bacterial species *Clostridium Autoethanogenum* (*C. autoethanogenum*) is a rod-shaped bacteria, first identified in rabbit feces in 1994 [17]. This micro-organism is part of the *Clostridium* genus, being a gram positive species, inhibiting soils and intestinal tracks of animals. *C. autoethanogenum* is found to be a non-dangerous species, not threatening to human health. The microbe is able to reduce mixtures of CO_2, CO and H_2 towards acetic acid, ethanol and butane-2,3-diol by means of its unique metabolism [18]. In addition, low quantities of lactic acid are observed as reaction product. Cultivation of *C. autoethanogenum* on fructose and xylose has also been shown to be possible, although leading to lower production compared to cultivation on the described gas mixture [19].

Figure 2.1 shows a schematic representation of *C. autoethanogenum*. Characteristic to gram-positive bacteria is that the cell wall structure consists out of two membranes. In contrast with gram-negative bacteria, they miss an extra rigid protein- and polysacharide-based membrane. In-between the outer membrane, or peptidoglycan, and inner plasma membrane, lies the periplasm or perisplasmic space. Several enzymatic complexes are situated on the inner plasma membrane. It is assumed that pH values in the periplasm are similar to pH values of the bacterial medium. All genetic material and enzymatic complexes to perform the conversion of gas substrates are found in the cytoplasm [20] and the inner plasma membrane.

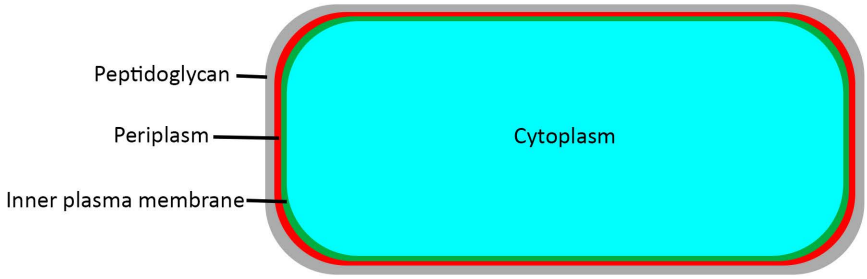

Figure 2.1: Schematic representation of a *Clostridium autoethanogenum* bacterium

2.1.1 Metabolism

Many research has been carried out examining the metabolism of *C. autoethanogenum*, understanding the different reactions involved in the conversion of H_2, CO_2 and CO into its products. The metabolic system of *C. autoethanogenum* consists of two parts: the catabolism and anabolism. The anabolism concerns reactions that consume energy. Reactions part of the catabolism provide

in this energy. The interaction between the anabolism and catabolism should eventually result in a net positive adenine triphospate (ATP) production [20]. This energy carrier is required for cell maintenance and cell reproduction. Accompanied is the release of the products acetic acid, ethanol and butane-2,3-diol. pH- and concentration changes of intracellular components can lead to changes in production and selectivity of the three described products, affecting the ATP-gain, thus cell reproduction and maintenance. The metabolism described in this chapter only focuses on the direct routes converting carbon into the described products and the energy conservation of *C. autoethanogenum*.

C. autoethanogenum utilises the Wood-Ljungdal Pathway (WLP) to fix carbon from both CO and CO_2 into acetyl Co-enzyme A (acetyl-CoA). This pathway, occuring in many acetogens, consists of a total of 8 reactions. Thereafter, acetyl-CoA can be converted using different reaction pathways, leading to four possible reaction products: acetic acid, ethanol, butane-2,3-diol and biomass.

A decent overview of the history and current understanding of the WLP and the pathways forming the four products is described by Ragsdale et al. [21], giving a general overview of reactions and enzymes involved.

Several reactions part of the metabolism, involved in reducing the carbon containing compound, require an oxidizing agent/ electron donor. *C. autoethanogenum* uses nicotinamide adenine dinucleotide phosphate (NADPH), nicotinamide-adenine-dinucleotide (NADH) and ferredoxin (Fd) as electron donors. Additionally, ATP functions as an energy carrier, and is used or produced in the metabolism. When NADPH, NADH and Fd are oxidised, *C. autoethanogenum* will reduce these compounds as they need to be re-used in the metabolism. Accompanied, ATP is produced. Four enzymatic complexes performing four reactions make up for the energy conservation mechanism.

Mock et al. [22] and Wang et al. [23] did great work determining the specific activities and specificities of all relevant enzymes in *C. autoethanogenum*. The set of chemical reaction equations describing the metabolism described in this work are largely based on these publications. These studies are backed-up with transcriptional genome analyses performed by Humphreys et al. [24] and Brown et al. [25], linking the enzymes to the specific genes in *C. autoethanogenum*. Enzymes performing reactions showing the highest specific activities as stated in these publications are used as the main reaction as presented in this work.

Several aspects of the WLP and the pathways to convert acetyl-CoA into the reaction products and biomass are still up for discussion. For these steps, a 'most-likely' scenario has been presented by the discussed publications. In the following sections, these cases are elaborated upon.

First, the four reactions making up the energy conservation mechanism are presented. Next, the reactions involved in the WLP are discussed, where-after all pathways leading to the described products are presented. When studying subsection 2.1.2 and section 2.2, it is recommended to simultaneously analyse Figure 2.2. This figure is attached to this report in A3 format, providing a complete overview of the metabolic reactions in *C. autoethanogenum*. In this figure, reactions are labelled similarly as presented in these sections.

For all reactions presented, the Enzyme Commission Number (EC) is included. For the reactions of which several types of the enzymes exists, the gene that was expressed most in Mock et al. and Wang et al. is provided (CAETHG-xxxx). A point of attention is that different reactions than stated in these publications are occasionally mentioned in the KEGG [26] and NCBI databases [27]. These databases are not fully up-to-date with the latest research and only show the gene products as stated by earlier work/ sequencing. These databases are however very useful in retrieving stoichiometrically correct reaction equations and additional information about the variety of enzymes present in *C. autoethanogenum*.

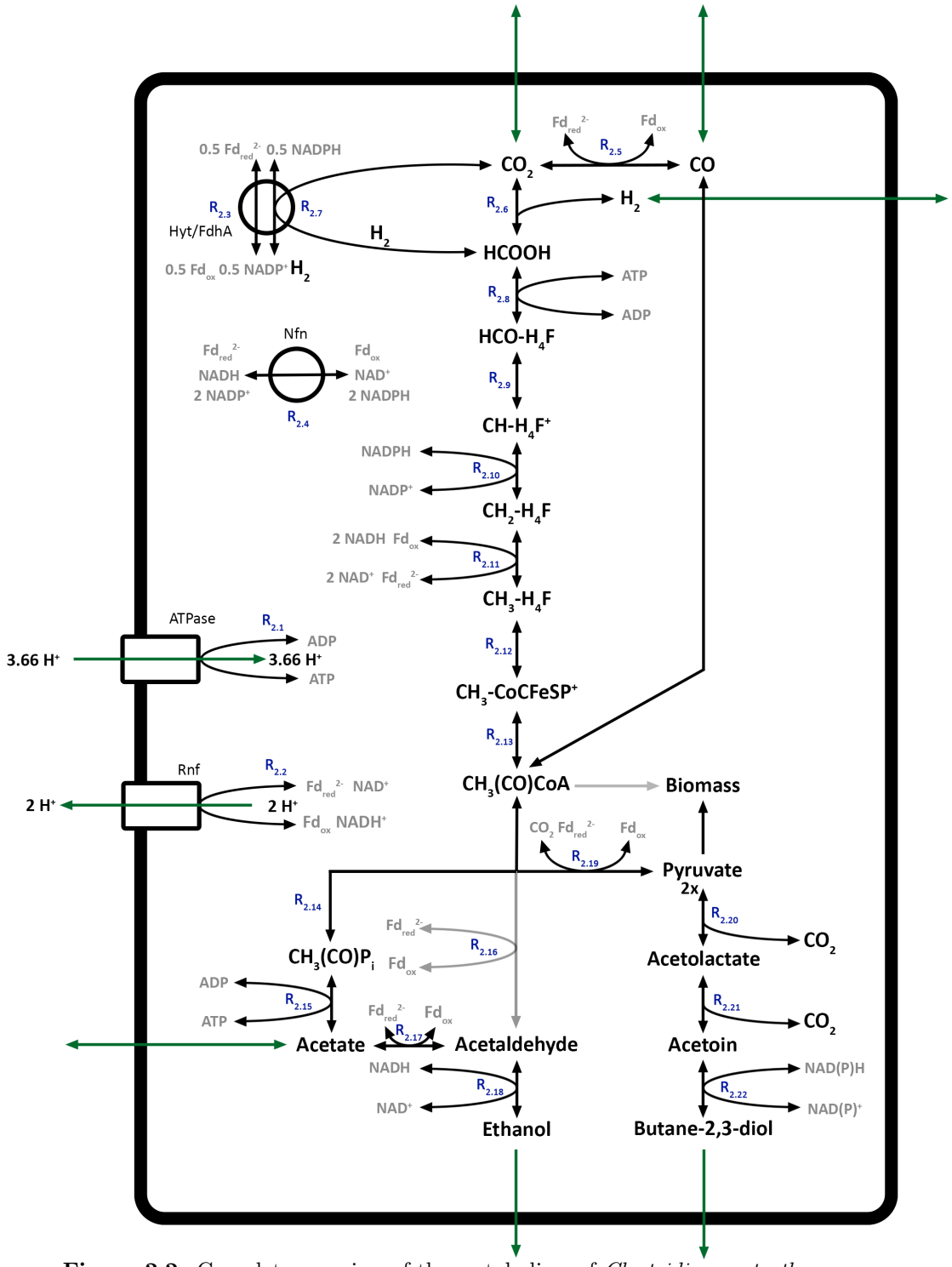

Figure 2.2: Complete overview of the metabolism of *Clostridium autoethanogenum*

2.1.2 Energy Conservation Mechanism

The energy conservation mechanism consists out of four enzymatic complexes. Half-reactions are provided, as well as the four overall reactions.

Acetogens conserve energy by the generation of an ion motive force, pumping ions in and out of the bacterial cell. For *C. autoethanogenum*, H^+ is used as a driving force for ATP synthesis. F_1F_0-ATP synthase (ATPase) converts adenine diphosphate (ADP) into ATP. It is assumed that pH levels in the bacterial cells is around 6 [22], whereas the bacterial medium has a medium between pH = 4.5-5.75. This implies that energy is gained when ATPase diffuses protons into the bacterial cell. This enzymatic complex is situated on the periplasmic membrane where the proton flow is with the proton concentration gradient, releasing energy to couple phosphate with ADP to form ATP. The c-ring protein-complex is part of ATPase in *Clostridia* and plays a role in transporting protons towards the cytoplasm. This c-ring contains a total of 11 subunits channeling protons. With every third of a rotation of this ring, one ATP molecule is formed, indicating that in *C. autoethanogenum* 3.66 (11/3) protons are required to synthesise 1 ATP molecule [28]. The full reaction is shown in Equation 2.1, where ${H_{in}}^+$ and ${H_{out}}^+$ refer to the protons in the cytoplasm and the protons in the periplasm respectively:

$$\mathrm{ADP} + \mathrm{P}_i + 3.66\,{\mathrm{H_{out}}}^+ \xrightleftharpoons{\mathrm{F_1F_0-ATPase}} \mathrm{ATP} + 3.66\,{\mathrm{H_{in}}}^+ + \mathrm{H_2O} \tag{2.1}$$

The second enzymatic complex is the ferredoxin, NAD+ dependent oxireductase (Rnf). Rnf is composed of 6 subunits (RnfA to -G) of which three are integral proteins located on the inner plamsa membrane. The function of Rnf is to balance the proton concentration gradient between cytoplasm and periplasm. Rnf is pumping protons out of the cytoplasm, hence, against the proton concentration gradient. The energy required to perform this is acquired by the oxidation of ferredoxin, alongside with the reduction of NAD+.

$$\begin{aligned} {\mathrm{Fd_{red}}}^{2-} &\rightleftharpoons \mathrm{Fd_{ox}} + 2\,\mathrm{e}^- \\ \mathrm{NAD}^+ + \mathrm{H}^+ + 2\,\mathrm{e}^- &\rightleftharpoons \mathrm{NADH} \end{aligned}$$

Overall:

$${\mathrm{Fd_{red}}}^{2-} + \mathrm{NAD}^+ + \mathrm{H}^+ + 2\,{\mathrm{H_{in}}}^+ \xrightleftharpoons{\mathrm{Rnf}} \mathrm{Fd_{ox}} + \mathrm{NADH} + 2\,{\mathrm{H_{out}}}^+ \tag{2.2}$$

The third enzymatic complex part of the energy conservation mechanism is hydrogenase (Hyt). Of the more than 10 hydrogenases encoded on *C. autoethanogenum*, HytABCDE1E2 was found to have the most significant expression during growth on CO_2, CO and H_2 according to Mock et. al (CAETHG2794-99) [22]. It turns out to be one of the highest expressed genes in *C. autoethanogenum*. This hydrogenase consists out of 6 subunits and is electron bifurcating. Electron bifurcation is the coupling of exergonic and endergonic redox reactions to simultaneously generate, or utilize, low- and high-potential electrons.

HytABCDE1E2 forms a tight complex with the selenium- and tungsten- dependent formate dehydrogenase FdhA (HytA-E/FdhA). The total complex plays a role in the formation of formate, which is discussed in section 2.2. The precise interaction between the two complexes on a molecular scale remains somewhat unclear. For Hyt, the following half reactions take place, with the overall reaction shown in Equation 2.3. When H_2 is present as a substrate, the equilibrium of the overall reaction is to the right. If no H_2 is present, only in the case of cultivation on CO, the equilibrium is to the left, forming H_2 for the formation of formic acid. More elaboration on this is provided in section 2.2.

$$\mathrm{H_2} \rightleftharpoons 2\,\mathrm{H^+} + 2\,\mathrm{e^-}$$
$$\mathrm{NADP^+} + \mathrm{H^+} + 2\,\mathrm{e^-} \rightleftharpoons \mathrm{NADPH}$$

$$\mathrm{H_2} \rightleftharpoons 2\,\mathrm{H^+} + 2\,\mathrm{e^-}$$
$$\mathrm{Fd_{ox}} + 2\,\mathrm{e^-} \rightleftharpoons \mathrm{Fd_{red}}^{2-}$$

Overall:

$$2\,\mathrm{H_2} + \mathrm{Fd_{ox}} + \mathrm{NADP^+} \overset{\mathrm{Hyt}}{\rightleftharpoons} \mathrm{Fd_{red}}^{2-} + \mathrm{NADPH} + 3\,\mathrm{H^+} \tag{2.3}$$

The last enzymatic complex performs the reduction of ferredoxin with NADPH in the presence of NAD+ in the so-called electron bifurcating ferredoxin-dependent transhydrogenase (Nfn). The *Nfn* gene in CO-grown *C. autoethanogenum* belongs to the most highly expressed genes [22]. Half reactions and overall reaction are shown in Equation 2.4

$$\mathrm{Fd_{red}}^{2-} \rightleftharpoons \mathrm{Fd_{ox}} + 2\,\mathrm{e^-}$$
$$\mathrm{NADP^+} + \mathrm{H^+} + 2\,\mathrm{e^-} \rightleftharpoons \mathrm{NADPH}$$

$$\mathrm{NADH} \rightleftharpoons \mathrm{NAD^+} + \mathrm{H^+} + 2\,\mathrm{e^-}$$
$$\mathrm{NADP^+} + \mathrm{H^+} + 2\,\mathrm{e^-} \rightleftharpoons \mathrm{NADPH}$$

Overall:

$$\mathrm{Fd_{red}}^{2-} + \mathrm{NADH} + 2\,\mathrm{NADP^+} + \mathrm{H^+} \overset{\mathrm{Nfn}}{\rightleftharpoons} \mathrm{Fd_{ox}} + \mathrm{NAD^+} + 2\,\mathrm{NADPH} \tag{2.4}$$

2.2 Metabolic system

In this section, all reactions making up the WLP converting gaseous substrates into acetyl-CoA for *C. autoethanogenum* are presented. Next, the reaction pathways reducing acetyl-CoA to form acetate, ethanol, butane-2,3-diol and biomass are provided. Stoichiometry checks for all reactions, atom and electrons balances are provided in Appendix A.

2.2.1 Wood Ljungdahl Pathway

The WLP begins with the CO hydrogenation reaction using the enzyme carbon monoxide hydrogenase (CODH) [EC 1.2.7.4] and uses ferredoxin as electron donor/ acceptor. This is an equilibrium reaction, depending on the available growth substrate, which could either be CO_2 or CO. Both CO and CO_2 are needed as components in the WLP. The half reactions and full reaction are as follows:

$$\begin{aligned} CO_2 + 2\,H^+ + 2\,e^- &\rightleftharpoons CO + H_2O \\ {Fd_{red}}^{2-} &\rightleftharpoons Fd_{ox} + 2\,e^- \\ CO_2 + 2\,H^+ + {Fd_{red}}^{2-} &\overset{CODH}{\rightleftharpoons} CO + H_2O + Fd_{ox} \end{aligned} \tag{2.5}$$

The next step is the conversion of CO_2 to formate (HCOOH), using the enzyme formate dehydrogenase (FdhA). As mentioned in subsection 2.1.2, this enzyme forms a tight complex with HytA-E forming HytA-E/FdhA. Depending on the available gaseous substrate, formate is formed in two different ways:

1. When CO_2 and H_2 are used as substrate, both molecules can be directly recombined as shown in Equation 2.6, known as the formate lyase reaction.

2. When *C. autoethanogenum* is cultivated on CO and H_2 is absent, H_2 first needs to be formed by the reaction in the HytABCDE1E2 complex, as shown in Equation 2.3. Recombination of H_2 with CO_2, the latter being either provided as a substrate or formed by Equation 2.5, will result in formate production. This overall reaction is shown in Equation 2.7. As can be observed, this reaction is a combination of the reverse Equation 2.3 and Equation 2.6.

$$\begin{aligned} CO_2 + H^+ + 2\,e^- &\rightleftharpoons HCOO^- \\ H_2 &\rightleftharpoons 2\,H^+ + 2\,e^- \\ CO_2 + H_2 &\overset{FdhA}{\rightleftharpoons} HCOO^- + H^+\,(HCOOH) \end{aligned} \tag{2.6}$$

$$2\,CO_2 + {Fd_{red}}^{2-} + NADPH + 3\,H^+ \overset{Hyt/FdhA}{\rightleftharpoons} 2\,HCOOH + Fd_{ox} + NADP^+ \tag{2.7}$$

After the formation of formate, a series of metabolic reactions take place to convert formate into a methyl group. This methyl group is eventually bonded with CO to form AcetylCoA.

The first reaction in this conversion is the ATP-dependent condensation of formate with tetrahydrofolate (H_4folate) forming 10-formyl$-H_4$folate. This reaction is performed by the enzyme 10-Formyl$-H_4$folate synthetase (FTL) [EC 6.3.4.3] (Equation 2.8):

$$\mathrm{HCOOH} + \mathrm{ATP} + \mathrm{H_4folate} \overset{\mathrm{FTL}}{\rightleftharpoons} \mathrm{10\text{-}HCO{-}H_4folate} + \mathrm{ADP} + \mathrm{P}_i \tag{2.8}$$

Next, a series of 3 reactions take place, converting the HCO-group on H_4folate to a CH_3-group. In the first reaction, the 10-HCO$-H_4$folate is converted to the intermediate product 5,10$-$methenyl$-H_4$folate$^+$ using 5,10$-$methenyl$-H_4$folate cyclohydrolase (MTC) [EC 3.5.4.9] (Equation 2.9). The next two steps further reduce the carbon atom taken up by the H_4folate. The second step is catalyzed by 5,10$-$methylene$-H_4$folate dehydrogenase (MTD) (Equation 2.10). Both NAD+ and NADP+ dependend forms of the enzyme exist. The genome of *C. autoethanogenum* contains the code to synthesise the NADP+ dependend form only [EC 1.5.1.5], CAETHG1616, as described by Mock et al. [22].

$$\mathrm{10\text{-}HCO{-}H_4folate} + \mathrm{H}^+ \overset{\mathrm{MTC}}{\rightleftharpoons} \mathrm{5,10{-}methenyl{-}H_4folate}^+ + \mathrm{H_2O} \tag{2.9}$$

$$\begin{aligned} \mathrm{5,10{-}methenyl{-}H_4folate}^+ + \mathrm{H}^+ + 2\,\mathrm{e}^- &\rightleftharpoons \mathrm{5,10{-}methylene{-}H_4folate} \\ \mathrm{NADPH} &\rightleftharpoons \mathrm{NADP}^+ + \mathrm{H}^+ + 2\,\mathrm{e}^- \end{aligned}$$

$$\mathrm{5,10{-}methenyl{-}H_4folate}^+ + \mathrm{NADPH} \overset{\mathrm{MTD}}{\rightleftharpoons} \mathrm{5,10{-}methylene{-}H_4folate} + \mathrm{NADP}^+ \tag{2.10}$$

The last step concerns the conversion of 5,10$-$methylene$-H_4$folate to 5-methyl$-H_4$folate using 5,10$-$methylene$-H_4$folate reductase (MTR). NAD, NADP and Fd_{ox} dependent forms of MTR exist. It remains unclear how this enzyme functions for *C. autoethanogenum*. In the activity experiments performed by Mock et al. [22], non of the three electron donors showed a significant activity on this enzyme. Activity was solely observed using benzyl viologen dyes. According to Mock et al., there are several explanations for the enzyme failing to show activities when purified, but could show these activities when present within the cell. This publication calculated for CO_2 and H_2 grown cells that positive ATP gains are only possible for NAD + Fd specific MTR. This would entail that MTR is electron bifurcating. Other NAD-specific electron bifurcating enzymes have been observed, for example in *Moorella Thermoacetica* [18].

Concluding, it is therefore most likely that MTR is electron bifurgating, performing the reaction as shown in Equation 2.11.

$$\begin{aligned} \mathrm{5,10{-}methylene{-}H_4folate} + 2\,\mathrm{H}^+ + 2\,\mathrm{e}^- &\rightleftharpoons \mathrm{5\text{-}methyl{-}H_4folate} \\ \mathrm{NADH} &\rightleftharpoons \mathrm{NAD}^+ + \mathrm{H}^+ + 2\,\mathrm{e}^- \end{aligned}$$

$$\begin{aligned} \mathrm{Fd_{ox}} + 2\,\mathrm{e}^- &\rightleftharpoons \mathrm{Fd_{red}}^{2-} \\ \mathrm{NADH} &\rightleftharpoons \mathrm{NAD}^+ + \mathrm{H}^+ + 2\,\mathrm{e}^- \end{aligned}$$

overall:

$$\mathrm{5,10{-}methylene{-}H_4folate} + 2\,\mathrm{NADH} + \mathrm{Fd_{ox}} \overset{\mathrm{MTR}}{\rightleftharpoons} \mathrm{5\text{-}methyl{-}H_4folate} + 2\,\mathrm{NAD}^+ + \mathrm{Fd_{red}}^{2-} \tag{2.11}$$

After H_4folate has a CH_3-group attached, it needs to be transferred to Co-enzyme A (CoA) forming acetyl-CoA. This transfer is performed in two steps, as proposed by Ragsdale [21], using the enzymes Methyl-H_4folate:CFeSP methyltransferase (MTS) [EC.2.1.1.258] and Acetyl-CoA synthase

(ACS) [2.3.1.169] (Equation 2.13). In the first step, the MTS enzyme transfers the methyl group from the H_4folate to a corridor protein (Co(I)CFeSP) containing a cobalt group (Equation 2.12). The second step is the key and final step in the WLP. Here, the CO group leaves the corridor protein and is combined with CoA and the methyl group by ACS to form acetylCoA ($CH_3(CO)CoA$). This is presented in Equation 2.13. As mentioned previously, when CO is used as the growth medium, it is directly included into this step. When CO_2 and H_2 are the growth medium, The CODH enzyme converts the CO_2 into CO using Equation 2.5, transferring it towards ACS.

It is proposed that the mechanism of the ACS enzyme works as follows [21]. CO is first bound to the Ni-complex of the ACS enzyme, initiating the carbonylation step. Next, the transmethylation step takes place, where the methyl group coming from the CFeSP-complex binds with the Ni-complex. Thereafter, the CH_3-group binds to the CO group forming an acetyl group, bound to the Ni-complex. Finalising, the acetyl group is transferred from the Ni-complex to CoA, forming AcetylCoA, concluding the Wood-Ljungdahl Pathway. The Ni-complex in the ACS enzyme can consequently be re-used again.

$$\text{5-methyl}-\text{H}_4\text{folate} + \text{Co(I)CFeSP} + \text{H}^+ \overset{\text{MTS}}{\rightleftharpoons} \text{H}_4\text{folate} + \text{methyl}-\text{Co(III)CFeSP}^+ \tag{2.12}$$

$$\text{CO} + \text{CoA} + \text{methyl}-\text{Co(III)CFeSP}^+ \overset{\text{ACS}}{\rightleftharpoons} \text{CH}_3\text{(CO)CoA} + \text{Co(I)CFeSP} + \text{H}^+ \tag{2.13}$$

2.2.2 AcetylCoA reduction

From acetylCoA, three reduction routes are observed. The first route is the reduction of acetate. This acetate can be further reduced to ethanol. The second route is the reduction of acetylCoA to acetaldehyde, which is the intermediate product to form ethanol. The third route is the reduction of acetylCoA to pyruvate, which is the intermediate to eventually form butane-2,3-diol. AcetylCoA can moreover be converted into biomass, since it is a building block to create sugars and genetic material. A fourth route forming lactate is not discussed here, since this compound is sparsely formed under the conditions discussed in this study [22].

The first route starts with the conversion of acetylCoA to acetyl$-\text{P}_i$ via the enzyme phosphate acetyltransferase (PTA) [EC. 2.3.1.8] (Equation 2.14). This is followed by the formation of acetate, where one molecule of ATP is released using the enzyme acetate kinase (ACK) [EC. 2.7.2.1] (Equation 2.15).

$$\text{CH}_3\text{(CO)CoA} + \text{P}_i \overset{\text{PTA}}{\rightleftharpoons} \text{CH}_3\text{(CO)P}_i + \text{CoA} \tag{2.14}$$

$$\text{CH}_3\text{(CO)P}_i + \text{ADP} \overset{\text{ACK}}{\rightleftharpoons} \text{Acetate} + \text{ATP} \tag{2.15}$$

The second route concerns the synthesis of acetaldehyde using the enzyme acetaldehyde dehydrogenase (ADA) [EC. 1.2.1.10] (Equation 2.16). In *C. autoethanogenum*, ADA forms a complex with alcohol dehydrogenase (ADH) and is encoded on the genes CAETHG3747-48. It is still uncertain whether the reduction of acetyl-CoA to acetaldehyde is NAD+ or NADP+ dependent.

$$\begin{aligned} \text{CH}_3\text{(CO)CoA} + 2\,\text{H}^+ + 2\,\text{e}^- &\rightleftharpoons \text{Acetaldehyde} + \text{CoA} \\ \text{NAD(P)H} &\rightleftharpoons \text{NAD(P)}^+ + \text{H}^+ + 2\,\text{e}^- \end{aligned}$$

$$\text{CH}_3\text{(CO)CoA} + \text{NAD(P)H} + \text{H}^+ \overset{\text{ADA}}{\rightleftharpoons} \text{Acetaldehyde} + \text{CoA} + \text{NAD(P)}^+ \tag{2.16}$$

This route is however found to be an unfavoured one in acetogenic bacteria, as this would result in almost all cases in a negative ATP gain [22]. Acetaldehyde can moreover be formed directly from acetate forming one molecule of ATP [29]. This direct reaction is catalyzed by the tungsten containing enzyme aldehyde ferredoxin oxireductase (AOR) [EC 1.2.7.5] and utilises ferredoxin as its electron donor (Equation 2.17).

$$\begin{aligned} \mathrm{Acetate} + 2\,\mathrm{H^+} + 2\,\mathrm{e^-} &\rightleftharpoons \mathrm{Acetaldehyde} + \mathrm{H_2O} \\ {\mathrm{Fd_{red}}}^{2-} &\rightleftharpoons \mathrm{Fd_{ox}} + 2\,\mathrm{e^-} \end{aligned}$$

$$\mathrm{Acetate} + 2\,\mathrm{H^+} + {\mathrm{Fd_{red}}}^{2-} \overset{\mathrm{AOR}}{\rightleftharpoons} \mathrm{Acetaldehyde} + \mathrm{H_2O} + \mathrm{Fd_{ox}} \tag{2.17}$$

From acetaldehyde, ethanol is synthesised using the enzyme alcohol dehydrogenase (ADH) in the ADA-ADH complex. Mock et al. has shown that the reduction of acetaldehyde in *C. autoethanogenum* is mainly NAD+ specific for growth on CO_2 and H_2 [EC: 1.1.1.1] [22]. However, Wang et al. also found a significant specific activity for NADP+ on CO-grown *C. autoethanogenum*. In most literature however, it is assumed that the reaction is NAD+ dependent.

$$\begin{aligned} \mathrm{Acetaldehyde} + 2\,\mathrm{H^+} + 2\,\mathrm{e^-} &\rightleftharpoons \mathrm{Ethanol} \\ \mathrm{NADH} &\rightleftharpoons \mathrm{NAD^+} + \mathrm{H^+} + 2\,\mathrm{e^-} \end{aligned}$$

$$\mathrm{Acetaldehyde} + \mathrm{NADH} + \mathrm{H^+} \overset{\mathrm{ADH}}{\rightleftharpoons} \mathrm{Ethanol} + \mathrm{NAD^+} \tag{2.18}$$

The third route is the synthesis of pyruvate from acetyl-CoA. Pyruvate can be converted into biomass and butane-2,3-diol. Pyruvate is synthesised using the pyruvate ferredoxin oxireductase enzyme (PFOR) [EC. 1.2.7.1] using ${\mathrm{Fd_{red}}}^{2-}$ and one molecule of CO_2 (Equation 2.19). When CO is used as the growth medium, a molecule of CO first needs to be converted into CO_2 by CODH (Equation 2.5) to perform this reaction.

$$\begin{aligned} \mathrm{CH_3(CO)CoA} + \mathrm{CO_2} + 2\,\mathrm{H^+} + 2\,\mathrm{e^-} &\rightleftharpoons \mathrm{Pyruvate} + \mathrm{CoA} \\ {\mathrm{Fd_{red}}}^{2-} &\rightleftharpoons \mathrm{Fd_{ox}} + 2\,\mathrm{e^-} \end{aligned}$$

$$\mathrm{CH_3(CO)CoA} + \mathrm{CO_2} + 2\,\mathrm{H^+} + {\mathrm{Fd_{red}}}^{2-} \overset{\mathrm{PFOR}}{\rightleftharpoons} \mathrm{Pyruvate} + \mathrm{Fd_{ox}} + \mathrm{CoA} \tag{2.19}$$

Pyruvate has a pivotal role in the formation of biomass, since it is the building block for cellular components like carbohydrates, amino acids, fatty acids and nucleotides. The conversion of pyruvate into biomass is discussed in subsection 2.2.3.

To convert pyruvate into butane-2,3-diol, two intermediates are formed. Acetolactate is the first intermediate formed by decarboxylating two molecules of pyruvate using acetolactate synthase (ALsS) [EC. 2.2.1.6], releasing CO_2 in the process (Equation 2.20). Following, acetolactate is converted to acetoin by another decarboxylating step using acetolactatedecarboxylase (ALDC) [EC 4.1.1.5] (Equation 2.21). The last step concerns the reduction of acetoin to butane-2,3-diol.

C. autoethanogenum contains two enzymes to perform this reaction, both butane-2,3- dioldehydrogenase (2,3-BDH) and the recently discovered C. auto alcohol dehydrogenase (CaADH). According to Wang et al., Both NAD and NADP dependend forms of the first enzyme exist, but it remains unknown which form is dominant. Köpke et al. has shown by cloning genes from *C. autoethanogenum* for the butane-2,3-diol pathway into *E.coli*, that CaADH, which is solely NADP

dependent, is capable of performing the same reaction as 2,3-BDH [30]. However, no information about the expressions of both enzymes is present. In conclusion, the reaction of acetoin reduction can be summarised as shown in Equation 2.22. Bioenenergetic calculations performed in this work assume the reaction to be NAD-dependend, as it usually done in literature [31].

$$2\,\text{Pyruvate} \overset{\text{ALsS}}{\rightleftharpoons} \text{Acetolactate} + \text{CO}_2 \tag{2.20}$$

$$\text{Acetolactate} \overset{\text{ALDC}}{\rightleftharpoons} \text{Acetoin} + \text{CO}_2 \tag{2.21}$$

$$\begin{aligned} \text{Acetoin} + 2\,\text{H}^+ + 2\,\text{e}^- &\rightleftharpoons \text{Butane}{-}2,3{-}\text{diol} \\ \text{NAD(P)H} &\rightleftharpoons \text{NAD(P)}^+ + \text{H}^+ + 2\,\text{e}^- \end{aligned}$$

$$\text{Acetoin} + \text{NAD(P)H} + \text{H}^+ \overset{\text{2,3-BDH/CaADH}}{\rightleftharpoons} \text{Butane}{-}2,3{-}\text{diol} + \text{NAD(P)}^+ \tag{2.22}$$

2.2.3 Biomass formation

For *C. autoethanogenum* to reproduce, building blocks for cellular components such as sugars, amino acids, nucleotides and fatty acids need to be formed. Pyruvate has a pivotal role in the formation of biomass, as it is used to form these building blocks. Acetyl-CoA could moreover be used to form these components. However, pyruvate is the major contributor in building cellular components. A set of very elaborate reaction schemes can describe the conversion of pyruvate towards these components, eventually building new copies of *C. autoethanogenum*. These processes all describe conversion requiring ATP [32].

Commonly, the amount of ATP required to form a certain amount of biomass is expressed in mmol ATP per gram dry cell weight (mmol ATP/ gDCW). Unfortunately, no publications are present providing values for *C. autoethanogenum*. However, a literature search of other *Clostridia* species showed values between 42 and 56 mmol ATP/gDCW [33]. In this work, a value of 47 mmol ATP/gDCW is used, approximating the mean.

To take the formation of biomass into account in the carbon balance and modelling of the metabolic pathway, a chemical formula describing biomass for *C. autoethanogenum* is needed. In Norman et al. [34], a complete overview of building blocks making up an average cell of *C. autoethanogenum* is given. Given the percentage of these building blocks being present in an average cell, a chemical formula can be set-up, approaching the average atomic composition of *C. autoethanogenum*. Building blocks, percentages used and calculations performed are presented in Appendix C. Final composition for biomass resulted in $CH_{1.52}N_{0.27}O_{0.46}S_{0.0059}P_{0.042}$, with a molecular weight of M_w = 24.62 g/mol. An attempt was made to verify this formula using elemental analysis of dry biomass from *C. autoethanogenum*. This attempt was however unsuccessful, and results are shown in Appendix E.

2.2.4 Simplified reactions

The reactions described under section 2.2 can be simplified into a set of 8 metabolic and 4 energy conservation reactions. The reactions in Equation 2.23 are the reactions performed by the CODH enzyme, being an equilibrium reaction. Reaction Equation 2.24 is the hydrogen lyase reaction, only performed under CO_2 and H_2 rich conditions. Equation 2.25 is the reaction performed by Hyt/FdhA as in Equation 2.7, only performed under CO_2 and H_2 poor conditions. The reaction shown in Equation 2.26 is the combination of 6 enzymatic reactions (Equation 2.8, Equation 2.9, Equation 2.10, Equation 2.11, Equation 2.12, Equation 2.13) and makes up most of the WLP. The reaction shown in Equation 2.27 is the branch that forms acetate (Equation 2.14, Equation 2.15).

Equation 2.28 shows the conversion of acetate to ethanol (Equation 2.17, Equation 2.18). Note that the pathway of Equation 2.16 is left out due to earlier mentioned reasons. Equation 2.29 concerns the conversion of acetylCoA to pyruvate (Equation 2.19). Equation 2.30 is the pathway from pyruvate to butane-2,3-diol (Equation 2.20, Equation 2.21, Equation 2.22). Reactions part of the energy conservation mechanism cannot be further simplified. Appendix A proves that that all reactions are stoichiometrically correct.

Reaction 1 and -1

$$CO_2 + 2\,H^+ + {Fd_{red}}^{2-} \underset{R_{-1}}{\overset{R_1}{\rightleftharpoons}} CO + H_2O + Fd_{ox} \tag{2.23}$$

Reaction 2a

$$CO_2 + H_2 \xrightarrow{R_2a} HCOOH \tag{2.24}$$

Reaction 2b

$$2\,CO_2 + {Fd_{red}}^{2-} + NADPH + 3\,H^+ \xrightarrow{R_2b} 2\,HCOOH + Fd_{ox} + NADP^+ \tag{2.25}$$

Reaction 3

$$\begin{aligned} HCOOH + ATP + H^+ + NADPH + 2\,NADH + Fd_{ox} + CO + CoA \xrightarrow{R_3} \\ CH_3(CO)CoA + ADP + P_i + H_2O + NADP^+ + 2\,NAD^+ + {Fd_{red}}^{2-} \end{aligned} \tag{2.26}$$

Reaction 4

$$CH_3(CO)CoA + ADP + P_i \xrightarrow{R_4} Acetate + CoA + ATP \tag{2.27}$$

Reaction 5

$$Acetate + 3\,H^+ + NADH + {Fd_{red}}^{2-} \xrightarrow{R_5} Ethanol + NAD^+ + H_2O + Fd_{ox} \tag{2.28}$$

Reaction 6

$$AcetylCoA + CO_2 + 2\,H^+ + {Fd_{red}}^{2-} \xrightarrow{R_6} Pyruvate + Fd_{ox} + CoA \tag{2.29}$$

Reaction 7

$$2\,Pyruvate + NAD(P)H + H^+ \xrightarrow{R_7} Butane{-}2,3{-}diol + NAD(P)^+ + 2\,CO_2 \tag{2.30}$$

Reaction 8

$$Pyruvate \xrightarrow{R_8} Biomass \tag{2.31}$$

Reaction E1

$$2\,H_2 + NADP^+ + Fd_{ox} \underset{E_{-1}}{\overset{E_1}{\rightleftharpoons}} NADPH + {Fd_{red}}^{2-} + 3\,H^+ \tag{2.32}$$

Reaction E2

$${Fd_{red}}^{2-} + NADH + 2\,NADP^+ + H^+ \underset{E_{-2}}{\overset{E_2}{\rightleftharpoons}} Fd_{ox} + NAD^+ + 2\,NADPH \tag{2.33}$$

Reaction E3

$${Fd_{red}}^{2-} + NAD^+ + 2\,H^+_{in} + H^+ \underset{E_{-3}}{\overset{E_3}{\rightleftharpoons}} Fd_{ox} + NADH + 2\,H^+_{out} \tag{2.34}$$

Reaction E4

$$ADP + P_i + 3.66\,H^+_{out} \underset{E_{-4}}{\overset{E_4}{\rightleftharpoons}} ATP + H_2O + 3.66\,H^+_{in} \tag{2.35}$$

Reaction	$NADP^+$	NAD^+	Fd^{2-}_{red}	Fd_{ox}	ATP	ADP	H^+	net ATP formed
$4\ CO + 2\ H_2O \rightarrow CH_3COOH + 2CO_2$	1.5	2	4	0.5	1	1	5.5	1.5
$6\ CO + 3\ H_2O \rightarrow CH_3CH_2OH + 4CO_2$	1.5	3	6	1.5	1	1	7.5	2.1
$11\ CO + 5\ H2O \rightarrow C_4H_{10}O_2 + 7CO_2$	3	5	11	3	0	2	13	1.6

Table 2.1: Stoichiometric reactions for acetic acid, ethanol and butane-2,3-diol production from CO. Formed metabolites, net proton consumption and net ATP gain per mole product.

2.2.5 Interaction catabolism and anabolsim

For every system where chemical reactions take place, the rule of 'in = out' holds. The reagents used for *C. autoethanogenum* are converted into acetate, ethanol, butane-2,3-diol and biomass. The stoichiometric ratios can be determined by experimental work and are shown for CO in Table 2.1 [23]. Based on the reaction scheme as described in section 2.2, one can work out the total amount of electron donors/ acceptors and energy carriers used to produce a certain reaction product. The energy conservation reactions are responsible for re-generating energy carriers. The production of reactants and the regeneration of energy carriers lead to a net decrease in proton concentration in the bacteria. To maintain the proton gradient over the inner-membrane of the bacteria, ATPase pumps these protons over the inner membrane space producing ATP. ATP is thereafter used for cell maintenance and cell-division [20].

Figure 2.3 shows a schematic representation of the behaviour of the energy conservation mechanism for the production of acetate. According to the reaction scheme, production of one mole of acetic acid from CO yields 1.5 mole of NADP+, 2 moles of NAD+, 4 moles of $Fd_{red}{}^{2-}$, 0.5 mole of Fd_{ox}, 1 mole of ATP and 1 mole of ADP. The Nfn, Hyt, and Rnf enzymes are able to convert these compounds to their redox couples according to the reaction as described in subsection 2.1.2. Total proton loss after this process is 5.5 mole H^+/ mol acetate. To restore the proton gradient over the membrane, ATPase pumps 5.5 mole H^+ back into the cytoplasm, producing net 1.5 mole ATP per mole of produced acetate.

In, Table 2.1, an overview of all produced energy compounds, net proton loss and ATP yield for acetate, ethanol and butane-2,3-diol are shown. Similar calculations as for acetate were performed for ethanol and butane-2,3-diol. Schematic representations of the bioenergetics for the production of these compounds are shown in Appendix B. This work uses the ATP yields and metabolic system as presented in further analyses.

ATP yield per mol consumed CO is highest for the production of acetic acid. It is therefore expected that this is the preferred product for *C. autoethanogenum*. However, several factors have an influence on the availability of energy carriers thus product selectivity of *C. autoethanogenum*. This in turn has an effect on pH in and outside the cell and redox potential inside the cell. These effects can lead to an increase or decrease in the proton gradient, changing activities of Rnf and ATPase, furthermore affecting product selectivity. Intracellular CO concentrations and rate of the different enzymes affects the concentrations of energy carriers, thus changing the redox potential and pH. In addition, both substrates and reaction products can have an inhibiting effect on *C. autoethanogenum*, affecting the product selectivity [35] [36]. Bacterial growth rate moreover has an effect on product selectivity, as the production of biomass requires the use of certain redox compounds [1]. Summarised, numrous factors can have an influence on the final product selectivity.

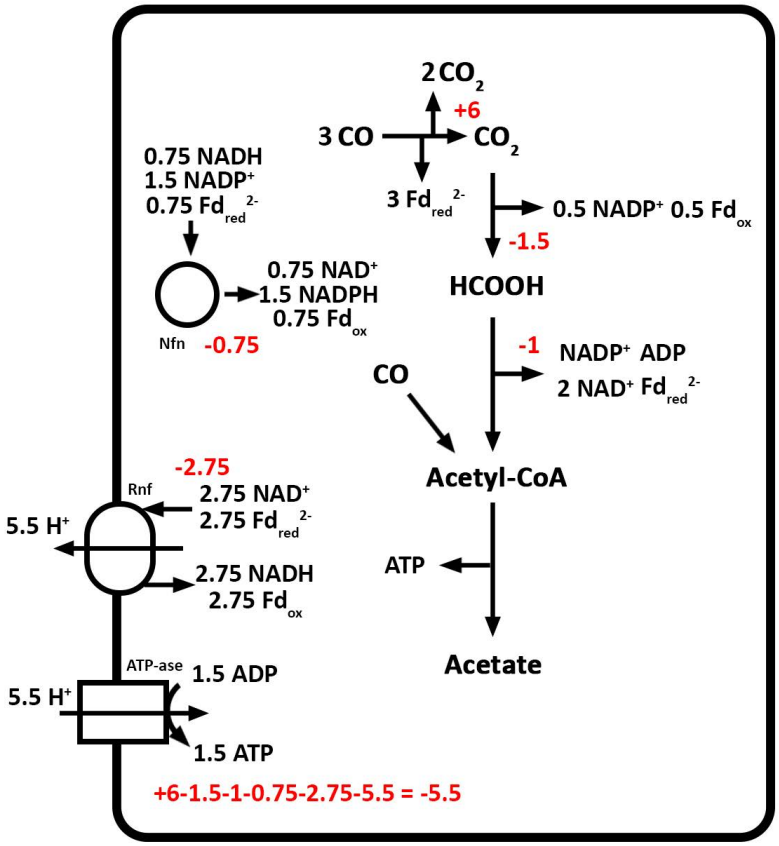

Figure 2.3: Bioenergetics of acetate formation from CO in *C. autoethanogenum* following $4\,CO + 2\,H_2O \longrightarrow CH_3COOH + 2\,CO_2$. The electron bifurcating HytA-E/FdhA complex reduces Fd, $NADP^+$, and CO_2. The Nfn complex is transferring electrons beteen Fd, NADH and NADPH. Excess $Fd_{red}{}^{2-}$ is oxidised by the Rnf complex, which reduces NAD^+, building up a H^+ gradient. This gradient drives ATP synthesis via the H+ dependent ATP synthase. Red numbers denote the production, consumption or transfer of protons.

2.3 Culturing microbes in bioreactors

In order to control the growth of microbes in bioreactors, the principles of bacterial growth are discussed. A bacterial culture can grow by performing cell division, driven by the metabolism of the bacteria. The created cells have a limited lifespan. The growth cycle of a bacterial cell can be divided into four phases which are respectively the lag-, exponential-, stationary- and death phase [20].

The lag phase starts when a microbe is inoculated into fresh growth medium. This growth medium consists of various nutrients the bacteria needs to start operating and sustaining its metabolism (vitamins, minerals, etc.). This phase is therefore used to construct enzymes and metabolites for the metabolism to operate. After this phase, cell division starts and the population doubles at regular intervals, entering the exponential phase. The bacterial cell is in its healthiest state during this phase. In a batch culture, the exponential phase is finite due to a lack of essential nutrients needed to continue cell maintenance and division. Moreover, produced components may inhibit further cell division. The stationary phase therefore entails a state where the metabolism operates at a reduced rate. Eventually, depletion of nutrients cause the culture to enter the death phase.

However, viable cells are able to re-enter the lag phase when re-exposed to nutrients can remain in the culture up to years [20].

To sustain a bacterial colony that is able to perform continuous production, both stationary and death phase should be omitted. This is possible when fresh nutrients and gas substrates are continuously provided to the bacteria. Additionally, medium has to be removed at the same rate to remain a constant liquid volume. The culture is said to be continuous if the culture volume, concentrations of products and cell density remain in equilibrium while being in the exponential phase.

Performing such processes in reactors requires regulation of in-flowing fresh medium and out-flowing reactor medium. This is described using the dilution rate (D), where $D = F/V_L$. In this equation, F is the volumetric flow rate of fresh and used medium entering and leaving the reactor. V_L is the total volume of the liquid present in the reactor. To achieve a steady state situation where the bacterial concentration is constant over time, dilution should be in equilibrium with the growth rate of the bacterial colony. The effects of the dilution rate on the specific growth rate and limiting nutrient is schematically shown in Figure 2.4. This figure shows that a viable range of dilution rates will result in a constant bacterial concentration. Here, the growth rate adjusts to the dilution rate. Too high dilution rates will result in a non-constant bacterial concentration as the colony cannot balance dilution with growth. This is commonly referred to as washout.

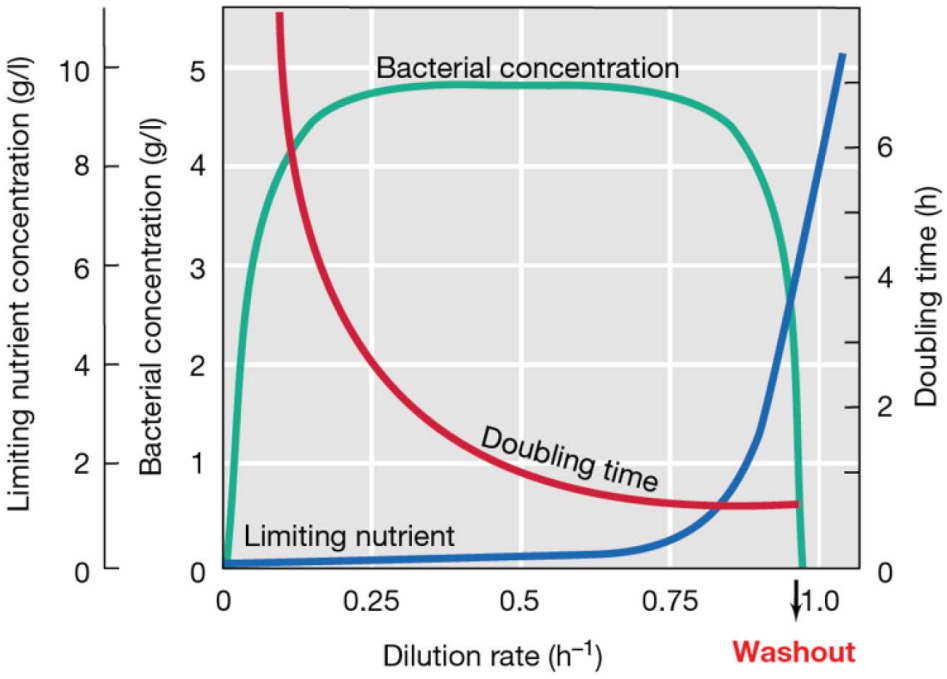

Figure 2.4: Effects of dilution rate on bacterial concentration and limiting nutrient. Both factors are observed to be constant during steady state. Although, doubling time varies as dilution rate increases. High values for D result in a washout of the colony.

2.4 Mass transfer in bioreactors

Next to continuous addition of fresh nutrients, gaseous substrates need to be dissolved in the bacterial medium for the microorganism to take up these substrates [37]. A low concentration of soluble gases in the bacterial medium (aqueous phases) result in a low maximum achievable cell

density, thus productivity. The gaseous substrates for *C. autoethanogenum* concern H_2, CO and CO_2 of which the first two in particular exhibit a low solubility [38]. Figure 2.5 shows a schematic representation of the mass transfer present in bacterial fermentation. The blue arrow depicts the mass transfer of gaseous substrates into the liquid phase. When dissolved in the liquid phase, the gaseous substrates need to be transferred through the bacterial cell wall. This is depicted by the red arrows. In the bacteria, gas substrates are converted into the products and biomass as described in section section 2.2. This figure shows that limitations in gas to liquid mass transfer affect the productivity of the fermentation process.

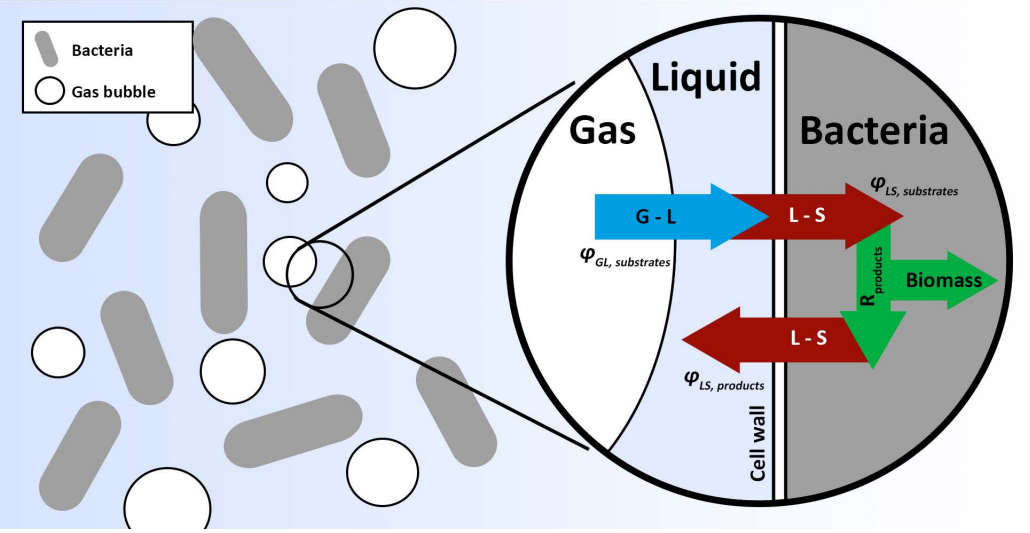

Figure 2.5: Overview of the different mass transfer steps in a gas-liquid-bacteria system. The blue arrow denotes the gas liquid mass transfer. Red arrows represent the mass transfer of both gas substrates and reaction products between the liquid phase and bacteria. Green arrows represent the conversion of gas substrates into reaction products or biomass

In order to quantify mass transfer of gaseous substrates and reaction products, a general mole balance is used (Equation 2.36). Here, m represents the component and n represents the phase (gas, liquid or bacteria) the component is in.

$$\frac{dN_{n,m}}{dt} = V_n \cdot \frac{dC_{n,m}}{dt} \tag{2.36}$$

In this section, mole balances for any substrate in the different phases are described for a continuous fermentation process with continuous gas in- and outflow. Complete derivations and descriptions of all variables are provided in Appendix F. To start, gaseous substrates are fed. For microorganisms to take-up these substrates, these need to be dissolved in the aqueous phase. A mole balance for gaseous components in continuous fermentation with continuous gas-flow is given in Equation 2.37

$$\frac{dC_{G,m}}{dt} = \frac{\phi_{G,in} P_0 y_{m,0}}{RTV_G} - \frac{\phi_G P y_m}{RTV_G} - k_L a_{GL}(PH_m - C_{L,m}) \tag{2.37}$$

In this equation, $k_L a_{GL}$ represents the gas-liquid volumetric mass transfer coefficient. This variable describes the hydrodynamic conditions at which mass is transferred from the gas phase towards the liquid phase. Attempts that are made to improve mass transfer consequently result in an increase of $k_L a_{GL}$.

As shown in Figure 2.5, the next step concerns the dissolved gas to be taken up by the bacteria. Equation 2.38 describes the concentration of both gaseous substrates and reaction products in the liquid phase. For gases, this concentration is dependent on the gas to liquid mass transfer rate, solubility of the gases and the rate at which the microorganisms consume the gases. The latter is described as mass transfer from the liquid phase into the micro-organism. For reaction products, the liquid concentration is only dependent on the mass transfer from the liquid to the bacterial phase. Mass transfer in and out of a bacteria is dependent on four factors: the permeability of component m through the bacterial cell wall (p_m) and the partition coefficient ($K_{p.m}$). Next, the total cellular surface area (A_{cell}) over the bacterial cell's volume (V_{cell}) determine the total surface area over which mass transfer can be performed. Mass transfer per unit of volume is moreover determined by the total bacterial concentration X. In the following equations, the concentrations of species m in the bacterial phase is indicated using 'B'.

$$\frac{dC_{L,m}}{dt} = k_L a_{GL} \frac{\epsilon_G}{\epsilon_L}(PH_m - C_{L,m}) - \frac{p_m}{K_{p,m}} \frac{A_{cell}}{V_{cell}} \left(\frac{C_{L,m}}{m_{LB}} - C_{B,m} \right) \frac{X}{\rho_b} - C_{L,m} D \tag{2.38}$$

C. autoethanogenum has a semi-permeable cell wall, consisting out of two membranes separated by the inner-membrane space or periplasm (Figure 2.1). Components need to pass both layers in order to enter or leave the environment where the metabolic reactions are performed. Concentrations of components in the bacteria are described by Equation 2.39. The concentration of species in the bacterial phase is both dependent on the mass transfer rate from the liquid phase into the bacteria and the rates of the performed reactions component m is involved in.

$$\frac{dC_{B,m}}{dt} = \frac{p_m}{K_{p,m}} \frac{A_{cell}}{V_{cell}} \left(\frac{C_{L,m}}{m_{LB}} - C_{B,m} \right) - \frac{\rho_B}{X V_L} \sum R_m \tag{2.39}$$

A mole balance describing the size of the bacterial phase is required, since this is a variable factor. The bacterial concentration (X) is determined both by the reactions inside the bacteria, eventually forming new biomass, and the death rate of the bacteria. As fresh medium is added and used medium containing bacteria is removed, the dilution rate should moreover be included in the mole balance.

$$\frac{dX}{dt} = \sum R_{biomass} - R_{death} - X * D \tag{2.40}$$

Using these mole balances and appropriate reaction expressions, a system performing a continuous fermentation process with continuous gasflow for *C. autoethanogenum* can be described.

2.5 Spinning Disk reactor

Currently, poor gas to liquid mass transfer is the main reason imposing limitations for bacterial syngas fermentation to be economically viable [39]. The rotor stator spinning disk reactor (rs-SDR) is a multiphase reactor capable of reaching high gas to liquid mass transfer rates [13]. The reactor consists out of one or multiple rotating discs, called rotors, enclosed in a housing, called the stator. Figure 2.6 shows a schematic representation of a rs-SDR containing only one rotor. The reaction mixture flows in at the top and leaves the reactor at the bottom. Due to rotation of the disk(s), high shear forces are created. rs-SDRs are capable of reaching rotational speeds up to a 4000 RPM. In a multiphase reaction condition, these forces result in the breaking-up of gas bubbles, causing the overall gas-liquid interfacial area a_{GL} to increase, leading to overall higher mass transfer rates [14] [15].

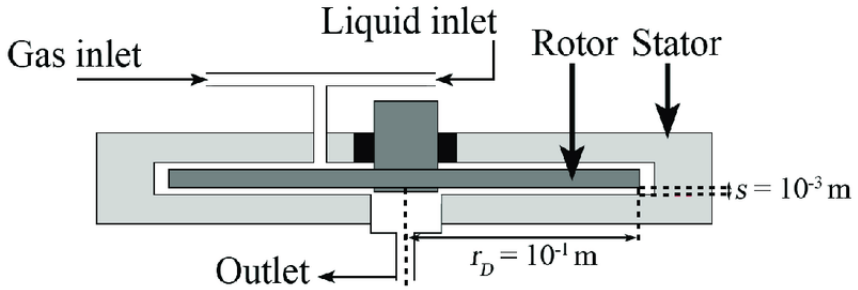

Figure 2.6: Schematic representation of a rotor stator spinning disk reactor with one rotor

Hydrodynamics generated by the rotation of the discs are governed by the rotational Reynolds number (Re_ω) and the aspect ratio of the cavity (G). Definitions of these variables are shown in equation Equation 2.41 and Equation 2.42 [14].

$$Re_\omega = \frac{\omega \cdot r_d^2}{\nu} \tag{2.41}$$

$$G = \frac{s}{r_d} \tag{2.42}$$

Here, ω describes the rotational speed, r_d describes the outer radius of the rotor and ν is the kinematic viscosity of the reaction mixture [40]. s is the gap distance between the housing and the rotor. Different flow regimes are observed in a rs-SDR as a function of Re_ω and G. An overview is depicted in Figure 2.7. The value for G is constant in a spinning disk reactor, indicating that flow regime is solely dependent on the value of Re_ω. The red line shown in Figure 2.7 indicates the working range of the rs-SDR used in this work. Following this red line towards higher values of Re_ω shows different hydrodynamic behaviour inside the reactor as a function of increasing values of ω. This inherently results in different mass transfer rates [13].

For economic reasons, it is important to consider the energy input needed to operate the reactor. The rotational speed ω of the disks is directly correlated with the required energy input. The value of the torque τ of the motor powering the rs-SDR is proportional to the energy dissipation rate as shown in Equation 2.43. Here, V_R is the reactor volume.

$$E_d = \frac{\tau \cdot \omega}{V_R} \tag{2.43}$$

Increasing rotational speed of the disk will lead to an increase energy dissipation rate. Consequently, increasing mass transfer requires higher energy input.

Figure 2.8 shows a comparison of the rs-SDR with other reactors. The range of achievable volumetric mass transfer coefficients as a function of required energy dissipation is presented. Current fermentation processes are limited to stirred tank reactors and bubble columns. Comparing these reactor configurations with the rs-SDR gives several insights.

First, the rs-SDR is capable of achieving one order of magnitude higher values for the mass transfer coefficient. Therefore, utilising the rs-SDR for bacterial fermentation processes could lead to significant intensification. Second, required energy input needed to operate the rs-SDR increases up to 3 orders of magnitude. The question therefore remains whether the benefits of the increase

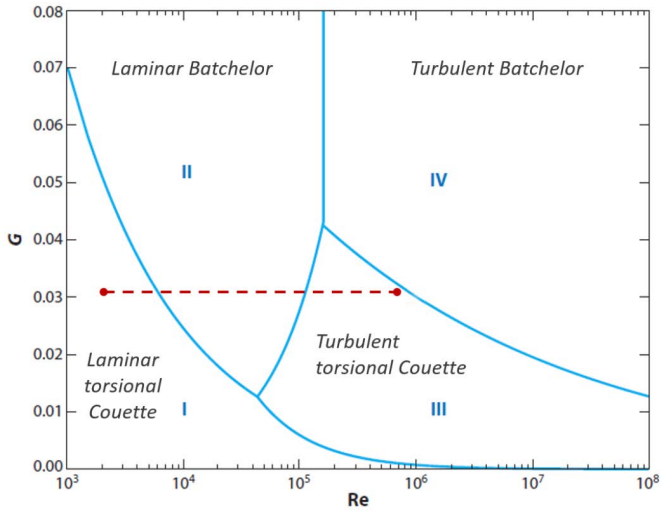

Figure 2.7: Different flow regimes in spinning disc reactors as function of rotational Reynolds number and the ratio of the cavity. The red line indicates the working range of the spinning disc reactor as used in this project.

in mass transfer in relation to the increase in cost due to higher energy use will yield economically viable fermentation processes. Nevertheless, many gas-to-liquid mass transfer limited processes have shown to potentially become more economically viable when the rs-SDR is used instead of traditional equipment [13].

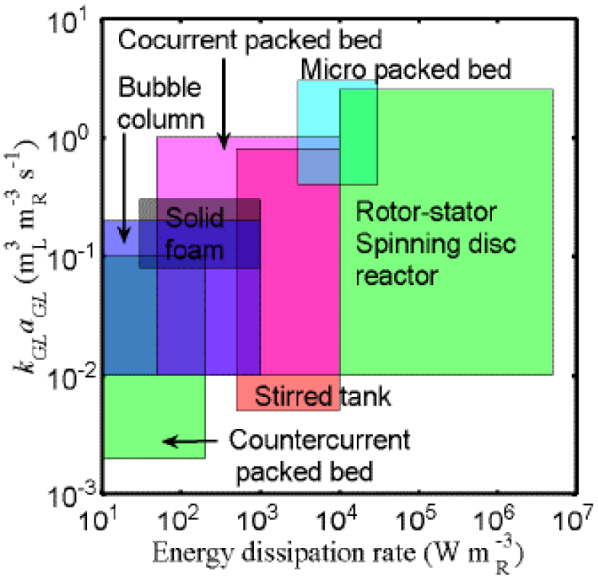

Figure 2.8: Comparison range of volumetric mass transfer coefficients and energy dissipation rates for different reactor configurations.

3. Method

This study performed three types of experiments to gain insight in enhancing productivity in continuous syngas fermentation. Fed-batch culturing was performed using glass cultivation bottles. These cultures were used for continuous fermentation experiments using a stirred vessel and a rs-SDR. The aim of each type of experiment is elaborated upon in its corresponding chapter. Furthermore, bacterial medium composition, experimental analyses and quantification techniques are discussed. At last, an attempt to model the metabolic pathway of *C. autoethanogenum* is presented.

3.1 Bacterial strain and growth conditions

Clostridium autoethanogenum was acquired from a derivative of DSM 10061, obtained from the DSMZ strain collection (Braunschweig, Germany). *C. autoethanogenum* was cultivated anearobically at 37 °C in a medium designed by Wageningen University and Research, The Netherlands, containing (per liter of medium): 0.4 g KH_2PO_4, 0.53 g $Na_2HPO_4 \cdot 2\,H_2O$, 0.3 g NH_4Cl, 0.3 g NaCl, 0.1 g $MgCl_2 \cdot 6\,H_2O$, 0.01 g $CaCl_2 \cdot 2\,H_2O$ and 0.5 mg resazurin. The medium was supplemented with the following trace-elements (per liter of medium): 1.8 mg HCl, 0.062 mg H_3BO_3, 0.061 mg $MnCl_2$, 0.944 mg $FeCl_2$, 0.065 mg $CoCl_2$, 0.013 $NiCl_2$, 0.067 $ZnCl_2$, 0.013 mg$CuCl_2$, 0.4 mg NaOH, 0.0173 mg Na_2SeO_3, 0.0294 mg Na_2WO_4, 0.0205 mg Na_2MoO_4. The medium was autoclaved using a pressure cooker, bringing total pressure up to 200 kPa and temperature of 133 °C. This was performed using 575 mL cultivation bottles capped with rubber stoppers and aluminium caps for 1.5 hours. When cooled down, 0.09 volume percent of a vitamin mixture was added containing (per liter vitamin mixture): 20 mg biotin, 200 mg nicotinamid, 100 mg p-aminobenzoic acid, 200 mg thiamin, 100 mg panthotenic acid, 500 mg pyridoxamine, 100 mg cyanocobalamine and 100 mg riboflavine. Cultivation was performed with 1 g yeast extract and 1 g tryptone per liter. Per liter, 3.88 g $NaHCO_3$ was added, acting as buffer. Per liter, 0.5 mg L-cysteine HCl and 0.235 mg $Na_2S \cdot 9\,H_2O$ were added acting as reducing agents. Unless stated otherwise, pH was set to 5.75 using NaOH or HCl. All notions of 'medium' in this study refer to this described mixture. Cultures were grown in the presence of 20mM acetate. Headspace of the bottles was refreshed by removing the gas in the headspace using a vacuum pump and adding the desired gas for a total of 5 times to maximise oxygen removal. *C. autoethanogenum* was grown with 180 kPa CO as sole substrate. Cultivation was done using a shaker at slow speed and constant temperature of 37 °C.

The culture was maintained by addition of NaOH or HCl to keep the pH close to the optimum growth value of 5.75. In addition, the headspace was refreshed regularly using CO when pressure decrease was observed. For longer fermentation times, part of the medium was replaced by fresh medium to ensure the presence of sufficient nutrients.

3.1.1 Experimental Analysis and quantification

Acetic acid and ethanol concentrations were analysed using high pressure liquid chromatography (HPLC) by Shimadzu of the type UFLC XR containing a LC-20AD pump, SIL-20A sampler and CTO-20AC oven, equipped with a Shimadzu Shim-pack GIST C:18 column. Measurements were performed using a Waters 2414 refractive index detector. The column operated at a temperature of 60 °C with 0.01 M H_3PO_4 eluent at a flow rate of 0.5 mL/min. Injected sample volume was 5 μL. Butane-2,3-diol concentrations were analysed via Gas Chromatography Mass Spectrometry (GCMS) by Shimadzu (GCMS QP2010) equiped with an Agilent JW DB-200 column (length: 30m, diameter: 0.25mm, film thickness: 0.50 μm). The column was operated at 50 °C at 65.7 kPa, using He as a carrier gas.

Bacterial concentration was quantified using a UV-2501PC UV-VIS, measuring optical density at 600 nm using dH_2O as reference sample. Samples were measured using 1 mL disposable cuvettes with a path length of 10 mm. A correlation between optical density and grams of dry

cellular weight per liter of medium was obtained (gDCW/L). Experimental results and procedure performed to obtain this correlation is described in Appendix D. pH measurements were performed using 3 mL samples with a 662-1382 probe and pH_2O control box by Consort. Microscopic analyses were performed with a Zeiss observer.D1m microscope with a magnification 1000x for the eye. The camera lens used a magnification of 67x. Microscope samples were prepared by placing a sample droplet in between two glass slides. A 10 minutes settling time was used before taking a picture

3.2 Fed-batch culturing

As a starting point, *C. autoethanogenum* was cultured in anearobic glass bottles with a total volume of 565 mL as described in section 3.1. To monitor performance, analysis was performed at regular intervals. This included headspace pressure measurements, pH measurements and optical density measurements to monitor CO consumption and production.

Cultures were created in two different cultivation bottles with varying gas and liquid holdups. The bottles were measured two times a day in order to monitor the activity of the bacteria for a time period of 10 days. Pressure, pH, optical density and HPLC measurements were conducted. No refreshment of the headspace or pH adjustments were made. After every sample, fresh medium was added with the same volume as the sample taken. Productivity and product selectivity for growth on CO was monitored as a function of gas holdup. Based on the obtained data, an attempt was made to close the carbon balance.

3.3 Continuous fermentation in stirred vessel

Next, continuous fermentation using a stirred vessel was performed. The aim of the experiments were to gain insight in the effects of elevated pressures on enhancing mass transfer to increase biomass and product concentrations. Preferably, continuous fermentation at steady state conditions is reached to accurately quantify differences in experimental outcome. The used set-up was able to continuously control and monitor the process and included in-line pH and Gas Chromatograph measurement equipment. In addition, a refreshment system is included, pumping fresh medium into, and excess medium out of the system, realising continuous fermentation.

3.3.1 Set-up description

Figure 3.1 shows the process flow diagram (PFD) of the used set-up. An enlarged version of the PFD P&ID of the set-up is provided in Appendix J and Appendix K. Numbers in the text correspond with the shown PFD.

The reactor set-up consists of a double loop system. The first loop is the reaction loop (stream 1 to 4) and contains an autoclave reactor with a volume of 2.6L. The reactor is equipped with a flat disk agitator, containing a pressure sensor and is heated by an electrical heating jacket. The autoclave can be heated up to a temperature of 150 °C. Reaction mixture is pumped out of the reactor using a Gather gear pump having a maximum throughput of 500 mL/min. Exact flow rate was monitored using a mini CORI-FLOW M12V14I by Bronckhorst. Gas enters the loop via a three-way connection (stream 3). Here, CO, CO_2, H_2 and N_2 can be fed separately. For the first three gasses, flow rates could be inserted up to a maximum op 20 mL/min each via a Bronckhorst mass flow controler. The multiphase flow re-enters the autoclave reactor after circa 1.5m of tubing, enhancing gas-liquid mass transfer. This concludes the reaction loop (stream 4). Tubing of the reaction loop is equipped with heat tracing, maintaining the set conditions of the process. Reactor pressure was regulated using a back pressure regulator (stream 15). Head space gas composition was monitored using an inline compact gas chromatograph (GC) of Interscience

(stream 16). Excess gas could be vented using stream 17 and 18.

The second loop in the set-up is the analysis and dilution loop, connected to the stirred vessel via stream 5 and 10. The analysis loop is connected to the reaction loop via 5 and 6. Stream 7 enters a 600 mL vessel, containing pressure and pH sensors. The pH probe used was a SP28X of Consort, coupled to a pH/ORP 350 control box. Furthermore, the vessel contains a sample port for offline measurements of liquid composition (stream 11). At last, dilution was controlled and connected via streams 12 and 13. Via stream 12, inflow of fresh medium in 2 L bottles was controlled using a HPLC pump of the type 101U/Shimadzu 10 AT. Outflow of medium was regulated via stream 13 using a peristaltic pump by Watson Marlow (type 101U), collecting the used medium in 2 L bottles. Depending on the dilution rate, bottles containing fresh and used medium needed to be replaced regularly. Both pumps required to operate at equal speed. In this way, an equilibrium is achieved between the addition of fresh medium and removal of excessive medium, keeping overall liquid volume constant. At last, liquid is pumped out of the reactor vessel using a Knauer HPLC pump. The mixture is able to re-enter the autoclave via stream 10.

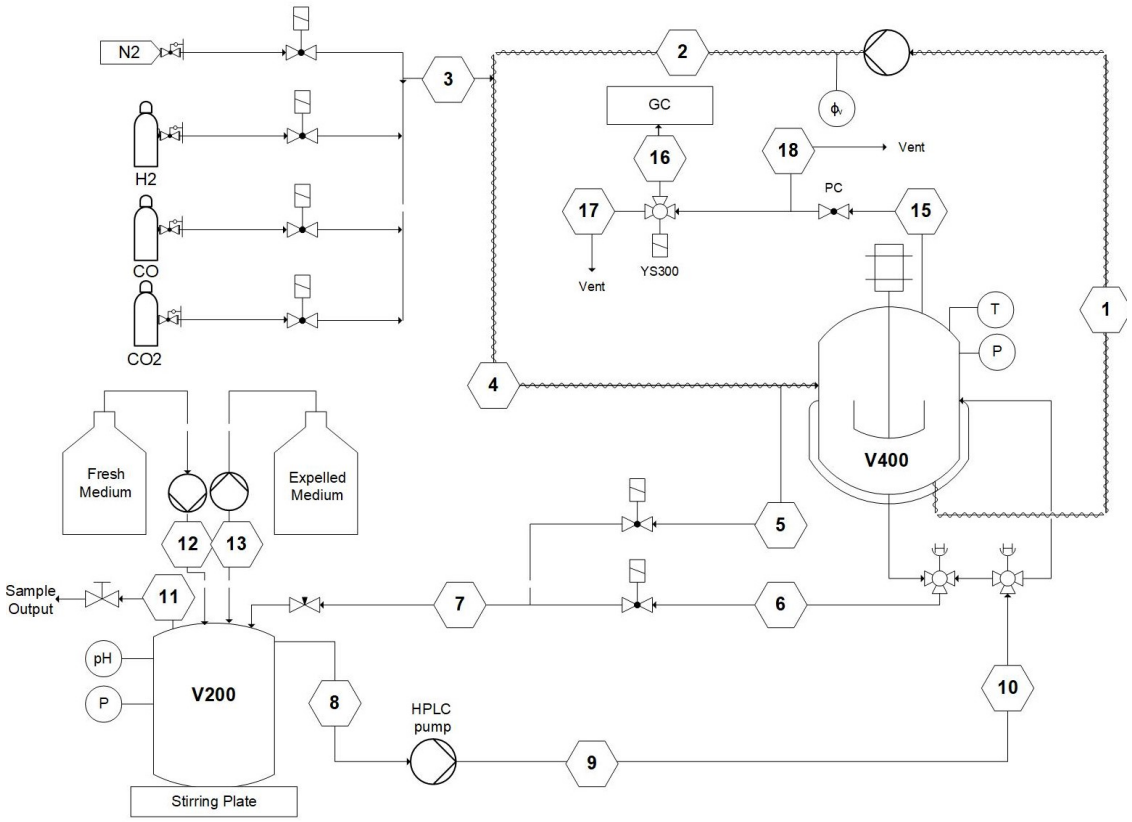

Figure 3.1: Schematic process flow diagram of the continuous stirred vessel reactor set-up

3.3.2 Experimental procedure

The set-up was initially cleaned flushing a 20 vol% H_2O_2 solution. Thereafter, the system was cleaned with multiple cycles of dH_2O and flushed with N_2 to ensure complete oxygen removal. Fresh medium as described in section 3.1 excluding vitamins, yeast extract, tryptone and reducing agents, was added and autoclaved at 121 °C for 1.5 hours. When cooled down to 37 °C, vitamins, yeast extract, tryptone and reducing agents were added. Thereafter, the set-up was flushed with the desired gaseous substrate (CO).

For the experiment performed, V_L^0 was 700 mL. 10 vol% of *C. autoethanogenum* cultivated in bottles was added with a biomass concentration of 0.136 gDCW/L. pH was set to 5.50. Initial acetic acid and ethanol concentrations in the reaction mixture were 29 mM and 5.9 mM respectively. Headspace was filled with 200 kPa CO.

Further cultivation of bacteria in the set-up was performed in the autoclave. This was done in a stagnant way, with a fixed headspace of CO, without the stirrer and pump operating. This was done to prevent built-up of excess intracellular $Fd_{red}{}^{2-}$. After growth was observed to 0.126 gDCW/L, continuous gas flow of CO was initiated with 5 ml/min, maintaining a pressure of 200 kPa. pH of the reaction mixture was adjusted daily, aiming to remain at a constant value of pH = 5.75. In addition, the pump of the reaction loop was started with a flow rate 100 ml/min, ensuring a multiphase flow, enhancing mass transfer. Agitation of the stirrer in the autoclave was kept off. After further growth, gas flow was set to 10 ml/min. Dilution was set to 300 mL/ day ($D = 0.42$) when steady state was reached. Steady state like behaviour was maintained for approximately four residence times (8 days) at 200 kPa.

Following, pressure was gradually increased with 6.25 kPa/h. After 48h, a pressure of 500 kPa was reached inside the autoclave. At this stage, gas flow rate for CO was increased to 20 mL/min. Dilution of the system was continued throughout and after the pressure increase. Reaction conditions at 500 kPa were maintained for a total of 7 days, reaching steady state-like behaviour. Liquid concentrations remained within 10% deviation for 4 days after which the experiment was terminated unexpectedly.

In total, the experiment ran for 28 days (666 hours). HPLC and GC samples were taken two times a day. pH measurement and adjustments were performed at least twice a day. Bacterial concentration was moreover measured twice a day using the UV-2501PC UV-VIS equipment. At last, in- and outflow rates of the refreshment system were monitored twice a day. Unfortunately, inflow of fresh medium was found to be consistently higher than outflow.

3.4 Fermentation in the spinning disk

Fermentation experiments were performed using a single stage rotor stator spinning disk reactor. The used set-up was able to induce a continuous liquid and gas flow. Furthermore, a refreshment system provided the opportunity to impose dilution and achieve continuous fermentation. The aim of the experiments was to monitor whether increasing mass transfer by varying rotation speed of the rs-SDR would lead to higher bacterial and product concentrations. The effect of high shear forces imposed by the rs-SDR on the bacteria was moreover investigated.

3.4.1 Set-up description

Figure 3.2 shows the process flow diagram of the used set-up. An enlarged version of the PFD can is provided in Appendix L. The reactor system consists of a loop including a rs-SDR (stream 1-7) and a bypass. Reaction vessel V400, with a volume of 600 mL, is placed in a water bath, heated using a heating and stirring plate. Using a thermometer, temperature of the mixture could be monitored and heating could be adjusted. Reaction mixture is pumped from V400 using a Cole Parmer Masterflex L/S peristaltic pump. After stream 2, a three-way valve is encountered. Via stream 3, the reaction mixture flows to the rs-SDR. Stream 6 is used to bypass the rs-SDR. CO and N_2 enters via stream 9. A pressure burst plate is in place as a safety measure. The multiphase mixture in stream 4 enters the rs-SDR from the top-side of the reactor. The mixture leaves the reactor at the bottom (stream 5) and re-enters V400 via stream 7. Excess gas can leave the system via stream 10, entering a three way valve. Via stream 11, gas samples can be taken for GC measurements. Gas leaves the system via stream 12. A refreshment system is in place

using two syringe pumps, ensuring the possibility to create continuous fermentation. Via stream 8, fresh medium can be added to the system. Via stream 13, excess medium can be removed.

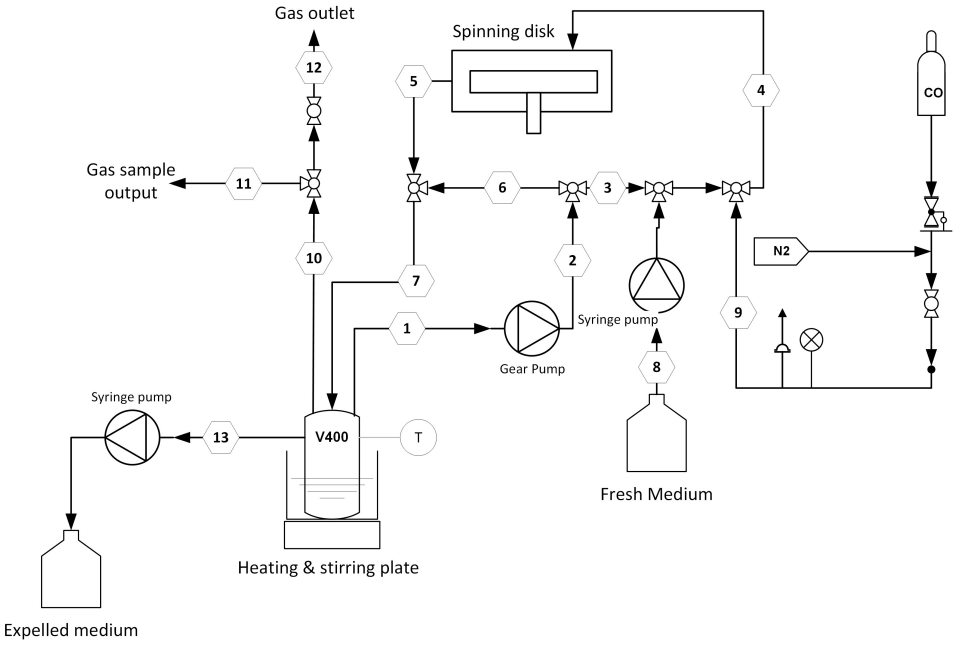

Figure 3.2: Schematic process flow diagram of the spinning disk reactor set-up

3.4.2 Experimental procedure

The set-up was cleaned by flushing a 20 vol% H_2O_2 solution. Thereafter, the system was cleaned with multiple cycles of dH_2O and flushed with N_2. The system was heated to 37 °C after which the dH_2O was removed. Thereafter, the system was flushed using CO to ensure complete oxygen removal. Next, an active bacterial colony cultivated in bottles was added. Liquid volumes were between 230-250 mL. Continuous CO flow was induced with flow rates between 17-7 mL/min. Liquid flow-rate was set to 141 mL/min.

Experiments were performed with rotational speeds of 100 RPM, 500 RPM and 1000 RPM. Analysis of the mixture was performed using offline equipment. 5 mL samples were taken on a daily basis, measuring pH and product composition using HPLC and UV-VIS. Fresh medium was added in equal volumes as the sample size. The bacterial colony was studied under the microscope, before and after every experiment. The effect of increased shear forces on the bacteria was investigated by analyzing shape and size using microscopical images and a MATLAB script. See Appendix O for the used MATLAB script.

3.5 Metabolic Pathway modelling

In addition to the experimental work, an attempt was made to model the metabolic system of *C. autoethanogenum*. A simplified but predictive model can eventually result in further understanding on the effects of process parameters on productivity and selectivity. Bacterial cells however contain many thousands of different interacting components, making it extremely hard to take all interactions into account. Many efforts have been made to create predictive models of microbes and *C. autoethanogenum* in particular. Dynamic Flux Balance Analasys (DFBA) is a dynamic simulation framework often used to model biochemical processes [41]. The essential information required to construct a stoichiometric model is a list of participating biochemical species (metabolites), a list

of the relevant intracellular reactions involving these species, and the stoichiometric coefficients for every species in each reaction. This method is often combined with genome-scale modeling, where chemical reactions are obtained by analysing the genome of the microbe in question [42]. This often results in a set of over a thousand reactions. To ensure a valid outcome, certain optimisations and end-conditions need to be set. Genome-scale DFBA has shown to achieve realistic results for numerous microbes, including *C. autoethanogenum*, giving insight to steer selectivity and productivity to increase production value [34]. However, a downside to this method is the need for optimisation and end-conditions.

For this work, a much more simplified approach is taken. In subsection 2.2.4, an overview of the simplified reactions making up the metabolsim of *C. autoethanogenum* are provided. Mole balances for all components active in these reactions were obtained and are shown in Appendix G. These differential equations all contain reaction rates in the bacterial phase, in which the component is either used as a substrate or formed as an intermediate or product. A total of 15 reaction terms are set-up and included in these differential equations. Since all reaction terms concern one, or a set of enzymatic reactions, kinetics are governed by several factors. Often, enzymatic kinetics are described by Michaelis Menten kinetics, taking into account the catalytic properties of enzymes. For this work however, a more simplified approach using mass action kinetics in combination with several assumptions was used. In Appendix H, an overview of all factors and assumptions leading to the obtained reaction terms are described. Final reaction rate expressions are presented in Appendix I. All reaction rate constants are assumed, since no experimental or kinetic data was obtained yet. Differential equations describing change in concentrations of components over time are modeled using MATLAB and solved by ode15s. Initial concentrations of metabolites were obtained from Norman et al [34]. The MATLAB script is found in Appendix P.

4. Results and Discussion

This section presents and discusses the results of all performed experiments. First, results of the bottle experiments are presented, followed by the results of the stirred vessel and spinning disk. At last, the results of the metabolic pathway modeling is presented.

4.1 Fed-batch culturing

In Figure 4.1, results of the bottle experiments are presented. Product concentration and pH over time are depicted together with pressure drop and biomass concentrations over time. No data for butane-2,3-diol concentrations are provided as the used analysis method was under development during the execution of this experiment.

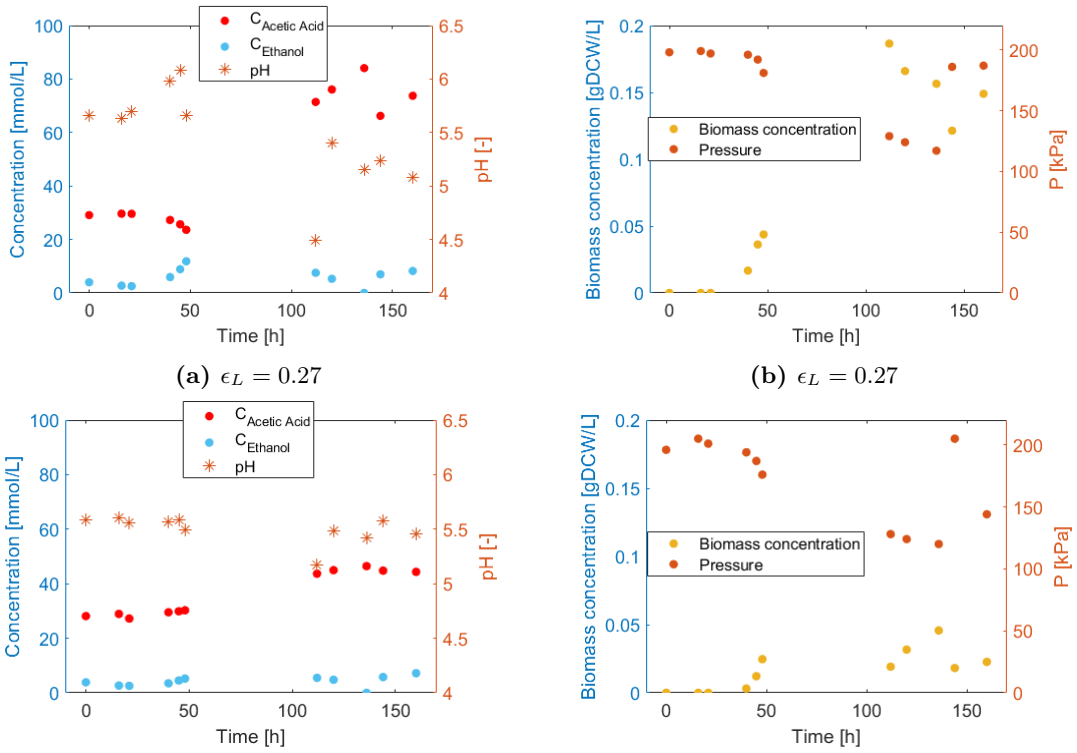

(a) $\epsilon_L = 0.27$ **(b)** $\epsilon_L = 0.27$

(c) $\epsilon_L = 0.54$ **(d)** $\epsilon_L = 0.54$

Figure 4.1: Product composition, pH and pressure decrease for bottle experiments for $\epsilon_L = 0.27$ (a,b) and $\epsilon_L = 0.54$ (c,b). pH was adjusted at t = 120 h. Headspace was refreshed at t = 144 h.

To start, it is observed that gas usage is highest during the exponential phase and product and biomass concentration increases. Furthermore, pH drops as a function of time as more CO is consumed and acetic acid is produced. Comparing both cases show the $\epsilon_L = 0.27$ experiment reaching higher concentrations for both acetic acid and biomass compared to $\epsilon_L = 0.54$. Pressure decrease in both cases show equal behaviour. Since more CO is available for $\epsilon_L = 0.27$, higher product concentrations are obtained.

Another interesting observation is the concentration profile for $\epsilon_L = 0.27$. A decrease in acetic acid and increase in ethanol concentrations are observed before t = 50 h. This is caused by an increase of $Fd_{red}{}^{2-}$ due to the CODH enzyme converting CO to CO_2 (Equation 2.5). The increase in intracellular $Fd_{red}{}^{2-}$ concentration causes a change in redox potential, favouring the conversion of acetic acid to ethanol, consuming $Fd_{red}{}^{2-}$ (Equation 2.17). Since no data points after t = 50

h are available, total consumption of acetic acid is not known. Eventually, after t = 100h, redox potentials reach a new equilibrium, leading to continued production of acetic acid.

Previous bottle experiments, without initial acetic acid present in the bacterial medium, showed no bacterial growth or productivity. This indicates that a too high CO uptake rate can cause the bacteria's redox potential to change significantly, stopping metabolic activity. To overcome this effect, initial acetic acid has to be added to be consumed by the bacteria. For $\epsilon_L = 0.54$, acetic acid consumption is not directly observed after t = 0 h. This indicates that the metabolic system reached a redox equilibrium at an earlier stage compared to $\epsilon_L = 0.27$. This is only possible if CO uptake rate is lower, giving the metabolism time to reach a redox equilibrium. The lower CO uptake rate is simply caused by a lower CO availability compared to $\epsilon_L = 0.27$.

After t = 100 h, bacterial concentration increases significantly. Concentrations for $\epsilon_L = 0.27$ are highest due to more CO being available. Consequently, acetic acid concentration increases. However, hardly any ethanol is produced. For $\epsilon_L = 0.27$, ethanol concentration even decreases. This could be explained by the rise of CO_2 concentrations in the headspace, produced as CO is converted. This leads to favourable conditions for ethanol to oxidise to acetate. According to Diender [43], a decrease in CO/CO_2 ratio changes ferredoxin redox potentials, favouring the oxidation of ethanol.

Knowing acetic acid and ethanol productivities, CO consumption and CO_2 production can be estimated using overall stoichiometric reaction equations as described in subsection 2.2.5. For both $\epsilon_L = 0.27$ and $\epsilon_L = 0.54$, these calculations show an almost complete CO consumption at t = 136 h, before the headspace was refreshed. GC samples taken do indeed show a significant rise in CO_2 levels in the headspace. This could be the reason that productivity halted around this time, as *C. autoethanogenum* is not capable to grow on CO_2 as its sole substrate. However, a slight increase in acetic acid concentration is still observed after t = 136 h. This could be due to a delay in the metabolic system, where pools of acetyl-CoA are still available and able to react towards acetic acid [44]. To ensure a constant productivity and product selectivity, bottle headspace should be refreshed regularly.

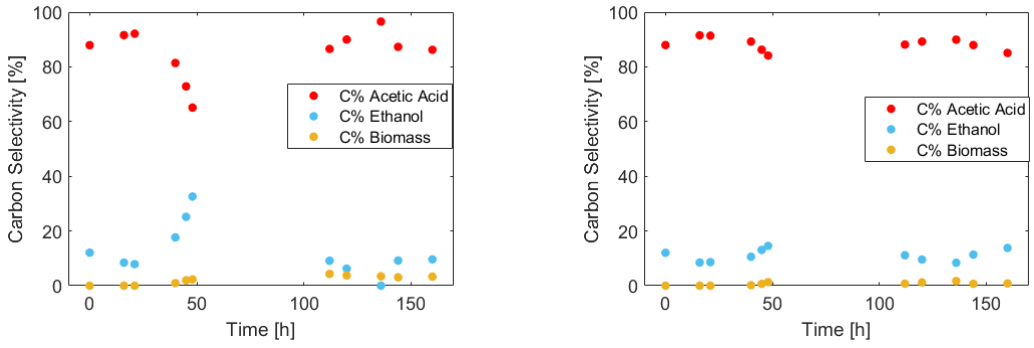

(a) $\epsilon_L = 0.27$ **(b)** $\epsilon_L = 054$

Figure 4.2: Product selectivity as a function of time for bottle experiments

Carbon selectivity over time is shown in Figure 4.2, highlighting the effects of changing ferredoxin redox potentials. It is observed that for most of the time, 80% of the carbon is channeled towards the production of acetic acid. Since butane-2,3-diol production are usually low, presented selectivities are credible. Another remarkable observation for both cases is the low selectivity towards biomass. Similar selectivity for growth of *C. autoethanogenum* on CO are however observed in literature [35] [43].

An attempt to close the carbon balance is made. Knowing the total product concentrations, theoretical CO consumption and CO_2 production can be calculated. Utilising this information, pressure decrease over time can be calculated and compared to the observed pressure decrease. For $\epsilon_L = 0.27$, total carbon balance overshoot is 25%. For $\epsilon_L = 0.54$, total carbon balance undershoot is 19%. The latter percentage could be due to a leakage in the bottle cap, allowing gas to escape. In these calculations, the assumption is made that all gaseous substrates are present in the gas phase. However, Henry coefficient values indicate a significant solubility for CO_2 at the given conditions. To perform a decent calculation for the carbon balance, this has to be taken into account. In addition, regular GC samples should be taken to determine the exact gas phase composition.

4.2 Continuous fermentation in stirred vessel

As described in section 3.4, a continuous fermentation experiment was performed for 28 days in a stirred vessel set-up. Steady state-like behaviour was maintained at 200 kPa for 8 days and at 500 kPa for 4 days. Liquid volume and dilution rate throughout the experiment were not constant however, with liquid volume slowly building up throughout the experiment. Therefore, a constant increase in liquid volume was assumed for calculations regarding this experiment. More information regarding this is provided in Appendix M. Nevertheless, product concentrations remained stable within an approximate range of 10%, making it possible to quantify and compare the results of both cases. Productivity, selectivity and conversion are discussed and compared for both cases of 200 kPa and 500 kPa.

A complete overview of the product concentrations over time for the entire experiment is presented in Figure 4.3. Here, the periods with steady state-like behaviour are indicated. Furthermore, changes in process conditions are shown. Biomass concentrations over time can be found in Figure M.1 in Appendix M.

Between t = 0 h and t = 120 h, a fixed CO headspace was implied on the reaction mixture. After an increase in bacterial concentration was observed, CO gas flow was increased to 5 mL/min at point **A**. An increase in product concentration is observed, slowly levelling out around t = 200 h. Refreshment of the reaction system was started at t = 168 h. Ethanol concentrations seem to decrease around this point. This is likely a result of dilution being faster than ethanol production by the bacteria. Calculated CO/CO_2 ratios at this point are close to a value of 3. As explained in Figure 4.1, this could favour ethanol oxidation towards acetic acid. This could moreover be a reason for the ethanol concentration decrease.

At point **B**, gas flow was increased to 10 mL/min, resulting in higher product concentrations. This could indicate the system to be mass-transfer limited, as a higher gas flow shows an increase in product concentration. Calculated CO conversion between points **A** and **B** is 24%, showing gas availability not being the rate limiting step. Since refreshment of the system started at t = 168 h, quantitative comparison between the 5 ml/min and 10 ml/min cases is not possible. Between t = 280 h and t = 474 h, steady state-like behaviour is observed. Deviations are likely caused by the inconsistent dilution rate, causing the system to be periodically over-diluted, decreasing product concentration. At point **C**, pressure is gradually increased with 6.25 kPa/h to 500 kPa at point **D**. Here, gas flow is increased to 20 mL/min. A rise in product concentrations is observed. After t = 618 h, steady state-like behaviour is observed.

Having two periods with steady state-like behaviour makes it possible to quantitatively compare output parameters as a function of pressure. In Figure 4.4, these periods are highlighted. In addition, Table 4.1 shows a comparison between the two periods given various outcome parameters. A footnote needs to be addressed concerning pH and biomass concentrations. By definition, steady state in defined as a state where values remain constant over time. However, during the supposed

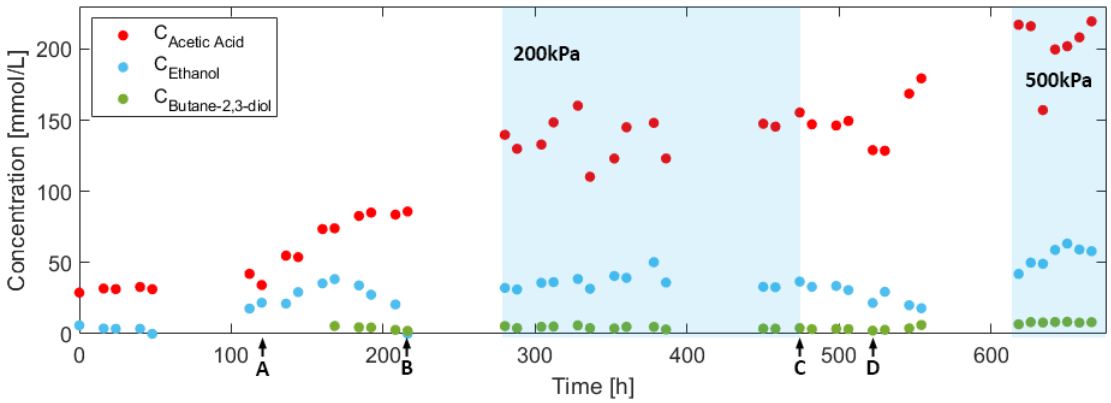

Figure 4.3: Complete overview of continuous fermentation experiment in stirred vessel. ϕ_R = 100 mL/min, T = 37 °C, $pH_{average}$ = 5.0, $V_{reactor}$ = 2.6 L, stirrer speed = 0 rpm. Blue zones indicate the period with steady state-like behaviour. At point **A**, gas flow is increased to ϕ_g = 5 mL/min. At point **B**, gas flow is set to ϕ_g = 10 mL/min. At point **C**, pressure increase starts with 6.25 kPa/h. At point **D**, p = 500kPa and gas flow is increased to ϕ_g = 20 mL/min.

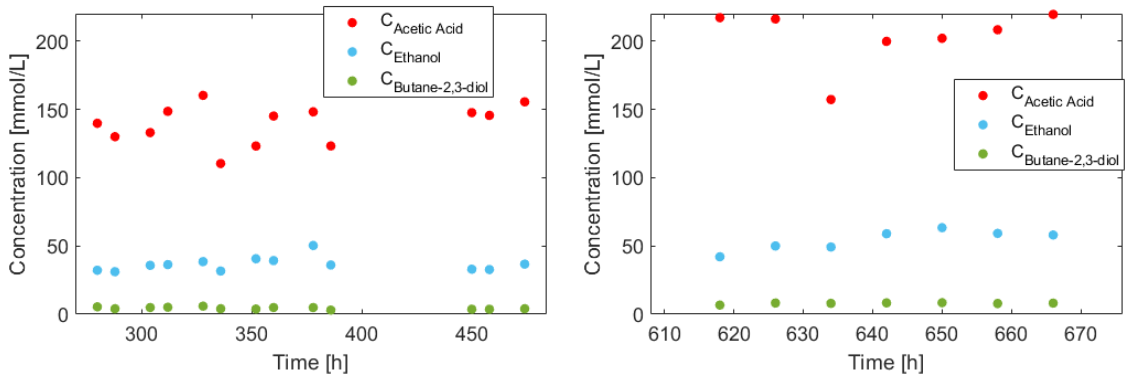

(a) 200 kPa **(b)** 500 kPa

Figure 4.4: Highlighted concentration profiles as a function of time for periods of steady state like behaviour for **(a)** 200 kPa and **(b)** 500 kPa.

steady state, deviation in pH was observed as a result of acetic acid production. Therefore, pH was corrected periodically by adding NaOH. Furthermore, biomass concentration varied, likely due to the variance in liquid volume. Taking these factors into consideration, obtained data is used for quantification, as previous conducted research moreover tolerates similar factors [35] [19].

Selectivity

In general, continuous refreshment of the headspace results in higher ethanol selectivitiy. As described earlier, significant presence of CO_2 leads to favourable conditions for ethanol oxidation. Low pH furthermore favours the production of ethanol. Since average pH was 5.1, this could explain the significant selectivity towards ethanol. Butane-2,3-diol is produced in small quantities, as total ATP gain is lowest for all three products. It is however remarkable that a relatively small portion of carbon is channeled to biomass. In literature, often higher carbon selectivies are described [32]. Biomass selectivity is directly related to intracellular ATP availability. Possibly, other intracellular processes demand ATP, leaving less for the production of biomass.

Apart from pH, selectivity is a strong function of dilution rate. Azevedo de Lima et al. [32] describe an increase in ethanol and butane-2,3-diol selectivity for higher dilution rates for *C. autoethanogenum* growing on CO. Biomass selectivity seems to be unaffected however by this increase.

	Acetic acid	sd	**Ethanol**	sd	**Butane-2,3-diol**	sd	**Biomass**	sd
200 kPa								
Concentration (mM)	139	14.4	36.5	4.15	4.40	0.83	0.29 gDCW/L	0.06
Carbon Selectivity (-)	0.728	0.025	0.191	0.025	0.046	0.024	0.034	0.011
Productivity (mmol/L/h)	0.944	2.27	0.239	0.48	0.013	0.17	0.118	0.74
Productivity (mmol/gDCW/h)	2.38	6.80	0.70	2.60	0.00	0.42	0.200	-
500 kPa								
Concentration (mM)	203	21.5	54.4	7.48	7.94	0.59	0.34 gDCW/L	0.02
Carbon Selectivity (-)	0.724	0.025	0.195	0.025	0.057	0.006	0.023	0.003
Productivity (mmol/L/h)	1.047	3.73	0.571	0.632	0.063	0.083	0.062	0.01
Productivity (mmol/gDCW/h)	3.50	11.42	1.73	2.000	0.185	0.239	0.164	-

Table 4.1: Average concentration, carbon selectivity and productivity for 200 kPa and 500 kPa. Note that biomass concentration is expressed in gDCW/L

Selectivity could be steered towards more valuable products like ethanol and butane-2,3-diol, by adjusting pH and dilution rate.

Comparing selectivies for 200 kPa and 500 kPa show 72% of carbon channeled towards acetic acid and 25% of carbon towards ethanol for both cases. Compared to 200 kPa, biomass selectivity decreases 30% and butane-2,3-diol selectivity increases 30 % for 500 kPa. This slight difference could possibly be attributed to a higher pressure, creating harsher conditions for bacteria to grow in [45]. However, differences are relatively small and overall biomass concentration increased for 500 kPa, making it hard to draw conclusions. In general, increase in pressure up to 500 kPa doesn't seem to have a significant effect on the way carbon is channeled within the metabolism of *C. autoethanogenum*. It is expected that longer fermentation times will moreover provide more conclusive answers.

Ample literature is available for gas fermentation at elevated pressures. No literature has been published so far investigating the effect of gas fermentation using *C. autoethanogenum* at elevated pressures. An overview of high pressure syngas fermentation studies using different strains of bacteria is provided by van Hecke et al. [45]. Stoll et al. showed for *C. ljungdahlii*, another *Clostridium* species often used for syngas fermentation, that selectivity is a strong function of pressure [46]. In contrast, this work shows that for *C. autoethangenum*, selectivity is not effected by pressure increase up to 500 kPa. Stoll et al. however induced a direct pressure increase on the reaction mixture, while this work performed a gradual pressure increase spanning multiple days. Furthermore, their work shows that a direct pressure increase to 700 kPa results in unstable cultivation.

Productivity and mass transfer

Comparing productivity in Table 4.1 show a significant increase for 500 kPa for all products. Values for productivity per gram of biomass increases approximately 23% for acetic acid, and more than double for the production of ethanol and butane-2,3-diol. As observed before, biomass productivity decreases, with values halving for 500 kPa compared to 200 kPa. This is in contrast with *C. ljungdahlii* and other work presented in Van Hecke et al., where biomass productivity did increase at elevated pressure [45].

The overall increase in productivity could be attributed to two possible factors: enhancement in gas-liquid mass transfer rate of CO or an increase in enzymatic kinetics within *C. autoethanogenum*.

Increase in mass transfer rate could be explained by two phenomena. First, gas flow rate is

increased to 20 mL/min, creating a higher gas-liquid interfacial area within the reactor set-up. Equation 4.1 shows the description of gas liquid mass transfer rate, moreover shown in the section 2.2. However, total liquid volume increased significantly for 500 kPa compared to 200 kPa. Approximated ϵ_L increases from 0.57 to 0.97 for 200 kPa to 500 kPa, decreasing the value of $k_L a$ in the overall reactor. Second, increase in pressure leads to an increase in gas solubility, as described by the Henry coefficient. Mass transfer rate depends on the partial pressure of CO, moreover shown in Equation 4.1. A pressure increase from 200 kPa to 500 kPa could theoretically result in a 2.5x higher solubility, resulting in 2.5x higher mass transfer rate.

$$\frac{dC_{i,m}}{dt} = k_L a_{GL}(P_m H_m - C_{L,m}) \tag{4.1}$$

An increase in enzymatic kinetics would suggest the system to be kinetically limited at 200 kPa. In this case, increase in pressure to 500 kPa would consequently result in a 2.5x increase in the kinetic rate constants of all enzymatic complexes to yield the observed increase in productivity. In general, pressure can have various effects on enzymatic reaction rate constants. Regardless the type of kinetics used, rate constants could both decrease, increase or stay constant as a function of pressure, depending on the enzyme [47]. Often, rate constants decrease due to denaturation (loss of activity). Since numerous different types of enzymes are involved in the metabolism of *C. autoethanogenum*, it would be unlikely that all enzymatic rate constants would increase.

Table Table 4.2 provides an overview of CO conversion and uptake rate for both 200 kPa and 500 kPa values. CO uptake rate is calculated using known productivity values for the reaction products and stoichiometric equations as defined in subsection 2.2.5. CO conversion for both cases is approximately 50%, moreover confirming CO availability in the gas phase not being rate limiting. In total, CO uptake rate in mmol/gDCW/h more than doubles for 500 kPa.

GC measurements of the gas headspace show an increase in CO/CO_2 ratio for 500 kPa. Although measurements not being very acurate, this result points towards an increase of solubility of both gases in the liquid phase. Since the Henry coefficient for CO_2 is an order of magnitude higher compared to CO, an increase in ratio should be observed. In addition, calculated values for the CO/CO_2 ratio in the total reaction mixture remain close to equal. If CO concentrations in the liquid phase would already have approached saturation values, the ratio measured by the GC would have been much higher.

Given the unlikeliness of increase in kinetic rate constants, there is a high probability that the increase in productivity and CO uptake rate is caused by an increase in mass transfer. This is supported by the works listed in van Hecke et al. [45]. This shows that poor CO solubility in the liquid phase can be overcome by an increase of pressure, resulting in higher CO uptake rates by *C. autoethanogenum*.

	CO conversion	Uptake rate (mmol/L/h)	Uptake rate (mmol/gDCW/h)	Calculated CO/CO2 ratio	Headspace CO/CO2 ratio by GC
200 kPa	49.5%	5.47	12.7	1.86	4.49
500 kPa	47.3%	8.31	26.58	1.98	10.68

Table 4.2: Average concentration, carbon selectivity and productivity for 200 kPa and 500 kPa. Note that biomass concentration is expressed in gDCW/L

Carbon and ATP balance

Attempts were made to close the carbon balance for both 200 kPa and 500 kPa cases. However, GC measurements of the headspace gas composition turned out to be unreliable. Obtained results for productivity could be used to theoretically calculate CO consumption and CO_2 production.

Headspace gas composition can be calculated given the Henry coefficients. Furthermore, adding an accurate gas flow meter to the set-up could measure decrease in gasflow, making it possible to quantitatively determine CO uptake rate, conversion and CO_2 production.

At last, an attempt was made to link ATP production with biomass production. As mentioned in subsection 2.2.5, according to literature, 47 mmol ATP is required to produce 1 gram of dry cell weight. Knowing total ATP yields for all products and knowing total productivity, the obtained value of 47 mmolATP/gDCW can be validated. For 200 kPa and 500 kPa, an average value of 767mmolATP/gDCW and 1863 mmolATP/gDCW was required. These values highly exceed the values provided by literature. Possibly, othe processes within the bacterial cell demand high levels of ATP.

4.3 Fermentation in the rs-SDR

In this section, all three fermentation experiments using the rs-SDR are discussed. Overall, no active production was observed. Several adjustments made after exploratory experiments moreover failed to show successful fermentation. An attempt was made to improve heat control to aim for stable temperature conditions. Next, CO flow rate was set to a rate equal to the experiment performed in the stirred vessel to reduce ${Fd_{red}}^{2-}$ redox pressure. In addition, extra acetic acid was added to the medium, moreover contributing to a reduced ${Fd_{red}}^{2-}$ redox pressure. However, non of these measures proved successful fermentation.

Figure 4.5 shows the results of concentration profiles and biomass concentration of the experiments performed at 100 rpm, 500 rpm and 1000 rpm. Process conditions are described in the caption of the figure. For the 100 rpm experiment, a colony with higher initial product and biomass concentrations was used compared to the other two cases. Butane-2,3-diol concentrations were too low for the 500 rpm and 1000 rpm cases for the GCMS to detect. For 500 and 1000 rpm, gas flow rate was reduced to aim for a reduced ${Fd_{red}}^{2-}$ redox pressure.

For all cases, production was absent and no bacterial growth was observed. Concentrations declined slowly over time due to fresh medium being added after 4 mL samples were taken. Several reasons could explain the absence of growth and production. First, poor temperature control could be a possibility. Reaction mixture temperature could vary slightly as a function of time. The reactor set-up was heated using a heating plate leading to small over- and undershoots of temperature. A 1 °C deviation from the optimal and set 37 °C was observed occasionally. Exposing *C. autoethanogenum* to higher temperatures for longer periods of time could possible lead to denaturation hence inactivation of enzymes [20].

A second explanation could be attributed to the increased shear forces caused by the spinning disk. These forces could have potentially damaged the bacteria, making them unable to create reaction products or reproduce. However, for both 100 and 1000 rpm cases, bacterial concentration only decreased gradually. One could state that exposing *C. autoethanogenum* to shear forces for longer periods of time would eventually lead to cell death. This could explain the decrease in biomass concentration for 100 and 1000 rpm. This is in contrast with the experiment at 500 rpm, where bacterial concentration remained constants for a period of 280h. Natural cell-death due to the inability of *C. autoethanogenum* to take-up and convert CO could moreover be an explanation for the observed bacterial concentration decrease.

For 100 rpm, an instant decrease in product and biomass concentration was observed around t = 320 h. This is explained by the addition of a large quantity of fresh medium. Approximately 60 mL of medium was evaporated between t = 240 h and t = 330 h, due to the effects of continuous gasflow and vapour pressure. This required the addition of extra medium, diluting product concentrations. To ensure a more stable temperature control, the reactor vessel was placed inside

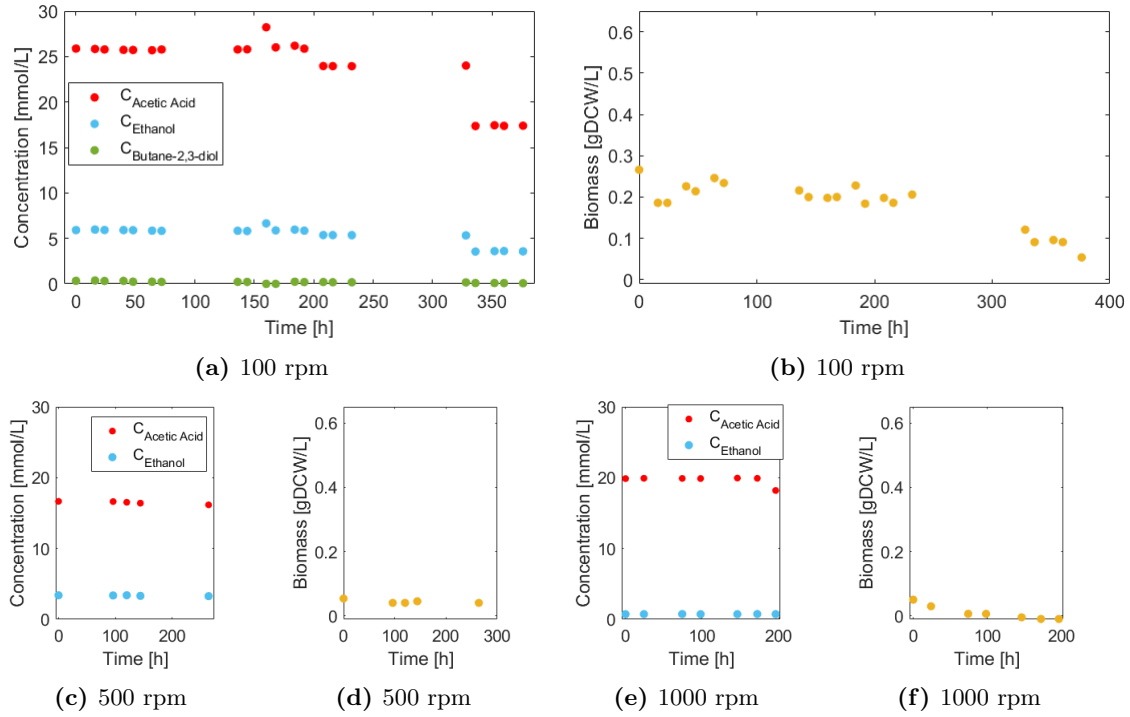

(a) 100 rpm **(b)** 100 rpm

(c) 500 rpm **(d)** 500 rpm **(e)** 1000 rpm **(f)** 1000 rpm

Figure 4.5: Concentration profiles and biomass concentration over time for fermentation experiments performed in the rs-SDR. **a,b** depicts the results for 100 rpm (ϕ_g = 17 mL/min, ϕ_R = 174 mL/min, T = 37 °C, $pH_{average}$ = 5.3, V_L = 240 mL, V_G = 560 mL.) **c,d** depicts the result for 500 rpm, (ϕ_g = 7 mL/min, ϕ_R = 174 mL/min, T = 37 °Cs, $pH_{average}$ = 5.4, V_L = 240 mL, V_G = 560 mL.) **e,f** depicts the result for 1000 rpm, (ϕ_g = 7 mL/min, ϕ_R = 174 mL/min, T = 37 °C, $pH_{average}$ = 5.2, V_L = 240 mL, V_G = 560 mL)

.

a water bath for the 500 and 1000 experiments. However, temperature control fluctuated nevertheless.

For 1000 rpm, biomass concentration decreased at a faster pace compared to the 100 rpm experiment. At t = 150 h, biomass concentrations had dropped to almost 0 gDCW/L. To investigate the condition of *C. autoethanogenum*, samples were analysed under the microscope at the start and at the end of each experiment, with the exception of the start of 100 rpm. Furthermore, average bacterial size was determined by taking microscopical picture and using a MATLAB script. Results are depicted in table Table 4.3. Microscopical images used can be found in Appendix N. The same bacterial culture that ended the 100 rpm experiment were used as a start for the 500 rpm experiment, explaining the similar values.

	100 rpm start	100 rpm end	500 rpm start	500 rpm end	1000 rpm start	1000 rpm end
Area $[mm^2]$	-	$4.949 \cdot 10^{-4}$	$4.949 \cdot 10^{-4}$	$4.879 \cdot 10^{-4}$	$4.404 \cdot 10^{-4}$	$4.841 \cdot 10^{-4}$
Standard deviation	-	$5.650 \cdot 10^{-4}$	$5.650 \cdot 10^{-4}$	$5.401 \cdot 10^{-4}$	$3.032 \cdot 10^{-4}$	$5.405 \cdot 10^{-4}$

Table 4.3: Average bacterial surface area of *C. autoethanogenum* before and after rs-SDR experiments

Overall, average bacterial size did not decrease after elongated exposure to higher shear forces for both 100, 500 and 1000 rpm. Microscopical analysis moreover showed most bacteria still being in normal conditions and moving around. However, cell-division wasn't observed. It is hard to say whether the absence of cell division and presence of spores can be attributed to the effect of shear forces.

Another observation that could possibly be encountered when bacterial cell death occurs is increase in pH. Average pH value inside *C. autoethanogenum* bacterial cells is 6. Cell-rupture would expose intracellular content to the liquid medium, consequently increasing pH. This phenomena was not observed however as pH values remained more or less constant.

4.4 Metabolic Pathway Modeling

In this section, the obtained results of kinetic modeling of the simplified metabolic pathway equations are discussed. Results are presented for syngas fermentation on CO. In Figure 4.6 and Figure 4.7, an overview of gas consumption and product formation in the bacteria is depicted.

The concentration profiles of the products seem to behave as observed in the experiments. Care should be taken however, since these graph only show the intracellular concentration profiles. CO concentrations remain constant as this was imposed in the model. For the gases, CO_2 concentration increases over time, as this is a byproduct of acetic acid, ethanol and butane-2,3-diol production. Furthermore, H_2 is produced as a result of the Hyt reaction. This H_2 is coupled with CO_2 to form formate.

Concentrations for all reaction products increase over time, however with a similar productivity. This is mostly determined by the set value for the reaction rate constant. Figure Figure 4.8 shows the intracellular concentration profiles of metabolites as a function of time. Initial concentrations were taken from Norman et al. [34]. To start, $Fd_{red}{}^{2-}$ concentrations first increases and later start to decrease. This behaviour is typical and observed in this work for CO-grown *C. autoethanogenum*. When analysing reaction rates over time, the model actually increases the rate towards ethanol production from acetate, which is in accordance with experimental observation.

Furthermore, ADP and ATP form an equilibrium within the cell after a short period of time. Used ADP quickly gets converted back to ATP. No net ATP gain over time is observed. However, a net decrease in intracellular pH is predicted over time. Since, intracellular pH is meant to be kept constant, additional ATP will be formed when these protons are transferred to the extracellular environment. This part was however not imposed in the model. Consequently, the shown metabolites concentration is not a good representation for longer periods of time. However, for shorter periods of time, it behaves in accordance to experimental results.

The concentration profiles give insight in the limiting components in the metabolic pathway. Nevertheless, reaction rate constants are assumed. Moreover, several assumptions, for example the reaction order and kinetic model reaction rate, are made. This furthermore affects concentration profiles. Therefore, no actual representation of a real system is obtained. As discussed previously, biomass concentrations, pH changes and inhibitory effects moreover have a profound effect on intracellular carbon fluxes. At last, most reactions were assumed to be irreversible, while enzymatic reactions are mostly reversible. Under certain conditions, this is possible for the metabolism, as shown in Figure 4.1. This all together shows that using a simplified approach to model metabolic behaviour is nonetheless a complex process.

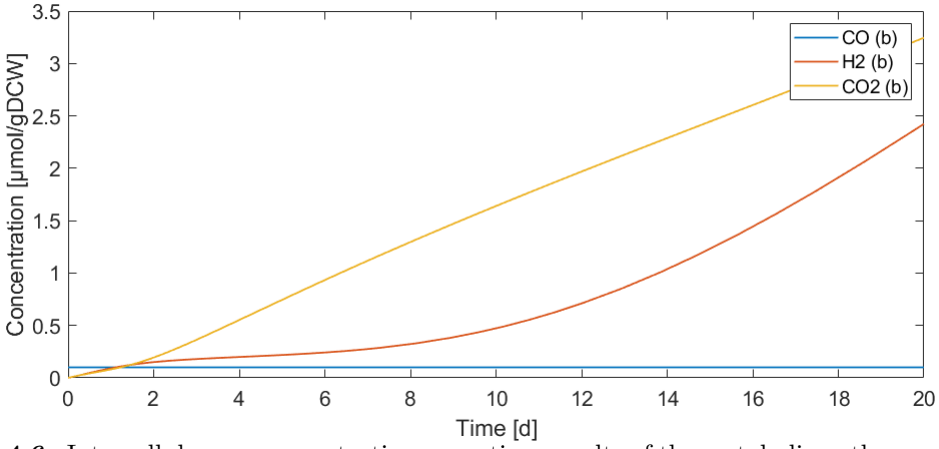

Figure 4.6: Intracellular gas concentrations over time results of the metabolic pathway modeling. Note that a continuous influx of CO is assumed and that no mass transfer from the bacteria to the liquid phase is imposed in the model

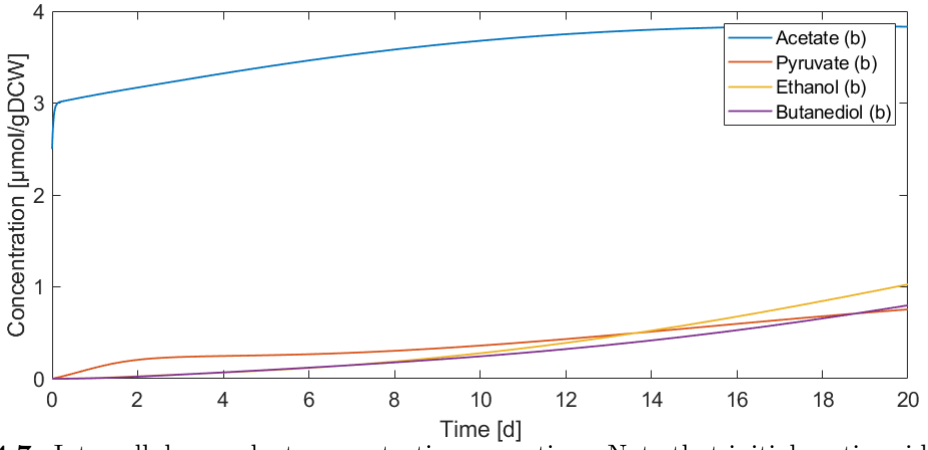

Figure 4.7: Intracellular product concentrations over time. Note that initial acetic acid concentrations are higher due to the current medium composition

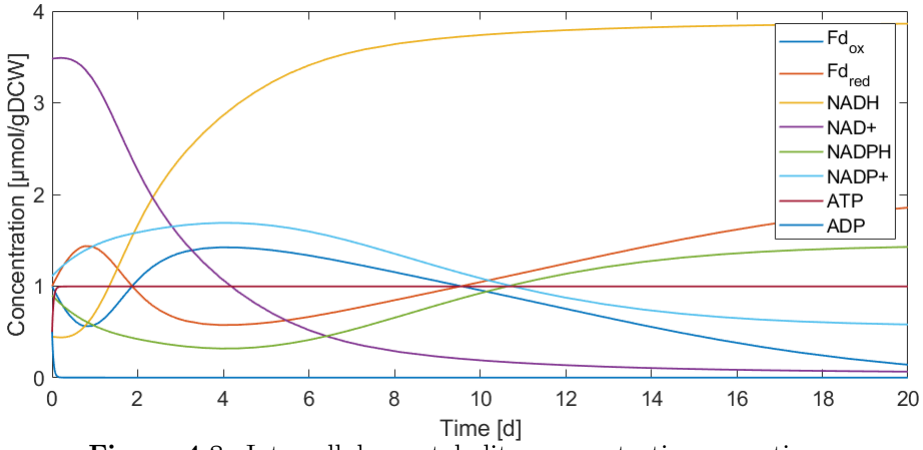

Figure 4.8: Intracellular metabolites concentrations over time.

5. Conclusions

This work demonstrates several aspects of the industrial process intensification of bacterial syngas fermentation using *Clostridium autoethanogenum*. As a starting point, microbes were cultured using CO as a gas substrate in glass cultivation bottles. Experiments with limited carbon supply showed a complete consumption of the gas substrate. A larger gas hold-up led to significantly higher product and biomass concentrations. Continuous supply of gas substrates is therefore preferred. Furthermore, two effects on product selectivity were demonstrated. First, increased pools of Fd^{2-}_{red} caused by the conversion of CO to CO_2 led to the conversion of extracellular acetic acid to ethanol, again consuming Fd^{2-}_{red}. Second, increase of the CO/CO_2 ratio, after the majority of CO was consumed, created favourable conditions for ethanol oxidation back to acetic acid.

To further increase productivity, continuous cultivation with constant refreshment of the headspace was performed using a stirred vessel set-up. This set-up was capable of performing fermentation experiments at elevated pressures. By conducting continious fermentation experiments, steady state can be reached. Despite efforts taken, biomass concentrations, pH and liquid volume were not kept constant throughout the experiment. However, it was observed that carbon distribution throughout the metabolic pathway stayed constant. In addition, it was possible to reach steady state-like behaviour, in which the the product concentration stayed within a 10% range from average value. This made it possible to vary process parameters and quantitatively compare these states, gaining insight into limitations.

A continuous fermentation experiments was performed reaching pressures of 200 kPa and 500 kPa, both periods reaching a state with constant productivity for multiple residence times. Pressure was increased gradually with 6.25 kPa/h. In addition, CO gas flow was doubled for the 500 kPa experiment. Product concentrations increased by 35% on average at elevated pressure. Product selectivity was unaffected for acetic acid and ethanol production. However, butane-2,3-diol selectivity increased slightly, as biomass selectivity decreased.

Additionally, CO uptake rate per gram biomass more than doubled at elevated pressures. This increase is attributed to an increase in gas liquid mass transfer rate, since it is a function of pressure. CO conversion was approximately 50% at both pressures, indicating availability of gas substrate not being the limiting factor. Moreover, enzymatic kinetics are not significantly affected by pressure. In contrast, plenty of enzymatic activity was available to realise this increase in productivity. This work is the first of its kind demonstrating fermentation using *Clostridium autoethanogenum* at elevated pressures. It shows that mass transfer limitations can be overcome by elevating pressure, increasing overall productivity.

Fermentation experiments were conducted using the rotor stator spinning disk reactor. No additional insights on the increase in mass transfer by this reactor were gained. No productivity or bacterial growth was observed in the experiments. Microscopic analysis of the bacteria didn't prove a significant change in bacterial morphology. However, since bacteria were unable to keep their metabolism active, no bacteria were present performing cell-devision.

Lastly, a reaction scheme describing the metabolism of *c. autoethanogenum* was proposed based on most recent insights and uncertainties were described. Metabolic reactions were verified and checked on carbon and electron balance. This set of reactions was further simplified to a total of 16 reactions. Using mass action kinetics, this set of reactions was modeled using MATLAB, making it possible to gain general insights in the behaviour of the metabolism given certain circumstances. However, kinetic data first need to be obtained to create a representative simulation of the pathway.

6. Recommendations

The results of the experiments presented in this worked have provided insights in the intensification of syngas fermentation using *Clostridium autoethanogenum*. By elevating pressure, gas liquid mass transfer limitations can be overcome, yielding higher productivity. However, additional mass transfer enhancement using a rs-SDR was not successful. In addition, several biochemical mechanisms part of the metabolism of *C.autoethanogenum* are not fully understood and need further investigation. Both factors determine product selectivity and productivity. To ensure economic success in the commercialisation of the revaluation of industrial waste gasses, additional research has to be performed.

By conducting fermentation experiments in steady state, varying important process conditions, valuable outcome parameters can be obtained. It is recommended to start focusing on achieving high biomass concentrations. This will both lead to higher productivity and faster experimentation times. Changes in outcome parameters as a function of varying process conditions are likely to become more visible when biomass concentrations are high. Focus should be placed on investigating process conditions enhancing mass transfer. This will lead to higher productivity, hence, increase in biomass concentrations.

This requires process control and accurate measurement of outcome parameters. The currently used stirred vessel set-up can be improved to further realise this. Multiple upgrades can be done contributing to achieving steady state. To compensate for manual and periodical pH adjustment, a pH control system can contribute to keeping overall pH constant during the process. Second, the dilution system showed to result liquid volume fluctuations over time. Currently, daily manual adjustments to the pumps need to be made to ensure a constant dilution. Determining the exact flow rate of the used pumps could contribute in omitting manual adjustments. Third, a method to constantly check liquid volume levels can be introduced to ensure a constant liquid volume. Possibly, adjustments to the autoclave can be made to achieve this.

Furthermore, changes can be made to better quantify flow rate of gas outflow. By introducing an accurate gas flow meter, total gas consumption can be measured and compared with calculated values. Moreover, determining exact gas composition using a GC was found to be difficult, as CO to interact with the stationary phase of the used column. Further calibration of the GC or possibly introducing a column better able to quantify CO levels could result in more accurate measurements. When both gas outflow and composition are known, gas uptake rate can be calculated and the carbon balance of the system can be closed. This will lead to accurate insights outcome parameters as a function of various process conditions.

Bacterial growth and productivity should be enhanced by extending research to overcome gas-liquid mass transfer limitations and by varying dilution rates. By introducing a rs-SDR in the stirred vessel set-up, effects of increasing mass transfer by means of introducing turbulence can be investigated. By varying rotational speed over a range between 0 and 2000 rpm, bacterial growth and productivity are likely to increase. Nevertheless, experiments investigating shear effects on *C. autoethanogenum* for longer periods of time do not yet provide conclusive results. In case of shear forces leading to an increased death rate, increasing k_La using a rs-SDR might not contribute to a gained advantage. However, increase in liquid viscosity due to high biomass concentrations might require the use of a rs-SDR. As an increase in viscosity decreases the value of k_La, extra shear forces creating more turbulence would therefore increase k_La again. As current insights in the use of rs-SDR do not provide conclusive insights in enhancing mass transfer for fermentation using *C. autoethanogenum*, additional research needs to be performed. To investigate possible cell rupture, measuring concentrations of intracellular components using specific optical density could be applied. This can be done by inserting a probe or UV meter in the set-up.

Moreover, this work proved to successfully overcome mass transfer limitations by elevating pressure. Broadening insights in this effect can lead to additional increase in biomass concentrations and productivity. Since the stirred vessel set-up is capable of reaching pressures up to 5000 kPa, it is highly recommended to further investigate the effect of elevated pressure on productivity. By gradually elevating pressure to higher values, mass transfer could be enhanced even further. It could be examined at which point *C. autoethanogenum* might be negatively affected by pressure. Possibly, increase in pressure up to a specific point might lead to decreased activity or denaturation of enzymatic complexes essential to the metabolism. Afterwhile, performing experiments at elevated pressure simultaneously operating the spinning disk reactor could lead to optimal mass transfer.

When high biomass concentrations are achieved, additional research could be performed steering product selectivity towards most economically viable products. pH of the bacterial medium has a significant influence on the energy regulatory processes of *C. autoethanogenum*. Understanding this effect could lead to steering selectivity to the desired products. Next, effects of gas composition could be investigated. By having a better understanding of the metabolic system, optimal gas substrate composition could be determined. Vice-versa, productivity and selectivity could be steered using the composition of available off-gases. These insights can be obtained both by experimental work as by modeling of the metabolic pathway. Next, the effect of dilution rate on selectivity and productivity can be investigated. Combining both insights will eventually lead to deeper understanding and control of the metabolic pathway of *C. autoethanogenum*.

By creating reaction conditions leading to optimal biomass concentrations, productivity and selectivity towards most economically viable products, a total technical-economical assessment of the fermentation process in the spinning disk can be performed. Productivity should outweigh energy input to operate the reaction system. Energy input required for the complete process, including product separation, should be taken into account.

Bibliography

[1] Jayarama Reddy Puthalpet. Mitigation of Climate Change. *The Daunting Climate Change*, pages 219–276, 2022. 1, 14

[2] E. A. Abdelaziz, R. Saidur, and S. Mekhilef. A review on energy saving strategies in industrial sector. *Renewable and Sustainable Energy Reviews*, 15(1):150–168, 2011. 1

[3] Matthew M. Yung, Whitney S. Jablonski, and Kimberly A. Magrini-Bair. Review of catalytic conditioning of biomass-derived syngas. *Energy and Fuels*, 23(4):1874–1887, 2009. 1

[4] Jun Ma, Nannan Sun, Xuelan Zhang, Ning Zhao, Fukui Xiao, Wei Wei, and Yuhan Sun. A short review of catalysis for CO2 conversion. *Catalysis Today*, 148(3-4):221–231, 2009. 1

[5] W. Walker Russell and Glenn H. Miller. Catalytic Hydrogenation of Carbon Dioxide to Higher Hydrocarbons. *Journal of the American Chemical Society*, 72(6):2446–2454, 1950. 1

[6] James Daniell, Michael Köpke, and Séan Simpson. Commercial biomass syngas fermentation. *Energies*, 5:5372–5417, 12 2012. 1

[7] L. G. Pereira, M. O.S. Dias, A. P. Mariano, R. Maciel Filho, and A. Bonomi. Economic and environmental assessment of n-butanol production in an integrated first and second generation sugarcane biorefinery: Fermentative versus catalytic routes. *Applied Energy*, 160(2015):120–131, 2015. 1

[8] Haris Nalakath Abubackar, María C Veiga, and Christian Kennes. Bioresource Technology Carbon monoxide fermentation to ethanol by Clostridium autoethanogenum in a bioreactor with no accumulation of acetic acid. *BIORESOURCE TECHNOLOGY*, 186:122–127, 2015. 1

[9] Michael Ko, Christophe Mihalcea, Fungmin Liew, Joseph H Tizard, Mohammed S Ali, Joshua J Conolly, Bakir Al-sinawi, and D Simpson. 2 , 3-Butanediol Production by Acetogenic Bacteria , an Alternative Route to Chemical Synthesis , Using Industrial Waste Gas †. 77(15):5467–5475, 2011. 1

[10] Konstantinos Asimakopoulos, Hariklia N Gavala, and Ioannis V Skiadas. Reactor systems for syngas fermentation processes : A review. *Chemical Engineering Journal*, 348(May):732–744, 2018. 1

[11] Pooya Lahijanid Maedeh Mohammadia, b, Ghasem D. Najafpourb,, 1, Habibollah Younesic and 1 Mohamad Hekarl Uzira, Abdul Rahman Mohameda,. Bioconversion of synthesis gas to second generation biofuels: A review. 2011. 1

[12] James K. Heffernan, Kaspar Valgepea, Renato de Souza Pinto Lemgruber, Isabella Casini, Manuel Plan, Ryan Tappel, Sean D. Simpson, Michael Köpke, Lars K. Nielsen, and Esteban Marcellin. Enhancing co2-valorization using clostridium autoethanogenum for sustainable fuel and chemicals production. *Frontiers in Bioengineering and Biotechnology*, 8, 2020. 1

[13] M. Meeuwse. *Rotor-stator spinning disc reactor*. PhD thesis, Chemical Engineering and Chemistry, 2011. 1, 18, 19, 20

[14] M. Meeuwse, J. Schaaf, van der, and J.C. Schouten. Multistage rotor-stator spinning disc reactor. *AIChE Journal*, 58(1):247–255, 2012. 1, 18, 19

[15] Arnab Chaudhuri. *Intensification of Multiphase Systems with Rotor-Stator Spinning Disk Reactors*. PhD thesis, 07 2021. 1, 18

[16] James J Orgill, Mike C Abboud, Hasan K Atiyeh, Mamatha Devarapalli, Xiao Sun, and Randy S Lewis. Bioresource Technology Measurement and prediction of mass transfer coe ffi cients for syngas constituents in a hollow fi ber reactor. 276(December 2018):1–7, 2019. 1

[17] Jamal Abrini, Henry Naveau, and Edmond-jacques Nyns. Hicrobinlegy. pages 345–351, 1994. 3

[18] Johanna Mock, Shuning Wang, Haiyan Huang, Jörg Kahnt, and Rudolf K. Thauer. Evidence for a hexaheteromeric methylenetetrahydrofolate reductase in Moorella thermoacetica. *Journal of Bacteriology*, 196(18):3303–3314, 2014. 3, 9

[19] Rachel M. Slivka, Mari S. Chinn, Amy M. Grunden, and José M. Bruno-Bárcena. An iterative approach to improve xylose consumption by Clostridium autoethanogenum: From substrate concentration to pH adjustment. *Biomass and Bioenergy*, 140(June), 2020. 3, 30

[20] Bender, Madigan, Buckley, Sattley, and Stahl. *Brock Biology of Microorganisms FIFTEENTH EDITION*. 2019. 3, 4, 14, 15, 16, 33, 58

[21] Stephen W. Ragsdale. Enzymology of the Wood-Ljungdahl pathway of acetogenesis. *Annals of the New York Academy of Sciences*, 1125:129–136, 2008. 4, 9, 10

[22] Johanna Mock, Yanning Zheng, Alexander P. Mueller, San Ly, Loan Tran, Simon Segovia, Shilpa Nagaraju, Michael Köpke, Peter Dürre, and Rudolf K. Thauer. Energy conservation associated with ethanol formation from H2 and CO2 in Clostridium autoethanogenum involving electron bifurcation. *Journal of Bacteriology*, 197(18):2965–2980, 2015. 4, 6, 7, 9, 10, 11

[23] Shuning Wang, Haiyan Huang, Haiyan Huang Kahnt, Alexander P. Mueller, Michael Köpke, and Rudolf K. Thauer. NADP-Specific electron-bifurcating [FeFe]-hydrogenase in a functional complex with formate dehydrogenase in clostridium autoethanogenum grown on CO. *Journal of Bacteriology*, 195(19):4373–4386, 2013. 4, 14

[24] Christopher M. Humphreys, Samantha McLean, Sarah Schatschneider, Thomas Millat, Anne M. Henstra, Florence J. Annan, Ronja Breitkopf, Bart Pander, Pawel Piatek, Peter Rowe, Alexander T. Wichlacz, Craig Woods, Rupert Norman, Jochen Blom, Alexander Goesman, Charlie Hodgman, David Barrett, Neil R. Thomas, Klaus Winzer, and Nigel P. Minton. Whole genome sequence and manual annotation of Clostridium autoethanogenum, an industrially relevant bacterium. *BMC Genomics*, 16(1):1–10, 2015. 4

[25] Steven D. Brown, Shilpa Nagaraju, Sagar Utturkar, Sashini De Tissera, Simón Segovia, Wayne Mitchell, Miriam L. Land, Asela Dassanayake, and Michael Köpke. Comparison of single-molecule sequencing and hybrid approaches for finishing the genome of Clostridium autoethanogenum and analysis of CRISPR systems in industrial relevant Clostridia. *Biotechnology for Biofuels*, 7(1), 2014. 4

[26] Minoru Kanehisa and Susumu Goto. KEGG: Kyoto Encyclopedia of Genes and Genomes. *Nucleic Acids Research*, 28(1):27–30, 01 2000. 4

[27] Erin E Dooley. National center for biotechnology information. *Environ. Health Perspect.*, 112(12):A674, August 2004. 4

[28] Thomas Meier, Scott A Ferguson, Gregory M Cook, Peter Dimroth, and Janet Vonck. Structural Investigations of the Membrane-Embedded Rotor Ring of the F-ATPase from Clostridium paradoxum . 188(22):7759–7764, 2006. 6

[29] Fungmin Liew, Anne M. Henstra, Michael Kpke, Klaus Winzer, Sean D. Simpson, and Nigel P. Minton. Metabolic engineering of Clostridium autoethanogenum for selective alcohol production. *Metabolic Engineering*, 40(May 2016):104–114, 2017. 11

[30] Michael Köpke, Monica L. Gerth, Danielle J. Maddock, Alexander P. Mueller, Fung Min Liew, Séan D. Simpson, and Wayne M. Patrick. Reconstruction of an acetogenic 2,3-butanediol pathway involving a novel NADPH-dependent primary-secondary alcohol dehydrogenase. *Applied and Environmental Microbiology*, 80(11):3394–3303, 2014. 12

[31] Alexander Katsyv and Volker Müller. Overcoming energetic barriers in acetogenic c1 conversion. *Frontiers in Bioengineering and Biotechnology*, 8, 2020. 12

[32] Lorena Azevedo de Lima, Henri Ingelman, Kush Brahmbhatt, Kristina Reinmets, Craig Barry, Audrey Harris, Esteban Marcellin, Michael Köpke, and Kaspar Valgepea. Faster Growth Enhances Low Carbon Fuel and Chemical Production Through Gas Fermentation. *Frontiers in Bioengineering and Biotechnology*, 10(April):1–14, 2022. 12, 30

[33] Kaspar Valgepea, Kim Q. Loi, James B. Behrendorff, Renato de S.P. Lemgruber, Manuel Plan, Mark P. Hodson, Michael Köpke, Lars K. Nielsen, and Esteban Marcellin. Arginine deiminase pathway provides ATP and boosts growth of the gas-fermenting acetogen Clostridium autoethanogenum. *Metabolic Engineering*, 41(September 2016):202–211, 2017. 12

[34] Rupert Norman, Rupert O J Norman, Thomas Millat, Sarah Schatschneider, Anne M Henstra, Ronja Breitkopf, Bart Pander, Florence J Annan, Pawel Piatek, Hassan B Hartman, Mark G Poolman, A David, Klaus Winzer, Nigel P Minton, and Charlie Hodgman. A genome-scale model of Clostridium autoethanogenum reveals optimal bioprocess conditions for high-value chemical production from carbon monoxide A genome-scale model of Clostridium autoethanogenum reveals optimal bioprocess conditions for high-value chemical production from carbon monoxide. (April):1–26, 2019. 12, 26, 35, 50

[35] Haris Nalakath Abubackar, Ánxela Fernández-naveira, María C Veiga, and Christian Kennes. Impact of cyclic pH shifts on carbon monoxide fermentation to ethanol by Clostridium autoethanogenum. *FUEL*, 178:56–62, 2016. 14, 28, 30

[36] Kaspar Valgepea, Renato De Souza Pinto Lemgruber, Tanus Abdalla, Steve Binos, Nobuaki Takemori, Ayako Takemori, Yuki Tanaka, Ryan Tappel, Michael Köpke, Séan Dennis Simpson, Lars Keld Nielsen, and Esteban Marcellin. H2 drives metabolic rearrangements in gas-fermenting Clostridium autoethanogenum. *Biotechnology for Biofuels*, 11(1):1–15, 2018. 14

[37] Pradeep Chaminda Munasinghe and Samir Kumar Khanal. Syngas fermentation to biofuel: Evaluation of carbon monoxide mass transfer coefficient (kla) in different reactor configurations. *Biotechnology Progress*, 26, 2010. 16

[38] Pradeep Chaminda Munasinghe and Samir Kumar Khanal. Syngas Fermentation to Biofuel : Evaluation of Carbon Monoxide Mass Transfer Coefficient (k L a) in Different Reactor Configurations. 2010. 17

[39] Muhammad Yasin, Yeseul Jeong, Shinyoung Park, Jiyeong Jeong, Eun Yeol Lee, Robert W. Lovitt, Byung Hong Kim, Jinwon Lee, and In Seop Chang. Microbial synthesis gas utilization and ways to resolve kinetic and mass-transfer limitations. *Bioresource Technology*, 177:361–374, 2015. 18

[40] D. A. Howey, A. S. Holmes, and K. R. Pullen. Radially resolved measurement of stator heat transfer in a rotor-stator disc system. *International Journal of Heat and Mass Transfer*, 53(1-3):491–501, 2010. 19

[41] Jose A Gomez, Kai Höffner, and Paul I Barton. DFBAlab : a fast and reliable MATLAB code for dynamic flux balance analysis. pages 1–10, 2014. 25

[42] Michael A. Henson. Genome-Scale Modeling of Microbial Metabolism with Temporal and Spatial Resolution. *Biochem Soc Trans*, 43(5):1164–1171, 2015. 26

[43] M. Diender. *Exploration of microbial systems as biocatalysts for conversion of synthesis gas to bio-based chemicals LK - https://wur.on.worldcat.org/oclc/1088405530*. PhD thesis, Wageningen Univeristy Research, 2019. 28

[44] Kaspar Valgepea, Renato de Souza Pinto Lemgruber, Kieran Meaghan, Robin William Palfreyman, Tanus Abdalla, Björn Daniel Heijstra, James Bruce Behrendorff, Ryan Tappel, Michael Köpke, Séan Dennis Simpson, Lars Keld Nielsen, and Esteban Marcellin. Maintenance of atp homeostasis triggers metabolic shifts in gas-fermenting acetogens. *Cell Systems*, 4(5):505–515.e5, 2017. 28

[45] Wouter Van Hecke, Richard Bockrath, and Heleen De Wever. Effects of moderately elevated pressure on gas fermentation processes. *Bioresource Technology*, 293(June):122129, 2019. 31, 32

[46] I. K. Stoll, N. Boukis, and J. Sauer. Syngas fermentation at elevated pressure – experimental results. *European Biomass Conference and Exhibition Proceedings*, (July):1255–1261, 2019. 31

[47] Eddie Morild. The theory of pressure effects on enzymes. *Advances in protein chemistry*, 34:93–166, 1981. 32

[48] A R Archibald and S Heptinstall. Short Communications. The teichoic acids of Micrococcus sp. 24. *Biochemical Journal*, 125(1):361–363, 11 1971. 50

A. Atom balances & simplified reactions

In the following section, the atom balance for all reactions discussed in section section 2.2 are shown. It proves that all reactions are stoichiometrically correct. The full reactions, similar to the simplified reactions of the metabolism as described in subsection 2.2.4 are also proven to be stoichiometrically correct. Reaction numbers used in this appendix are similar to the numbers in this section.

Reaction 1 and -1:

$$\mathrm{CO_2 + 2\,H^+ + Fd_{red}{}^{2-} \overset{\mathrm{CODH}}{\rightleftharpoons} CO + H_2O + Fd_{ox}}$$
$$\mathrm{CO_2 + H_2 + Fd \overset{CODH}{\rightleftharpoons} CO + H_2O + Fd}$$

Reaction 2a:

$$\mathrm{CO_2 + H_2 \overset{FdhA}{\rightleftharpoons} HCOO^- + H^+}$$
$$\mathrm{CO_2 + H_2 \overset{FdhA}{\rightleftharpoons} HCO_2 + H}$$

Wood-Ljungdahl Pathway:

$$\mathrm{HCOOH + ATP + H_4folate \overset{FTL}{\rightleftharpoons} 10\text{-}HCO{-}H_4folate + ADP + P_{\mathit{i}}}$$
$$\mathrm{CH_2O_2 + C_{10}H_{15}N_5O_{13}P_3 + C_{19}H_{23}N_7O_6 \rightleftharpoons C_{20}H_{23}N_7O_7 + C_{10}H_{14}N_5O_{10}P_2 + H_3PO_4}$$

$$\mathrm{10\text{-}HCO{-}H_4folate + H^+ \overset{MTC}{\rightleftharpoons} 5{,}10{-}methenyl{-}H_4folate^+ + H_2O}$$
$$\mathrm{C_{20}H_{23}N_7O_7 + H \rightleftharpoons C_{20}H_{23}N_7O_6 + H_2O}$$

$$\mathrm{5{,}10{-}methenyl{-}H_4folate^+ + NADPH \overset{MTD}{\rightleftharpoons} 5{,}10{-}methylene{-}H_4folate + NADP^+}$$
$$\mathrm{C_{20}H_{22}N_7O_6 + C_{21}H_{30}N_7O_{17}P_3 \rightleftharpoons C_{20}H_{23}N_7O_6 + C_{21}H_{29}N_7O_{17}P_3}$$

$$\mathrm{5{,}10{-}methylene{-}H_4folate + 2\,NADH + Fd_{ox} \overset{MTR}{\rightleftharpoons} 5\text{-}methyl{-}H_4folate + 2\,NAD^+ + Fd_{red}{}^{2-}}$$
$$\mathrm{C_{20}H_{23}N_7O_6 + 2\,C_{21}H_{29}N_7O_{14}P_2 + Fd \rightleftharpoons C_{20}H_{25}N_7O_6 + 2\,C_{21}H_{28}N_7O_{14}P_2 + Fd}$$

$$\mathrm{5\text{-}methyl{-}H_4folate + Co(I)CFeSP + H^+ \overset{MTS}{\rightleftharpoons} H_4folate + methyl{-}Co(III)CFeSP^+}$$
$$\mathrm{C_{20}H_{25}N_7O_6 + H + Co(I)CFeSP \rightleftharpoons C_{19}H_{23}N_7O_6 + Co(III)CFeSP{-}CH_3}$$

$$\mathrm{CO + CoA + methyl{-}Co(III)CFeSP^+ \overset{ACS}{\rightleftharpoons} CH_3(CO)CoA + Co(I)CFeSP + H^+}$$
$$\mathrm{CO + C_{21}H_{36}N_7O_{16}P_3S + Co(III)CFeSP{-}CH_3 \rightleftharpoons C_{23}H_{38}N_7O_{17}P_3S + Co(I)CFeSP + H^+}$$

Reaction 3: Full equation from HCOOH to acetylCoA;

$$\mathrm{HCOOH + ATP + H^+ + NADPH + 2\,NADH + Fd_{\mathit{o}}x + CO + CoA \rightleftharpoons}$$
$$\mathrm{CH_3(CO)CoA + ADP + P_{\mathit{i}} + H_2O + NADP^+ + 2\,NAD^+ + Fd_{red}{}^{2-}}$$

$$\mathrm{CH_2O_2 + C_{10}H_{15}N_5O_{13}P_3 + H + C_{21}H_{30}N_7O_{17}P_3 + 2\,C_{21}H_{29}N_7O_{14}P_2 + Fd + CO +}$$
$$\mathrm{C_{21}H_{36}N_7O_{16}P_3S \rightleftharpoons C_{23}H_{38}N_7O_{17}P_3S + C_{10}H_{14}N_5O_{10}P_2 + H_3PO_4 + H_2O +}$$
$$\mathrm{C_{21}H_{29}N_7O_{17}P_3 + 2\,C_{21}H_{28}N_7O_{14}P_2 + Fd}$$

Pathway from acetylCoA to acetate:

$$\mathrm{CH_3(CO)CoA + P}_i \overset{\mathrm{PTA}}{\rightleftharpoons} \mathrm{CH_3(CO)P}_i + \mathrm{CoA}$$
$$\mathrm{C_{23}H_{38}N_7O_{17}P_3S + H_3PO_4} \rightleftharpoons \mathrm{C_2H_5O_5P + C_{21}H_{36}N_7O_{16}P_3S}$$

$$\mathrm{CH_3(CO)P}_i + \mathrm{ADP} \overset{\mathrm{ACK}}{\rightleftharpoons} \mathrm{Acetate + ATP}$$
$$\mathrm{C_2H_5O_5P + C_{10}H_{14}N_5O_{10}P_2} \rightleftharpoons \mathrm{C_2H_4O_2 + C_{10}H_{15}N_5O_{13}P_3}$$

Reaction 4: Full equation from AcetylCoA to acetate

$$\mathrm{CH_3(CO)CoA + ADP + P}_i \rightleftharpoons \mathrm{Acetate + CoA + ATP}$$
$$\mathrm{C_{23}H_{38}N_7O_{17}P_3S + C_{10}H_{14}N_5O_{10}P_2 + H_3PO_4} \rightleftharpoons \mathrm{C_2H_4O_2 + C_{21}H_{36}N_7O_{16}P_3S + C_{10}H_{15}N_5O_{13}P_3}$$

Pathway direct to acetaldehyde:

$$\mathrm{CH_3(CO)CoA + NAD(P)H + H^+} \overset{\mathrm{ADA}}{\rightleftharpoons} \mathrm{Acetaldehyde + CoA + NAD(P)^+}$$
$$\mathrm{C_{23}H_{38}N_7O_{17}P_3S + C_{21}H_{30}N_7O_{17}P_3 + H} \rightleftharpoons \mathrm{C_2H_4O + C_{21}H_{36}N_7O_{16}P_3S + C_{21}H_{29}N_7O_{17}P_3}$$

Pathway from acetate to ethanol:

$$\mathrm{Acetate + 2\,H^+ + Fd_{red}{}^{2-}} \overset{\mathrm{AOR}}{\rightleftharpoons} \mathrm{Acetaldehyde + H_2O + Fd_{ox}}$$
$$\mathrm{C_2H_4O_2 + 2\,H + Fd} \rightleftharpoons \mathrm{C_2H_4O + H_2O + Fd}$$

$$\mathrm{Acetaldehyde + NADH + H^+} \overset{\mathrm{ADH}}{\rightleftharpoons} \mathrm{Ethanol + NAD^+}$$
$$\mathrm{C_2H_4O + C_{21}H_{29}N_7O_{14}P_2 + H} \rightleftharpoons \mathrm{C_2H_6O + C_{21}H_{28}N_7O_{14}P_2}$$

Reaction 5: Full equation from acetate to ethanol:

$$\mathrm{Acetate + 3\,H^+ + NADH + Fd_{red}{}^{2-}} \rightleftharpoons \mathrm{Ethanol + NAD^+ + H_2O + Fd_{ox}}$$
$$\mathrm{C_2H_4O_2 + 3\,H + C_{21}H_{29}N_7O_{14}P_2 + Fd} \rightleftharpoons \mathrm{C_2H_6O + C_{21}H_{28}N_7O_{14}P_2 + H_2O + Fd}$$

Reaction 6: Pathway + full equation from acetyl-CoA to pyruvate:

$$\mathrm{AcetylCoA + CO_2 + 2\,H^+ + Fd_{red}{}^{2-}} \overset{\mathrm{PFOR}}{\rightleftharpoons} \mathrm{Pyruvate + Fd_{ox} + \mathit{CoA}}$$
$$\mathrm{C_{23}H_{38}N_7O_{17}P_3S + CO_2 + 2\,H + Fd} \rightleftharpoons \mathrm{C_3H_4O_3 + Fd + C_{21}H_{36}N_7O_{16}P_3S}$$

Pathway from pyruvate to butane-2,3-diol:

$$\mathrm{2\,Pyruvate} \overset{\mathrm{ALsS}}{\rightleftharpoons} \mathrm{Acetolactate + CO_2}$$
$$\mathrm{2\,C_3H_4O_3} \rightleftharpoons \mathrm{C_5H_8O_4 + CO_2}$$

$$\mathrm{Acetolactate} \overset{\mathrm{ALDC}}{\rightleftharpoons} \mathrm{Acetoin + CO_2}$$
$$\mathrm{C_5H_8O_4} \rightleftharpoons \mathrm{C_4H_8O_2 + CO_2}$$

$$\text{Acetoin} + \text{NAD(P)H} + \text{H}^+ \overset{\text{2,3-BDH/CaADH}}{\rightleftharpoons} \text{Butane-2,3-diol} + \text{NAD(P)}^+$$
$$\text{C}_4\text{H}_8\text{O}_2 + \text{C}_{21}\text{H}_{30}\text{N}_7\text{O}_{17}\text{P}_3 + \text{H}^+ \rightleftharpoons \text{C}_4\text{H}_{10}\text{O}_2 + \text{C}_{21}\text{H}_{29}\text{N}_7\text{O}_{17}\text{P}_3$$

Reaction 7: Full Equation from pyruvate to butane-2,3-diol:

$$2\,\text{Pyruvate} + \text{NAD(P)H} + \text{H}^+ \rightleftharpoons \text{Butane-2,3-diol} + \text{NAD(P)}^+ + 2\,\text{CO}_2$$
$$2\,\text{C}_3\text{H}_4\text{O}_3 + \text{C}_{21}\text{H}_{30}\text{N}_7\text{O}_{17}\text{P}_3 + \text{H} \rightleftharpoons \text{C}_4\text{H}_{10}\text{O}_2 + \text{C}_{21}\text{H}_{29}\text{N}_7\text{O}_{17}\text{P}_3 + 2\,\text{CO}_2$$

B. Bioenergetics C. autoethanogenum

Bioenergetics for the formation of acetic acid (Figure B.1), ethanol (Figure B.2) and butane-2,3-diol (Figure B.3) from CO. Red numbers denote the consumption, production or transfer of protons. Calculations presented in red denotes the net proton loss after after the production of acetic acid. This loss is restored by the transfer of protons by ATPase, creating ATP.

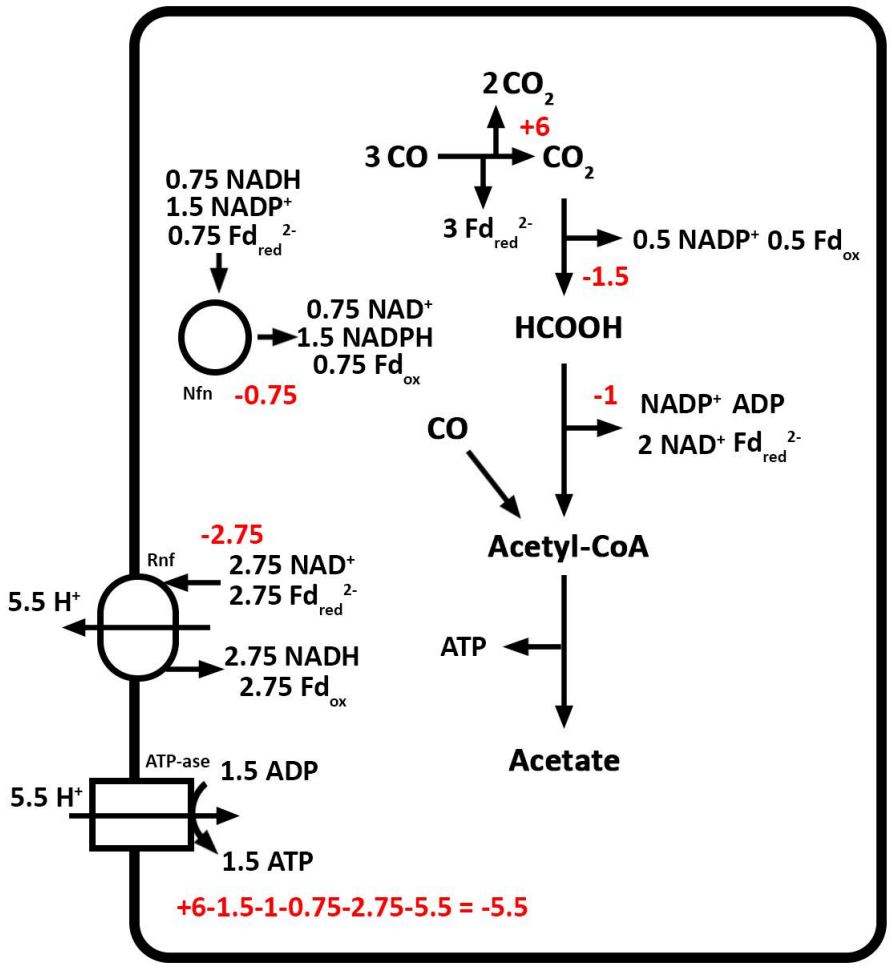

Figure B.1: Bioenergetics for acetic acid production from CO

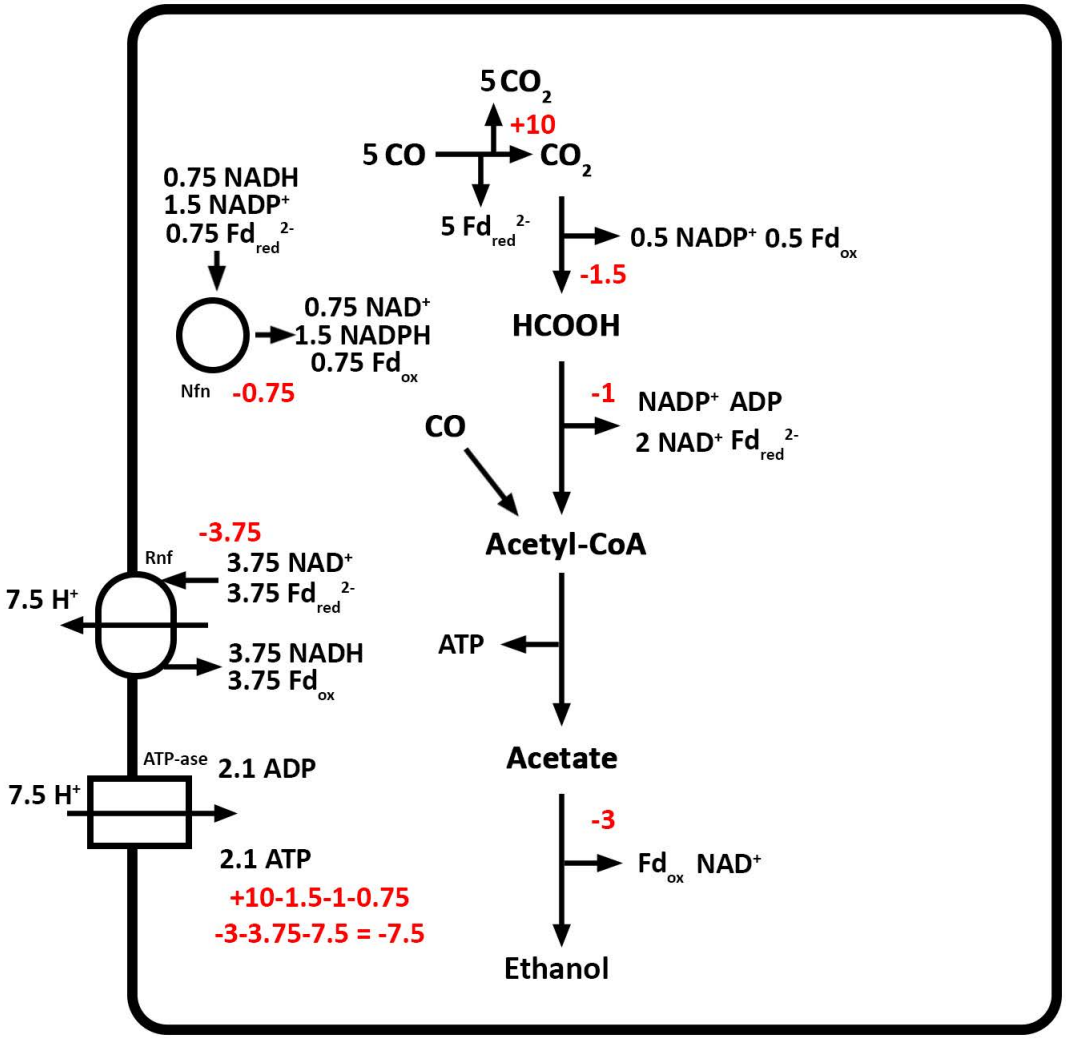

Figure B.2: Bioenergetics for ethanol production from CO

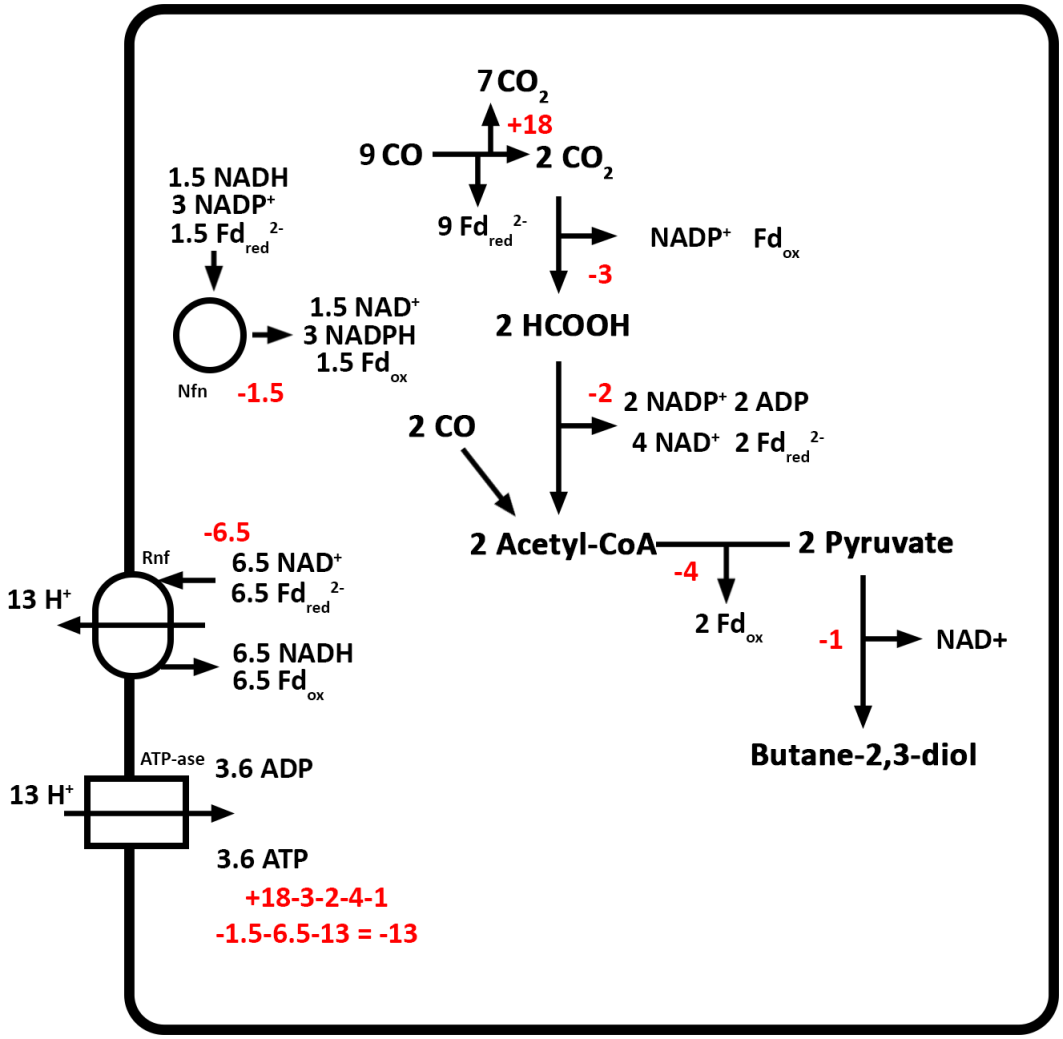

Figure B.3: Bioenergetics for butane-2,3-diol production from CO

C. Biomass formula

A chemical formula for *C.autoethanogenum* has to be used to perform calculations and modeling. In Norman et al. [34], computational work was conducted estimating the average percentages of types of macromolecules making up *C.auto*. These numbers are shown in the 3rd column of Table C.1.

Average elemental compositions of these macromolecules was set-up as follows. In Norman et al. [34], the amino acid proportions present in *C.autoethanogenum* have been estimated. Using this information, the average elemental composition for proteins of *C.autoethanogenum* was calculated. The same is done for the 'other' components, which consisted mainly of cellular metabolites (NADH, CoA, H_4Folate etc.). The elemental composition of RNA, DNA and carbohydrates have been extracted from previous work. The elemental composition for lipids are determined assuming a phospholipid/ neutral fat ratio of 4:1. The corresponding compositions of these species are $CH_{1.91}O_{0.23}N_{0.02}P_{0.02}$ and $CH_{1.84}O_{0.12}$. For Teuchoic acid, the structural formula of the repeat unit found in *Micrococcaceae*, a bacteria alike *C.autoethanogenum*, has been used [48].

Macromolecule	Elemental composition	percent by weight
Protein	$CH_{1.58}O_{0.33}N_{0.29}S_{0.0077}P_{0.10}$	26,3
DNA	$CH_{1.15}O_{0.62}N_{0.39}P_{0.10}$	14,6
RNA	$CH_{1.25}O_{0.75}N_{0.38}P_{0.11}$	17,9
Lipids	$CH_{1.89}O_{0.21}N_{0.016}P_{0.016}$	21,0
Polysacharide	$CH_{1.67}O_{0.83}$	10,2
Teuchoic acid	$CH_{2.15}N_{0.076}O_{1.31}$	0,6
Other	$CH_{1.33}N_{0.34}O_{1.61}S_{0.0048}P_{0.087}$	9,4

Table C.1: Biomass composition estimate for *C.autoethanogenum*

Averaging out, the elemental composition of *C.autoethanogenum* equals $CH_{1.52}N_{0.28}O_{0.46}S_{0.0059}P_{0.042}$.

D. Dry Cellular Weight

To convert measured optical density at 600 nm (OD_{600}) to dry cellular weight per liter (gDCW/L), a calibration was made. An already existing calibration obtained by a BSc student (Usama Nazeem) was checked and expanded.

Two 60 mL samples with OD_{600} values of 0.410 and 0.816 were taken from obtained bacterial colonies. Samples were centrifuged at 15000 rpm for 2.5 hours, creating a biomass 'cake' and liquid. The liquid was removed and replaced with 60 mL dH_2O. Samples were centrifuged again for 30 minutes. The formed biomass cake was spread over a alumina cup and placed in the oven at 80 °C for 48 hours to ensure complete removal of all liquid. Initial weight of the alumina cups was noted down. After 48 hours, samples are weighted again. Subtracting this weight from the initial weight of the alumina cup yields the dry cellular weight for 60 mL of the bacterial colony. This results in a relation between measured OD_{600} and gram dry cellular weight per liter.

For OD_{600} = 0.410, an average value of 0.136 gDCW/L was obtained (sd = 0). For OD_{600} = 0.816, an average value of 0.270 gDCW/L was obtained (sd = 0.0012). The previously obtained correlation was $gDCW/L = \frac{OD_{600}-0.1477}{1.9962}$. In Figure D.1, the fit between experimental points and this correlation is shown. For OD_{600} = 0.410, this correlation yields an outcome of 0.1314 gDCW/L, a 3 % deviation from the measured value. For the For the OD_{600} = 0.816, this correlation yields an outcome of 0.3348 gDCW/L, deviating 20% from the measured value. This concludes that the correlation is less suitable for higher OD_{600} values.

By conducting this experiment for a wide range of OD_{600} values, a more accurate correlation describing dry cellular weight can be obtained.

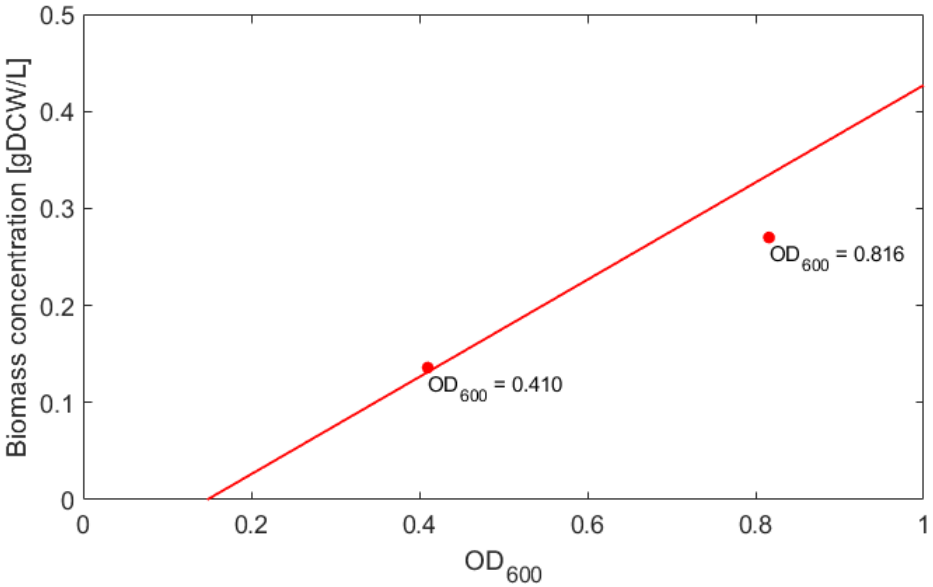

Figure D.1: Correlation between OD_{600} and grams of dry cellular weight

E. Elemental analysis of biomass experiment

An attempt was made to determine the atomic biomass composition using an elemental analyzer. A biomass sample was obtained by centrifuging and drying using the same procedure as described in Figure D. Samples were packed in alumina and analysed in a Thermo Scientific Elemental Analyser to determine carbon, hydrogen, nitrogen and sulfur ratios. Samples were analysed in duplicate, yielding the following average elemental composition of biomass: C: 0.189%, H: 71.021%, N: 10.049 %. Converting this to a chemical formula for biomass yields $\mathbf{CH_{3.75}N_{0.51}}$.

Comparing this formula to the obtained value as described in Appendix C shows a much higher presence of hydrogen. This could possibly be explained by traces of H_2O still present in the sample. By vacuuming the sample before analysis, these traces might be removed. It is therefore advised to repeat the experiment and exposing the sample to a vacuum for a long period of time. The outcome of the experiment can be compared to the currently obtained formula. In addition, oxygen percentage can be determined using the elemental analyser.

F. Complete mass balances

In this section, the general gas, liquid and solid(bacterial) balances for a reactor system with continuous fermentation is shown. A continuous gas flow is present in the reactor, leading to a describe this phase as a CSTR. In reality, for a spinning disk reactor, the gas phase should be modeled by CSTRs in series. The liquid phase is recycled in the set-up. In addition, a certain amount of liquid is extracted and refreshed with new medium. This is expressed using the dilution factor D in $\frac{1}{h}$. For the solid or 'bacterial' balances, ideal mixing within the bacteria is assumed. At last, no mass transfer between the gas phase and the bacteria is assumed.

F.0.1 Gas Balance

$$\frac{dN_{G,m}}{dt} = V_G \frac{dC_{G,m}}{dt} = \phi_{G,in} C_{0,m} - \phi_G C_{G,m} - k_L a_{GL} (PH_m - C_{L,m}) V_R \tag{F.1}$$

$$\frac{dC_{G,m}}{dt} = \frac{\phi_{G,in} P_0 y_{m,0}}{RTV_G} - \frac{\phi_G P y_m}{RTV_G} - k_L a_{GL} (PH_m - C_{L,m}) \tag{F.2}$$

Where

- $\frac{dC_{G,m}}{dt} = \left[\frac{mol_G}{m_G^3 \cdot h}\right]$
- ϕ_G = Gas flow $\left[\frac{m_G^3}{h}\right]$
- P = Pressure $\left[\frac{kg}{m_G \cdot s^2}\right]$ or $[Pa]$
- y_m = Partial gas fraction $[-]$
- R = Gas constant $\left[\frac{\frac{kg \cdot m_G^3}{s}}{mol \cdot K}\right]$
- T = Temperature in $[K]$
- V_G = Gas volume in reactor $[m_G^3]$
- k_L = Gas liquid mass transfer coefficient, $\left[\frac{m_L^3}{m_{int}^2 \cdot h}\right]$
- a_{GL} = Gas liquid mass transfer interfacial area $\left[\frac{m_{int}^2}{m_G^3}\right]$
- H_m = Henry's coefficient $\left[\frac{mol}{Pa \cdot m_L^3}\right]$
- $C_{L,m}$ = Liquid concentration of component m $\left[\frac{mol}{m_L^3}\right]$

Unit check

$$\frac{mol}{m_G^3 \cdot h} = \frac{m_G^3}{h} \cdot \frac{kg}{m_G \cdot s^2} \cdot - \cdot \frac{mol \cdot K \cdot s^2}{kg \cdot m_G^2} \cdot \frac{1}{K} \cdot \frac{1}{m_G^3} - \frac{m_L^3}{m_{int}^2 \cdot h} \frac{m_{int}^2}{m_G^3} \left(\frac{kg}{m_G \cdot s^2} \cdot \frac{mol}{\frac{kg}{m_G \cdot s^2} m_L^3} - \frac{mol}{m_L^3} \right) \tag{F.3}$$

F.0.2 liquid balance

$$\frac{dN_{L,m}}{dt} = V_L \frac{dC_{L,m}}{dt} = k_L a_{GL}(PH_m - C_{L,m})V_R - k_{LB}a_{LB}\left(\frac{C_{L,m}}{m_{LB}} - C_{B,m}\right)V_B - V_L C_{L,m} D \quad \text{(F.4)}$$

Devide by V_L add in dependencies

$$\frac{dC_{L,m}}{dt} = k_L a_{GL}\frac{\epsilon_G}{\epsilon_L}(PH_m - C_{L,m}) - \frac{D_{L\to B}}{\delta_{cellwall}}\frac{A_{cell}}{V_{cell}}\left(\frac{C_{L,m}}{m_{LB}} - C_{B,m}\right)\frac{\frac{XV_L}{\rho_B}}{V_L} - C_{L,m}D \quad \text{(F.5)}$$

$$\frac{dC_{L,m}}{dt} = k_L a_{GL}\frac{\epsilon_G}{\epsilon_L}(PH_m - C_{L,m}) - \frac{p_m}{K_{p,m}}\frac{A_{cell}}{V_{cell}}\left(\frac{C_{L,m}}{m_{LB}} - C_{B,m}\right)\frac{X}{\rho_b} - C_{L,m}D \quad \text{(F.6)}$$

Where

- $\frac{dC_{L,m}}{dt} = \left[\frac{mol}{m_L^3 \cdot h}\right]$
- P = Pressure $\left[\frac{kg}{m_G \cdot s^2}\right]$ or $[Pa]$
- k_L = Gas liquid mass transfer coefficient, $\left[\frac{m_L^3}{m_{int}^2 \cdot h}\right]$
- a_{GL} = Gas liquid mass transfer interfacial area $\left[\frac{m_{int}^2}{m_G^3}\right]$
- ϵ_G = Gas fraction $\left[\frac{m_G^3}{m_R^3}\right]$
- ϵ_L = Liquid fraction $\left[\frac{m_L^3}{m_R^3}\right]$
- H_m = Henry's coefficient $\left[\frac{mol}{Pa \cdot m_L^3}\right]$
- p_m = Permeability $\left[\frac{m_{B,int}}{h}\right]$
- $K_{p,m}$ = Partition coefficient $[-]$
- A_{cell} = Superficial area bacteria cell $[m_{B,int}^2]$
- V_{cell} = Superficial volume bacteria cell $[m_B^3]$
- m_{LB} = Distribution coefficient $\left[\frac{m_B^3}{m_L^3}\right]$
- $C_{B,m}$ = Concentration of component m in bacteria $\left[\frac{mol}{m_B^3}\right]$
- X = Bacteria concentration $\left[\frac{kg}{m_L^3}\right]$
- ρ_B = Bacteria density $\left[\frac{kg_B}{m_B^3}\right]$
- D = Dilution rate $\left[\frac{1}{h}\right]$

$$\frac{mol}{m_L^3 \cdot h} = \frac{m_L^3}{m_{int}^2 \cdot h}\frac{m_{int}^2}{m_G^3} \cdot \frac{m_G^3}{m_R^3} \cdot \frac{m_R^3}{m_L^3}\left(\frac{kg}{m_G \cdot s^2} \cdot \frac{mol}{\frac{kg}{m_G \cdot s^2} m_L^3} - \frac{mol}{m_L^3}\right) - \frac{m_{B,int}}{s}\frac{m_{B,int}^2}{m_B^3}\left(\frac{mol}{m_L^3} \cdot \frac{m_L^3}{m_B^3} - \frac{mol}{m_B^3}\right) \cdot \frac{kg}{m_L^3} \cdot \frac{m_B^3}{kg} - \frac{mol}{m_L^3} \cdot \frac{1}{h}$$

F.0.3 Solid/ Bacteria Balances

$$\frac{dN_{B,m}}{dt} = V_B \frac{dC_{B,m}}{dt} = k_{LB} a_{LB} \left(\frac{C_{L,m}}{m_{LB}} - C_{B,m} \right) V_B - \sum R_m \tag{F.7}$$

$$\frac{dC_{B,m}}{dt} = \frac{p_m}{K_{p,m}} \frac{A_{cell}}{V_{cell}} \left(\frac{C_{L,m}}{m_{LB}} - C_{B,m} \right) - \frac{\rho_B}{X V_L} \sum R_m \tag{F.8}$$

- $\frac{dC_{B,m}}{dt}$ = Change in concentration of component m in bacterial cells $[\frac{mol}{m_B^3 \cdot h}]$
- p_m = Permeability $\left[\frac{m_{B,int}}{h}\right]$
- $K_{p,m}$ = Partition coefficient $[-]$
- A_{cell} = Superficial area bacteria cell $[m_{B,int}^2]$
- V_{cell} = Superficial volume bacteria cell $[m_B^3]$
- m_{LB} = Distribution coefficient $\left[\frac{m_B^3}{m_L^3}\right]$
- $C_{B,m}$ = Concentration of component m in bacteria $\left[\frac{mol}{m_B^3}\right]$
- X = Bacteria concentration $\left[\frac{kg}{m_L^3}\right]$
- ρ_B = Bacteria density $\left[\frac{kg_B}{m_B^3}\right]$

Unit check

$$\frac{mol}{m_B^3 \cdot h} = \frac{m_{B,int}}{h} \frac{m_{B,int}^2}{m_B^3} \left(\frac{mol}{m_L^3} \cdot \frac{m_L^3}{m_B^3} - \frac{mol}{m_B^3} \right) - \frac{kg}{m_B^3} \cdot \frac{m_L^3}{kg} \cdot \frac{1}{m_L^3} \sum \frac{mol}{h}$$

G. Bacterial mass balances

Here, all reactions terms are defined per intracellular component.

$$\frac{dC_{CO}}{dt} = R_1 - R_{-1} - R_3 \tag{G.1}$$

$$\frac{dC_{H_2}}{dt} = -R_{2a} - 2R_{E_1} + 2R_{E_{-1}} \tag{G.2}$$

$$\frac{dC_{CO2}}{dt} = -R_1 + R_{-1} - R_{2a} - 2R_{2b} - R_6 + 2 * R_7 \tag{G.3}$$

$$\frac{dC_{HCOOH}}{dt} = +R_{2a} + 2R_{2b} - R_3 \tag{G.4}$$

$$\frac{dC_{CoA}}{dt} = -R_3 + R_4 + R_6 \tag{G.5}$$

$$\frac{dC_{AcetylCoA}}{dt} = +R_3 - R_4 - R_6 \tag{G.6}$$

$$\frac{dC_{Acetate}}{dt} = +R_4 - R_5 \tag{G.7}$$

$$\frac{dC_{Pyruvate}}{dt} = +R_6 - 2R_7 \tag{G.8}$$

$$\frac{dC_{Ethanol}}{dt} = +R_5 \tag{G.9}$$

$$\frac{dC_{Buta-2,3-diol}}{dt} = +R_7 \tag{G.10}$$

$$\frac{dC_{H+}}{dt} = -2R_1 + 2R_{-1} - 3R_{2b} - R_3 - 3R_5 - R_7 + 3R_{E_1} - 3R_{E_{-1}} - R_{E_2} + R_{E_{-2}} - R_{E_3} \tag{G.11}$$

$$\frac{dC_{Fd_{ox}}}{dt} = R_1 - R_{-1} + R_{2b} - R_3 + R_5 + R_6 - R_{E_{-1}} + R_{E_1} + R_{E_2} - R_{E_{-2}} + R_{E_3} \tag{G.12}$$

$$\frac{dC_{Fd_{red}}}{dt} = -R_1 + R_{-1} - R_{2b} + R_3 - R_5 - R_6 + R_{E_{-1}} - R_{E_1} - R_{E_2} + R_{E_{-2}} - R_{E_3} \tag{G.13}$$

$$\frac{dC_{NADH}}{dt} = -2R_3 - R_5 - R_{E_2} + R_{E_{-2}} + R_{E_3} \tag{G.14}$$

$$\frac{dC_{NAD+}}{dt} = +2R_3 + R_5 + R_{E_2} - R_{E_{-2}} - R_{E_3} \tag{G.15}$$

$$\frac{dC_{NADPH}}{dt} = -R_{2b} - R_3 - R_7 + R_{E_1} - R_{E_{-1}} + 2R_{E_2} - 2R_{E_{-2}} \tag{G.16}$$

$$\frac{dC_{NADP+}}{dt} = R_{2b} + R_3 + R_7 - R_{E_1} + R_{E_{-1}} - 2R_{E_2} + 2R_{E_{-2}} \tag{G.17}$$

$$\frac{dC_{ATP}}{dt} = -R_3 + R_4 + R_{E_4} \tag{G.18}$$

$$\frac{dC_{ADP}}{dt} = +R_3 - R_4 - R_{E_4} \tag{G.19}$$

$$\frac{dC_{Pi}}{dt} = +R_3 - R_4 - R_{E_4} \tag{G.20}$$

H. Assumptions reaction terms

In this section, assumptions for the reaction terms as stated in Appendix I are defined.
To start, current rate expressions describe one, or a combination of enzymatic reactions, as described in subsection 2.2.4 and Appendix A. The reaction rate of an enzymatic reaction is dependent on both substrate and enzyme concentration, pH and temperature. Given a fixed enzyme concentration, the reaction rate increases as the substrate concentration increases, until a certain maximum substrate concentration is reached. At this point, all reaction sites of the available enzymes are occupied and the reaction rate is at its maximum [20].

In biology, enzymatic reaction rates are often expressed using Michaelis Menten kinetics [20]. These expressions contains the term '$Vmax$', the enzym's maximum rate where an increase in substrate concentration doesn't lead to an increase in reaction rate anymore. These kinetics also contain the term 'Km', the substrate concentration at which the rate is $0.5 \cdot Vmax$ to describe the rate as a function of the substrate concentration. This means that the reaction rates of the reactions present in the metabolism of *C. autoethanogenum* has one fixed maximum rate, at the point when the saturation substrate concentration is reached.
This leads to the following questions:

1. What are the substrates' saturation concentrations for the enzymes included in the enzymatic reaction schemes? What enzymes are usually performing at their maximum rate?

2. What is the maximum reaction rate when the substrate saturation concentration is reached?

3. What is the pH an T optimum for each enzyme?

4. What is the total enzyme concentration? Can C.auto increase the enzyme concentration depending on changing circumstances within the cell?

To answer these questions, it is important to discuss the purpose of the model. Its purpose is to demonstrate what the effect of varying gas compositions and pH environments have on the product composition. It is therefore assumed that reaction rates directly describing product concentrations don't have a fixed value and are dependent on substrate concentrations. This will otherwise always lead to the same distribution of product concentrations. This concerns reactions R_4, R_5, R_6, and R_7 in subsection 2.2.4.

The next step is to define the reaction terms. Both mass action kinetics and Michaelis Menten kinetics could be used. To avoid imposing boundaries that aren't present by introducing random values for Vmax, mass action terms are used. The reaction terms are shown in Appendix H. The assumptions are made leading to the described reaction term:

1. for R_1 and R_{-1}, it is assumed that the substrate saturation concentration is reached, meaning that the reaction rate has a constant value. This assumption can be made when a large enough inflow of CO or CO2 into the bacteria is present. To keep the flux through the WLP constant, and enhance the effect of changing product compositions, the equilibrium describing the CODH enzyme, thus R_1 and R_{-1} is assumed to be constant. This means that the reaction is zero-th order in CO_2, H^+, Fd, CO and H_2O. The resulting reaction term is shown in Appendix I.

2. When CO_2 and H_2 are present as a gas substrate reaction, R_{2a} is the preferred reaction. When CO_2 and H_2 are not present in the gas feed, CO_2 has to react via R_{2b}. For the model, it is assumed that the substrate concentrations have reached the saturation concentration, resulting in R_{2a} and R_{2b} having one fixed reaction rate. This moreover implies that E_{-1} is the preferred reaction under CO_2 and H_2 poor conditions. As R_{2b} and E_1 are equal reactions, E_{-1} needs to be switched off in the model under CO2 and H2 poor conditions.

3. R_3 is a combination of 6 enzymatic reactions. One of these is rate limiting, determining the reaction rate. With 6 reactions, it can be assumed that this one rate limiting reaction performs at its maximum rate, leading to the assumption that the combination of reactions under R_3 perform at one fixed rate. This leads to the assumption that the reaction is zeroth order in all components.

4. After R_1 - R_3, acetylCoA is formed. It is assumed that two pathways are possible from now on; leading to the formation of acetate or pyruvate (R_4 and R_6). One could assume that the concentration of acetylCoA have an influence on the reaction rates of these reactions. Looking at the substrates of both reactions, only ADP + Pi is needed for R_4 and for R_6, CO_2, H^+ and Fd^{2-}_{red} is needed. The same assumption for CO_2 being at the saturation concentration can moreover be made. Furthermore the assumption is made that enough protons are present to reach the substrate saturation concentration. This leads to the assumption that the rate of R_4 is only dependent on the concentration of ADP and that the rate of R_6 is only dependent on Fd^{2-}_{red}. When acetylCoA is included, this has not really an influence, as now two different components (ADP and Fd^{2-}_{red} determine the ratio of reaction rates R_4/R_6.

5. R_5 is the next reaction that needs to be discussed. In *C. autoethanogenum*, acetate can both diffuse in and out of the bacterial cell as well as react further to ethanol. Acetate can only react and diffuse in its protonated form. The cell wants to prevent a too acidic environment, thus releasing acetate into the environment or converting it to ethanol. As the model doesn't implement mass transfer of components from the cell to the liquid medium, the acetate concentration will build up. Therefore, it is more convenient to cut the dependency of the rate of R_5 on the acetate concentration and let R_5 only be dependent on the NADH and Fd^{2-}_{red} concentration.

6. R_7 concerns the combination of reactions leading to the formation of butane-2,3-diol. Pyruvate concentrations will keep on rising in the cell as no conversion to biomass is implemented yet. It is therefore assumed that this component has a zeroth order dependency on R_7, however depending on the concentration of NADPH.

7. Reactions $E_1 - E_4$ are key in determining the concentration of electron donors and ATP in the cell. It is assumed that the reactions all do depend on the concentrations of the different electron donors and their oxidized forms. For $E_3 - E4$, the proton pumps are dependent on disturbances in the proton gradient between the cell wall and the periplasm. As this isn't included in the model yet, one could do two things: make reaction E_3 dependent on Fd^{2-}_{red} and NAD^+ and include in the model that 2 protons are created when this reaction is carried out. One could state that then reaction E_4 should be carried out to account for the extra protons created in E3 at a similar rate. However, extra protons could be created or consumed during the rest of the metabolism; changing the proton gradient. As E_4 requires protons coming from the periplasm, this concentration isn't included in the rate expression. As E_3 has to make sure that enough protons are pumped out of the cell to keep the proton concentration constant so that ATPase (E_4) can pump the protons back into the cell, one could impose a boundary that if the proton concentration goes under a certain concentration reaction E_4 will instantly pump protons back into the cell until the concentration is constant again.

An important thing to note is the reaction scheme in case of a purely CO-fed case. In this case reaction 2A does not take place, as well as E_1, as these reactions are practically combined into one. E_{-1} can however still take place

1. The next question is what reaction rate constant value is picked for the reactions. Important here is that a too large acetylCoA concentration in the cell is prevented. Furthermore, the reaction constant of the different reactions may not differ too much, as than the effect of electron donor concentrations is not shown. Key here is the speed of the energy reactions,

one of those should not be dominating and depleting the other, as it is shown in section 2.2 that the system can function in a very balanced way. Therefore, the reaction rate constants for all reactions roughly have the same value, but for rate expressions that have two or more substrates, a higher value is picked, as the substrate concentrations are given a value under 1, otherwise leading to a very slow reaction rate.

2. At last, values have to be picked for the initial concentrations. These are very determining for the final product composition. Experimental data for certain conditions for the concentration of the energy carriers is available in literature. These initial concentrations fluctuate depending the gas feed composition. We looking at the purpose of the model, its goal is to highlight the change in product composition given varying gas compositions. To highlight this, a fixed initial concentration is picked.

I. Reaction terms

$$R_1 = k_1 \cdot [\mathrm{CO}]^0 \cdot [Fd_{ox}]^0 \tag{I.1}$$

$$R_{-1} = k_{-1} \cdot [\mathrm{H^+}]^0 \cdot [\mathrm{CO_2}]^0 \cdot [Fd_{red}^{-2}]^0 \tag{I.2}$$

$$R_{2a} = k_{2a} \cdot [\mathrm{CO_2}]^0 \cdot [\mathrm{H_2}]^0 \tag{I.3}$$

$$R_{2b} = k_{2b} \cdot [CO2]^0 \cdot [Fd_{red}^{-2}]^0 \cdot [NADPH]^0 \cdot [H+]^0 \tag{I.4}$$

$$R_3 = k_3 \cdot [\mathrm{HCOOH}]^0 \cdot [\mathrm{H^+}]^0 \cdot [ATP]^0 \cdot [NADPH]^0 \cdot [NADH]^0 \cdot [Fd_{ox}]^0 \cdot [\mathrm{CO}]^0 \cdot [CoA]^0 \tag{I.5}$$

$$R_4 = k_4 \cdot [\mathrm{CH_3(CO)CoA}]^0 \cdot [ADP] \cdot [P_i]^0 \tag{I.6}$$

$$R_5 = k_5 \cdot [Acetate]^0 \cdot [H+]^0 \cdot [NADH] \cdot [Fd_{red}^{2-}] \tag{I.7}$$

$$R_6 = k_6 \cdot [AcetylCoA]^0 \cdot [\mathrm{CO_2}]^0 \cdot [\mathrm{H^+}]^0 \cdot [Fd_{red}^{2-}] \tag{I.8}$$

$$R_7 = k_7 \cdot [Pyruvate]^0 \cdot [H+]^0 \cdot [NADH] \tag{I.9}$$

$$R_{E_1} = k_{E_1} \cdot [\mathrm{H_2}]^0 \cdot [NADP+] \cdot [Fd_{ox}] \tag{I.10}$$

$$R_{E_{-1}} = k_{E_{-1}} \cdot [\mathrm{NADPH}] \cdot [Fd_{red}^{2-}] \cdot [H+]^0 \tag{I.11}$$

$$R_{E_2} = k_{E_2} \cdot [\mathrm{Fd_{red}}^{2-}] \cdot [NADH] \cdot [NADP+] \cdot [H+]^0 \tag{I.12}$$

$$R_{E_{-2}} = k_{E_{-2}} \cdot [\mathrm{Fd_{ox}}] \cdot [NAD+] \cdot [NADPH] \tag{I.13}$$

$$R_{E_3} = k_{E_3} \cdot [Fd_{red}^{2-}] \cdot [NAD+] \cdot [H^+]^0 \tag{I.14}$$

$$R_{E_4} = k_{E_4} \cdot [ADP] \cdot [NAD+] \tag{I.15}$$

J. P&ID stirred vessel set-up

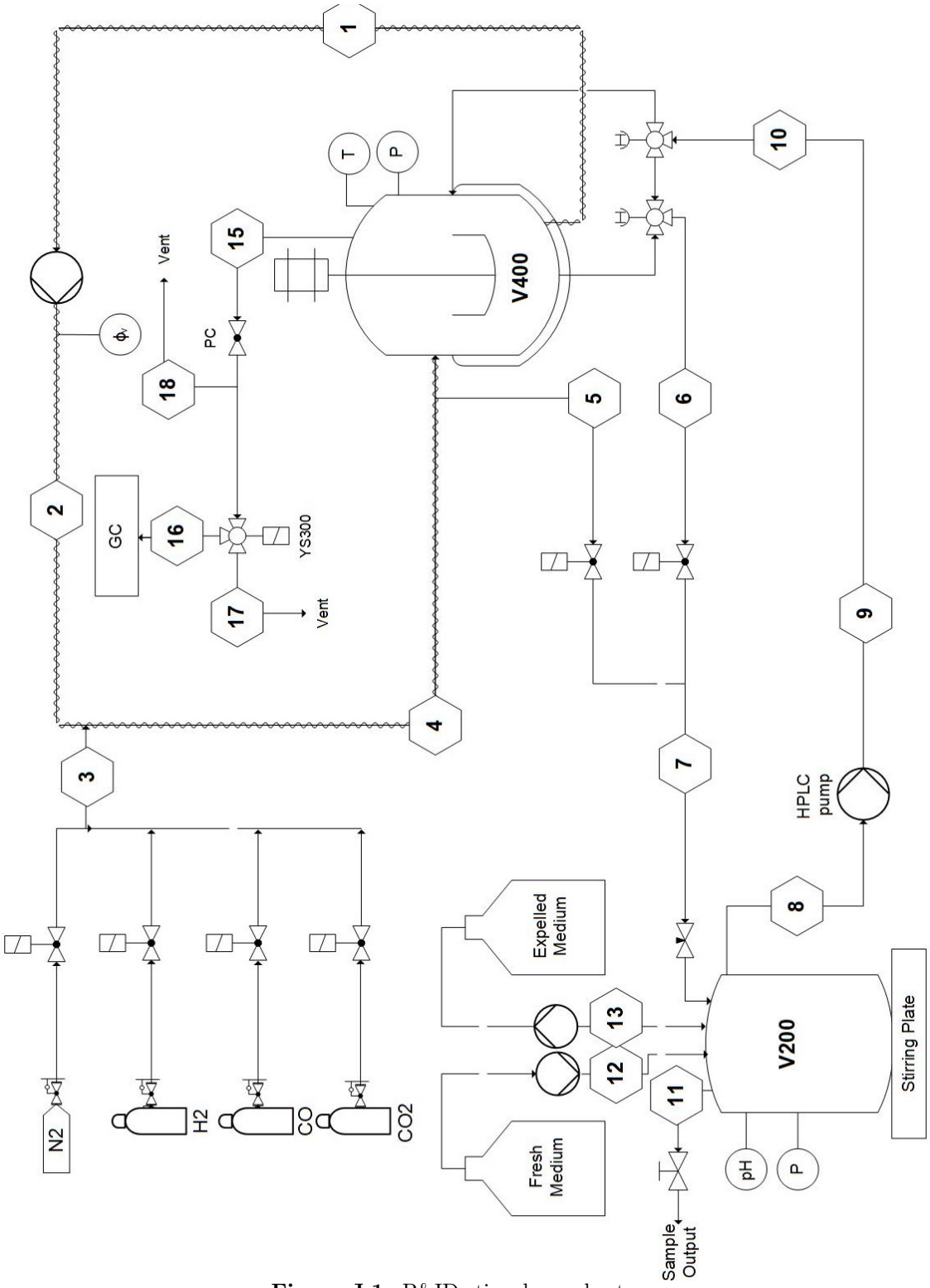

Figure J.1: P&ID stirred vessel set-up

K. Extended P&ID for stirred vessel set-up

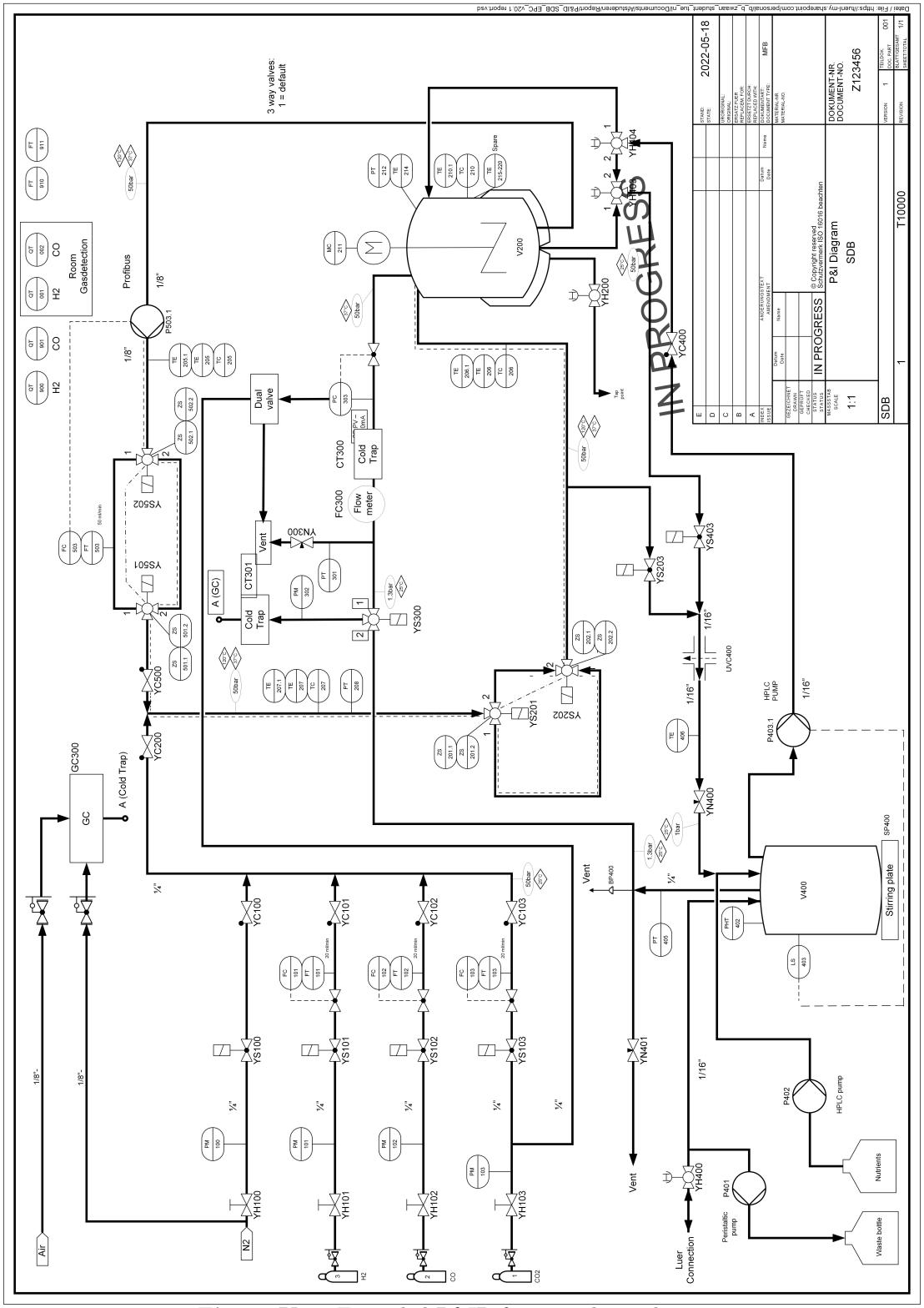

Figure K.1: Extended P&ID for stirred vessel set-up

L. P&ID for rs-SDR set-up

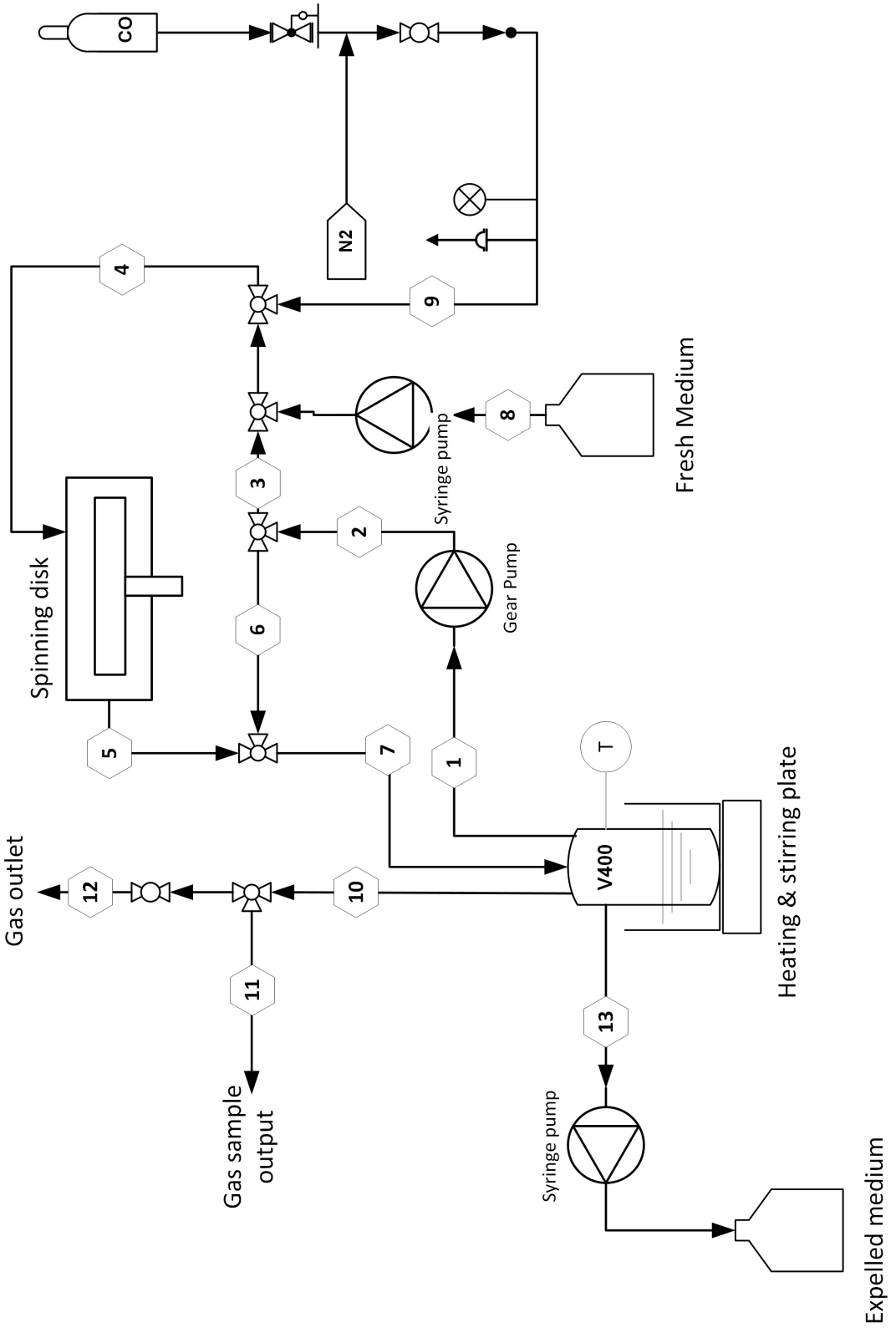

Figure L.1: P&ID for rs-SDR set-up

M. Addition experimental results stirred vessel experiment

This appendix shows additional graphs giving insight in the experiment performed in the stirred vessel set-up. In figure Figure M.1, biomass concentration is shown as a function of time. In figure Figure M.2, assumed liquid volume increase over time is depicted.

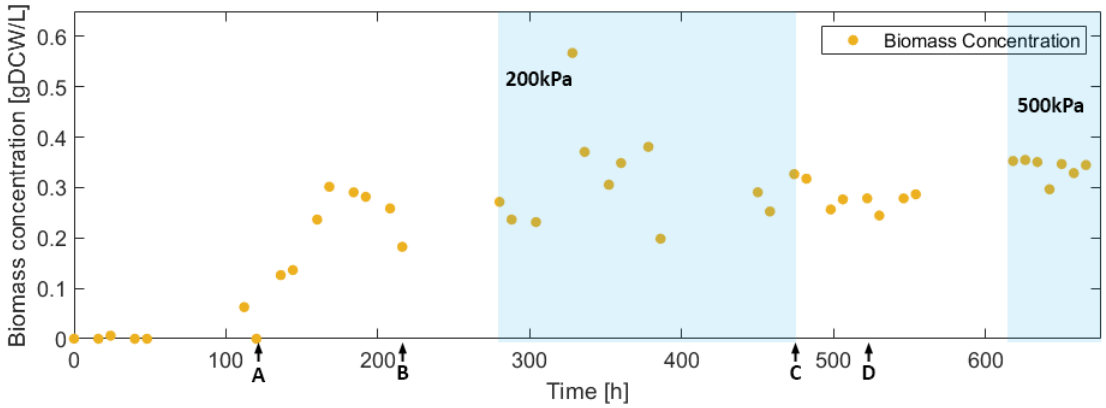

Figure M.1: Complete overview of biomass concentrations during continuous fermentation experiment in stirred vessel. ϕ_R = 100 mL/min, T = 37 , $pH_{average}$ = 5.0, $V_{reactor}$ = 2.68 L, stirrer speed = 0 RPM. Blue zones indicate the period with steady state like behaviour. At point **A** gas flow is increased to ϕ_g = 5 mL/min. At point **B** gasflow is set to ϕ_g = 10 mL/min. At point **C**, pressure increase starts with 6.25 kPa/h. At point **D**, p = 500kPa and gas flow is increased to ϕ_g = 20 mL/min.

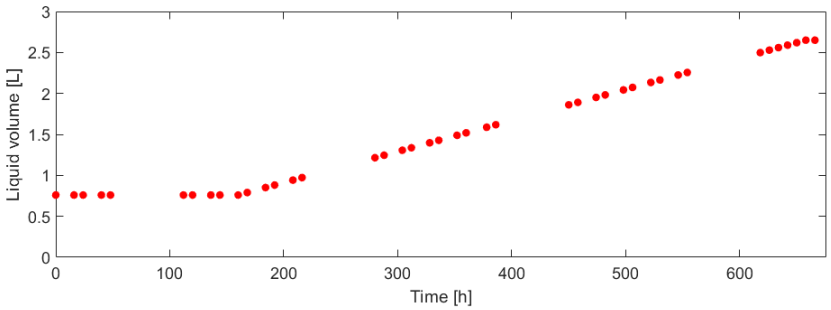

Figure M.2: Increase in liquid volume in stirred vessel experiment over time

N. Microscopical pictures C. autoethanogenum rs-SDR experiments

In this appendix, images used to analyse bacterial area using the MATLAB script as presented in Appendix O are shown.

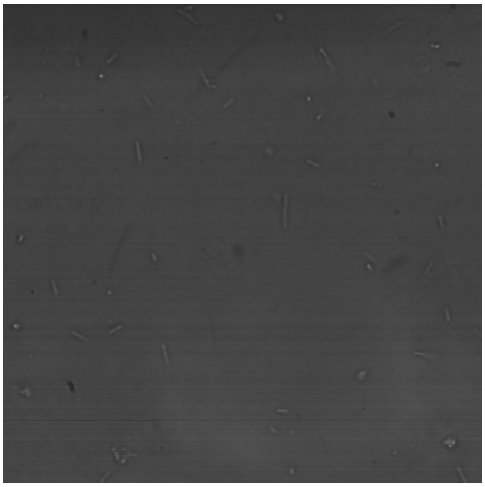

(a) Picture taken at the end of 100rpm experiment/ at the start of 500 rpm experiment

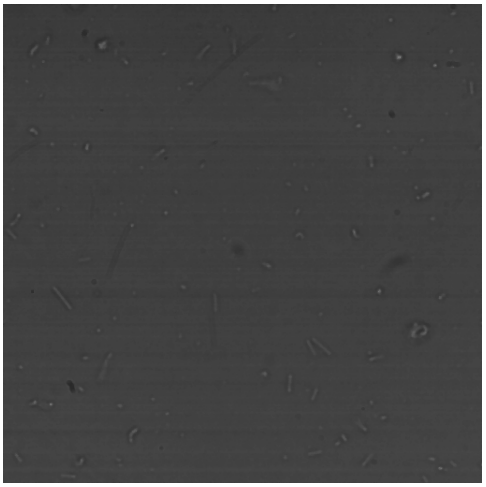

(b) Picture taken of bacteria at the end of 500 rpm experiment

(c) Picture taken of bacteria at the start of 1000 rpm experiment

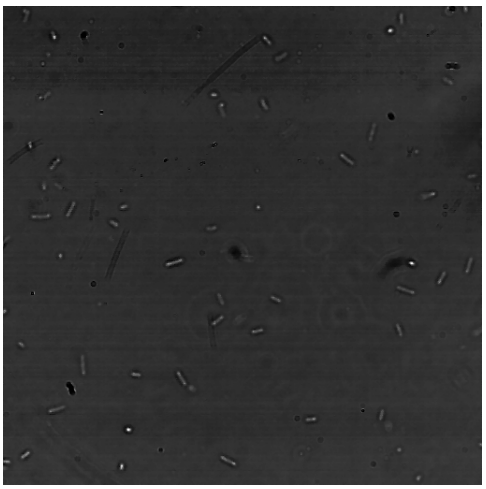

(d) Picture taken at the end of 1000 rpm experiment

Figure N.1: Microscopical pictures taken of samples extracted before and after fermentation experiments in the rs-SDR

O. Bacterial area analysis MATLAB script

```
close all; clear;

%% picture analysis constants
T = 5;          % Threshold value, below T pixels, the object neglected
P_mm = 200;     % 200 pixels per mm, determined with 1000x.tif
Nbin = 20;      % Number of bins for the Histogram
margin = 30;    % Amount of cropped pixels (remove half cells and text)

% Graph stuff
fontsize = 14;
titlesize = 14;
MS = 8;

f_col = ['b'; 'r'; 'g'; 'm'; 'c'; 'k'];
shapes = ['o'; 's'; 'd'; '^'];

%% Analysis of the images
Files = dir(fullfile("*.jpg"));     % Select all files that end with .jpg

% loop over all selected files
for i = 1:(length(Files))

    % Import figure into Matlab
%     figure(1)
    Im = imread(Files(i).name);
    imshow(Im)

    % Apply contrast based on the threshold value T
    bw = imbinarize(Im, 'adaptive');
    bw1 = bwareaopen(bw,T);

    % Show normal image and image with contrast next to each other
    imshowpair(Im,bw1,'montage')

    % Crop image, remove half cells at the boundaries and text
    croppedImage = imcrop(bw1, [0, margin, 512, 512]);
    bw1 = imclearborder(croppedImage);
    bw1 = logical(padarray(bw1, margin));

    % Create boundaries on the cells
    [B,L] = bwboundaries(bw1,'noholes');

    % Show the cells with highlighted boundaries
%     figure(2)
%     imshow(label2rgb(L,@jet,[.5 .5 .5]))
    hold on
    for k = 1:length(B)
      boundary = B{k};
      plot(boundary(:,2),boundary(:,1),'w','LineWidth',2)
    end

    % Measure the bounded cells and returns the area
    stats = regionprops(L,'Area');

    % loop over the boundaries
    for k = 1:length(B)

      % obtain (X,Y) boundary coordinates corresponding to label 'k'
      boundary = B{k};

      % obtain the area calculation corresponding to label 'k'
      area(k) = stats(k).Area;

    end

    % Convert determined area in pixels^2 to mm^2
```

```
67      area_real{i} = area*(1/P_mm)^2;
68
69  end
70
71  %% Statistical analysis of the Histrograms
72
73  clear time
74  clear RPM
75  clear rpm
76  clear i_rpm
77  clear i_time
78  clear Time
79  clear avg
80  clear mod
81  clear STD
82  clear Average
83  clear n_times
84
85  rpm = 0;
86  r = 0;
87  k = 1;
88
89  for j = 2:(length(Files) + 1)
90
91      % Split file name into parts
92      Name = split(Files(j-1).name, '_');
93      Number = split(Name{3}, '.');
94
95      % Convert string into scalar
96      rpm(j) = str2num(Name{1});
97      Time(j-1) = str2num(Name{2});
98      n = str2num(Number{1});
99
100     if rpm(j-1) ≠ rpm(j)
101         r = r + 1;
102         t = 1;
103         i_rpm(j) = j;
104     end
105
106     if n == 4
107         l = 1;
108
109         Time_mat = 1;
110         for s = k:(j-1)
111             size = length(area_real{s});
112
113             if size > l
114                 l = size;
115                 Time_mat = zeros(n,l);
116             end
117         end
118
119         for p = k:(j-1)
120             Time_mat(p,:) = sort(area_real{j-1});
121         end
122
123         Time_area = sum(Time_mat)./sum(Time_mat≠0);
124         Time_area = nonzeros(Time_area);
125
126         k = j - 1;
127         t = t + 1;
128         i_time(j) = j;
129
130         % Plot Histogram
131         if j > 2
132
133             figure(r)
```

```
134             histogram(Time_area, Nbin, 'DisplayName', Name{2}, ...
135                 'facecolor',f_col(t),'facealpha',0.7,'edgecolor','none','Normalization','probability')
136             hold on
137             title(Name{1},'interpreter','latex')
138             xlabel('Area (mm$^2$)','interpreter','latex');
139             ylabel('Normalized Count', 'Interpreter','latex');
140             set(gca,'TickLabelInterpreter','latex', 'fontsize', fontsize);
141 
142         end
143 
144     end
145 
146 legend show
147 
148     n_times{r}(t) = n;
149 
150     % Determine the average value, modulus and standard deviation
151     avg{r}(t,n) = mean(area_real{j-1}(1,:));
152     mod{r}(t,n) = mode(area_real{j-1}(1,:));
153     STD{r}(t,n) = std(area_real{j-1}(1,:));
154 
155 end
156 
157 %% Placing the data into the correct arrays
158 
159 % Remove the zeros from the index arrays
160 i_time(1) = 1;
161 Time(1) = 0;
162 i_rpm = nonzeros(i_rpm);
163 i_time = nonzeros(i_time);
164 
165 % Create rpm and Time array
166 RPM =  rpm(i_rpm(1:end));
167 time = Time(i_time(1:end));
168 time(1) = [];
169 
170 w = 0;
171 m = 1;
172 
173 for T = 1:length(time)
174 
175     if time(T) == 0
176         w = w + 1;
177         m = 1;
178     end
179 
180     Average{w}(m) = sum(avg{w}(m,:))/sum(avg{w}(m,:)≠0);
181     Modulus{w}(m) = sum(mod{w}(m,:))/sum(mod{w}(m,:)≠0);
182     Stand_dev{w}(m) = sum(STD{w}(m,:))/sum(STD{w}(m,:)≠0);
183 
184     m = m + 1;
185 end
186 
187 %% Plotting part
188 
189 % Plotting the Average size
190 figure
191 time_ = time;
192 
193 for i = 1:length(RPM)
194 
195     h = length(n_times{i});
196     % errorbar(time_(1:h),Average{i}, Stand_dev{i}, 'o', 'Color', ...
            'k','MarkerSize', MS, 'MarkerFaceColor', f_col(i), 'LineWidth', 1)
197     plot(time_(1:h),Average{i}, 'o', 'Color', 'k','MarkerSize', MS, ...
            'MarkerFaceColor', f_col(i), 'LineWidth', 1)
198     hold on
```

```
199
200     time_(1:h) = [];
201
202 end
203
204 title('Size VS time','interpreter','latex')
205 ylabel('Averaged Area (mm$^2$)','interpreter','latex');
206 xlabel('Time (h)', 'Interpreter','latex');
207 set(gca,'TickLabelInterpreter','latex', 'fontsize', fontsize);
208 xlim([-5 75])
209 legend(num2str(RPM(1)),num2str(RPM(2)),num2str(RPM(3)),num2str(RPM(4)), ...
        'Location', 'best')
210
211 figure
212 errorbar(RPM(1),mean(Average{1}), std(Average{1}), 'o', 'Color', ...
        'k','MarkerSize', MS, 'MarkerFaceColor', f_col(1), 'LineWidth', 1)
213 hold on
214 errorbar(RPM(2),mean(Average{2}), std(Average{2}), 'o', 'Color', ...
        'k','MarkerSize', MS, 'MarkerFaceColor', f_col(1), 'LineWidth', 1)
215 errorbar(RPM(3),mean(Average{3}), std(Average{3}), 'o', 'Color', ...
        'k','MarkerSize', MS, 'MarkerFaceColor', f_col(1), 'LineWidth', 1)
216 errorbar(RPM(4),mean(Average{4}), std(Average{4}), 'o', 'Color', ...
        'k','MarkerSize', MS, 'MarkerFaceColor', f_col(1), 'LineWidth', 1)
217
218 title('Area VS RPM','interpreter','latex')
219 ylabel('Time Averaged Area (mm$^2$)','interpreter','latex');
220 xlabel('Rotational velocity (rpm)', 'Interpreter','latex');
221 set(gca,'TickLabelInterpreter','latex', 'fontsize', fontsize);
222 xlim([0 1700])
223
224 % Plotting the modulus
225 figure
226 time_ = time;
227
228 for i = 1:length(RPM)
229
230     h = length(n_times{i});
231 %     errorbar(time_(1:h),Modulus{i}, Stand_dev{i}, 'o', 'Color', ...
        'k','MarkerSize', MS, 'MarkerFaceColor', f_col(i), 'LineWidth', 1)
232     plot(time_(1:h),Modulus{i}, 'o', 'Color', 'k','MarkerSize', MS, ...
            'MarkerFaceColor', f_col(i), 'LineWidth', 1)
233     hold on
234
235     time_(1:h) = [];
236
237 end
238
239 title('Modulus VS time','interpreter','latex')
240 ylabel('Modulus (mm$^2$)','interpreter','latex');
241 xlabel('Time (h)', 'Interpreter','latex');
242 set(gca,'TickLabelInterpreter','latex', 'fontsize', fontsize);
243 xlim([-5 75])
244 legend(num2str(RPM(1)),num2str(RPM(2)),num2str(RPM(3)),num2str(RPM(4)), ...
        'Location', 'best')
245
246 figure
247 errorbar(RPM(1),mean(Modulus{1}), std(Modulus{1}), 'o', 'Color', ...
        'k','MarkerSize', MS, 'MarkerFaceColor', f_col(1), 'LineWidth', 1)
248 hold on
249 errorbar(RPM(2),mean(Modulus{2}), std(Modulus{2}), 'o', 'Color', ...
        'k','MarkerSize', MS, 'MarkerFaceColor', f_col(1), 'LineWidth', 1)
250 errorbar(RPM(3),mean(Modulus{3}), std(Modulus{3}), 'o', 'Color', ...
        'k','MarkerSize', MS, 'MarkerFaceColor', f_col(1), 'LineWidth', 1)
251 errorbar(RPM(4),mean(Modulus{4}), std(Modulus{4}), 'o', 'Color', ...
        'k','MarkerSize', MS, 'MarkerFaceColor', f_col(1), 'LineWidth', 1)
252
253 title('Modulus VS RPM','interpreter','latex')
```

```
254  ylabel('Time Averaged Modulus (mm$^2$)','interpreter','latex');
255  xlabel('Rotational velocity (rpm)', 'Interpreter','latex');
256  set(gca,'TickLabelInterpreter','latex', 'fontsize', fontsize);
257  xlim([0 1700])
```

P. Metabolic pathway modeling MATLAB script

```
%% Script bioreactor
%In this script, a bioreactor containing c.auto is modeled.
%Here, a coontinious gas flow is present containing CO, CO2 and H2. The
%liquid phase is continiously refreshed with fresh medium.

clc, clear, close, close all
p = Parameters_C_auto();

%% ODE-solver


C0_reactants = [0.1 0 0 0];

C0_AC = [0.1 0];

C0_products = [ 2.5 0 0 0 ];

C0_pH = [0.0001];

C0_energycariers = [ 1.0 1.0 0.45 3.48 0.9 1.11 0.5 0.5 0.5 ]; % in micromol/gDCW


C0 = [C0_reactants C0_AC C0_products C0_pH C0_energycariers];


tau = 20;
options = odeset('NonNegative', 1:20);
[t,C] = ode15s(@Metabolism_Cauto2, [0 tau], C0, options, p);

%% Plot data
% Gas concentrations
figure
x0=10;
y0=10;
width=1000;
height=420;
set(gcf,'position',[x0,y0,width,height])
plot(t,C(:,1:3),'LineWidth',1.2)
legend('CO (g)','H2 (g)','CO2 (g)')
xlabel('Time [d]','Fontsize',13)
ylabel('Concentration [ mol /gDCW]','Fontsize',13 )


figure
x0=10;
y0=10;
width=1000;
height=420;
set(gcf,'position',[x0,y0,width,height])
plot(t,C(:,7:10),'LineWidth',1.2)
legend('Acetate (b)','Pyruvate (l)','Ethanol (l)','Butanediol (l)')
xlabel('Time [d]','Fontsize',13)
ylabel('Concentration [ mol /gDCW]','Fontsize',13)

figure
x0=10;
y0=10;
width=450;
height=420;
set(gcf,'position',[x0,y0,width,height])
plot(t,C(:,11),'LineWidth',1.2)
legend('H+')
xlabel('Time [d]','Fontsize',13)
ylabel('Concentration [ mol /gDCW]','Fontsize',13)
```

```
65
66  figure
67  x0=10;
68  y0=10;
69  width=1000;
70  height=420;
71  set(gcf,'position',[x0,y0,width,height])
72  plot(t,C(:,12:19),'LineWidth',1.2)
73  legend('Fd_ox','Fd_red','NADH','NAD+','NADPH','NADP+','ATP','ADP','Pi')
74  xlabel('Time [d]','Fontsize',13)
75  ylabel('Concentration [ mol /gDCW]','Fontsize',13)
76
77
78  function dCdt = Metabolism_Cauto2(t,C,p)
79
80  %% Reactions
81  % In this part, the implificied reactionterms are given. In this case, only
82  % the energy carriers determine the reaction rate. For reactions 2 and 3, only ...
        one rate is active. For reactions concerning
83  % ATP, ADP and Pi, only the concentration of Pi is left out.
84
85  % Reaction order:
86  n = 0;
87
88      % Reaction 1:
89      R_1 =  p.k1 * C(1)^n * C(12)^n;
90
91      % Reaction 1 (reverse):
92      R_rev1 = p.k_rev1 * C(11)^n * C(3)^n * C(13)^n;
93
94      % Reaction 2a
95      if C(1) <= 0
96          R_2a = p.k2a * C(3)^n * C(2)^n ;
97      end
98      if C(1) > 0
99          R_2a = 0;
100     end
101
102     % Reaction 2b
103     R_2b = p.k2b * C(3)^n * C(13)^n * C(16)^n * C(11)^n;
104
105     % Reaction 3
106     R_3 = p.k3 * C(4)^n * C(11)^n * C(18)^n * C(16)^n * C(14)^n * C(12)^n * ...
            C(1)^n * C(5)^n;
107
108     % Reaction 4
109     R_4 = p.k4 * C(6)^n * C(19) * C(20)^n  ;
110
111     % Reaction 5
112     R_5 = p.k5 * C(7)^n * C(11)^n * C(14) * C(13);
113
114     % Reaction 6
115     R_6 = p.k6 * C(6)^n * C(3)^n * C(11)^n * C(13);
116
117     % Reaction 7
118     R_7 = p.k7 * C(11)^n * C(12)^n * C(8);
119
120     % Reaction E1
121         if C(1) <= 0
122         R_E1 = p.kE1 * C(2)^0 * C(17) * C(12);
123         end
124     if C(1) > 0
125         R_E1 = 0;
126     end
127
128     % Reaction E_rev1
129     R_Erev1 = p.kE_rev1 * C(16) * C(13) * C(11)^n;
```

```
130
131      % Reaction E2
132      R_E2 = p.kE2 * C(13) * C(14) * C(17) * C(11)^n;
133
134      % Reaction E2_rev
135      R_Erev2 = p.kE_rev1 * C(12) * C(15) * C(16);
136
137      % Reaction E3
138      R_E3 = p.kE3 * C(13) * C(15) * C(11); %actually dependend on the gradient
139
140      % reaction E4
141      R_E4 = p.kE4 * C(19) * C(11); %actually dependend on the gradient
142
143
144  %% Macrobalances
145  dCdt = zeros(20,1);
146  C(C<0) = 0;
147
148      % 1: C_CO (b) - dC_CO+/dt [mol/m^3_b/h]
149      dCdt(1) = 0; %R_1 - R_rev1 - R_3 + (0.1 - dCdt(1));
150
151       % 2: C_H2 (b) - dC_H2/dt [mol/m^3_b/h]
152      dCdt(2) = - R_2a - 2*R_E1 + 2*R_Erev1;
153
154       % 3: C_CO2 (b) - dC_CO2/dt [mol/m^3_b/h]
155      dCdt(3) = - R_1 + R_rev1 - R_2a - 2*R_2b -R_6 + 2*R_7 -0.5;
156
157       % 4: C_HCOOH (b) - dC_HCOOH/dt [mol/m^3_b/h]
158      dCdt(4) = R_2a + 2*R_2b - R_3;
159
160       % 5: C_CoA (b) - dC_CoA/dt [mol/m^3_b/h]
161      dCdt(5) = -R_3 + R_4 + R_6;
162
163       % 6: C_AcetylCoA (b) - dC_AcetylCoA/dt [mol/m^3_b/h]
164      dCdt(6) = R_3 - R_4 - R_6;
165
166       % 7: C_Acetate (b) - dC_Acetate/dt [mol/m^3_b/h]
167      dCdt(7) = R_4 - R_5;
168
169       % 8: C_Pyruvate (b) - dC_Pyruvate/dt [mol/m^3_b/h]
170      dCdt(8) = R_6 - 2*R_7;
171
172       % 9: C_Ethanol (b) - dC_Ethanol/dt [mol/m^3_b/h]
173      dCdt(9) = R_5;
174
175       % 10: C_Butane-2,3-diol (b) - dC_Butane-2,3-diol/dt [mol/m^3_b/h]
176      dCdt(10) = R_7;
177
178       % 11: C_H+ (b) - dC_H+/dt [mol/m^3_b/h]
179      dCdt(11) = - 2*R_1 + 2*R_rev1 - 3*R_2b - R_3 - 3*R_5 - R_7 + 3*R_E1 - ...
             3*R_Erev1 - R_E2 + R_Erev2 + 2*R_E3 - 3.66*R_E4;
180
181       %   dCdt(11) = 0.01;
182
183
184       % 12: C_Fd_ox (b) - dC_Fd_ox/dt [mol/m^3_b/h]
185      dCdt(12) = R_1 - R_rev1 + R_2b - R_3 + R_5 + R_6 - R_Erev1 + R_E1 + R_E2 - ...
             R_Erev2 + R_E3;
186
187       % 13: C_Fd_red (b) - dC_Fd_red/dt [mol/m^3_b/h]
188      dCdt(13) = - R_1 + R_rev1 - R_2b + R_3 - R_5 - R_6 + R_Erev1 - R_E1 - R_E2 + ...
             R_Erev2 - R_E3;
189
190       % 14: C_NADH (b) - dC_NADH/dt [mol/m^3_b/h]
191      dCdt(14) = -2*R_3 - R_5 - R_E2 + R_Erev2 + R_E3;
192
193       % 15: C_NAD+ (b) - dC_NAD+/dt [mol/m^3_b/h]
```

```
194       dCdt(15) = 2*R_3 + R_5 + R_E2 - R_Erev2 - R_E3;
195
196        % 16: C_NADPH (b) - dC_NADPH/dt [mol/m^3_b/h]
197       dCdt(16) = -R_2b - R_3 - R_7 + R_E1 - R_Erev1 + 2*R_E2 - 2*R_Erev2;
198
199        % 17: C_NADP+ (b) - dC_NADP+/dt [mol/m^3_b/h]
200       dCdt(17) = R_2b + R_3 + R_7 - R_E1 + R_Erev1 - 2*R_E2 + 2*R_Erev2;
201
202        % 18: C_ATP (b) - dC_ATP/dt [mol/m^3_b/h]
203       dCdt(18) = -R_3 + R_4 + R_E4;
204
205        % 19: C_ADP (b) - dC_ADP/dt [mol/m^3_b/h]
206       dCdt(19) = R_3 - R_4 - R_E4;
207
208        % 20: C_Pi (b) - dC_Pi/dt [mol/m^3_b/h]
209       dCdt(20) = R_3 - R_4 - R_E4;
210
211
212   end
```